CR 86295

Design Of A Satellite Instrument For Measurement Of The Millimeter Characteristics Of Atmospheric Ozone

FINAL REPORT

CONTRACT NAS 12-117

Prepared for:
Electronics Research Center
National Aeronautics and Space Administration
Cambridge, Massachusetts 02139

EWEN KNIGHT

DESIGN OF A SATELLITE INSTRUMENT FOR MEASUREMENT OF THE MILLIMETER CHARACTERISTICS OF ATMOSPHERIC OZONE

FINAL REPORT

CONTRACT NAS 12-117

PREPARED FOR:
ELECTRONICS RESEARCH CENTER
NATIONAL AERONAUTICS AND SPACE ADMINISTRATION
CAMBRIDGE, MASSACHUSETTS 02139

TABLE OF CONTENTS

LIST OF FIGURES

LIST OF FIGURES

LIST OF TABLES

1.0 PROGRAM OBJECTIVES

The objective of this investigation was to develop the design approach for a satellite-measurement instrument capable of detecting atmospheric ozone concentration and motion. Detailed knowledge of the global vertical temperature distribution, water vapor concentration, pressure gradients, and the structure of air mass flow is of crucial importance to global numerical weather prediction. A new generation of meteorological sensors is required to provide this needed information. This investigation was the first step in the development of one of these future generation meteorological satellite measurement instruments.

The relationship between weather conditions and the vertical distribution of ozone is not, as yet, well-documented on a global scale, as a consequence of insufficient geographically distributed daily observations. Though the role of ozone in determining the weather pattern is not thoroughly understood at this time, there is strong evidence to indicate that a measure of ozone concentration and motion would provide a valuable source of information to further the understanding of global air mass circulation. In this sense, ozone may be considered in the role of a "tracer element" which may allow us to observe the global structure of air mass circulation under those conditions where visible indicators such as clouds are not available.

Photochemical equilibrium computations suggest that variations in ozone content, particularly at the lower altitudes are less subject to change than actually observed. It has been concluded that the observational data supports the theory of atmospheric circulation processes, which redistribute the photochemically formed ozone. One such circulation pattern which could account for the observed ozone distribution is based on a cycle of ascending motion through the equatorial tropopause, northward motion, descending motion at higher latitudes, and a return flow at lower altitudes toward the equator to complete a meridional circulation pattern. In opposition to the circulation theories, there remains considerable controversy over the possibility that one observes "local ozone transport vectors," rather than a meridional circulation pattern.

Extension of present knowledge is needed concerning the vertical distribution of ozone in the atmosphere, the global and temporal variations of this distribution, and the influence upon it of such external factors as solar activity. The accumulation of this knowledge can proceed more rapidly through global measurements obtained from the vantage point of an earth orbiting space platform. Such data might then be combined with data obtained from other atmospheric sensors located on earth-based, airborne and space platforms to provide a more complete view of atmospheric characteristics in the spatial, frequency, and time domains. The broader the frequency range over which the electromagnetic properties of the atmosphere are determined and understood, the greater the possibility to derive its composition and the distribution of its constituents, and from that point of understanding, useful numerical weather prediction criteria.

This investigation was specifically directed to determining the potential utility of passively sensing the microwave emission from atmospheric ozone in order to derive from the observed characteristics the vertical profile distribution. The concept was predicated on prior analytical efforts and related experimental data which suggested the possibility of resolving a single resonant line profile. With sufficient signal-to-noise ratio, the measured characteristics of the line profile could then be translated through an inversion process, to the vertical density profile of ozone in the atmosphere.

The program objective was a unique challenge to microwave radiometer technology, since it is well-known that the intensity of ozone resonant lines increase rapidly with increasing frequency; however, the state-of-the-art in microwave radiometer sensitivity decreases rapidly with frequency. For example, the strongest ozone lines near 3 mm are nearly two orders of magnitude more intense than those near a wavelength of 8 mm. Achievable radiometric sensitivity, at the time that this investigation was initiated, was more than two orders of magnitude poorer at a wavelength of 3 mm, than at 8 mm. The questions to be resolved by this investigation were then:

1) Are the predicted resonant ozone line profiles at short millimeter wavelengths valid?

2) What applicable improvements in radiometer sensitivity at millimeter wavelengths appear reasonable?

3) What instrument techniques and component capabilities are most suitable for the sateilite instrument?

In summary, the objective was to select an ozone resonant line with sufficient intensity which could be detected with a signal-to-noise ratio adequate to allow resolution of the line profile to the precision required for inversion. A further stipulation, of course, was that the techniques and components incorporated in the design of the satellite instrument be at, or near, the current state-of-the-art.

2.0 APPROACH AND RESULTS

The technical approach to the achievement of program objectives is shown in flow diagram form in Figure 2-1. The three major areas of effort were: Analysis, Design, and Measurement. The function of measurements was to verify predictions derived from both the theoretical analysis of the problem, as well as the instrument design analysis. These inter-relationships are depicted in Figure 2-1. The following brief description of the philosophy of approach will be aided by reference to that Figure.

Theoretical analysis of the problem preceded with an investigation of the physical properties of ozone molecular transitions in the millimeter domain and the influence of atmospheric parameters on the millimeter characteristics of the line structure. Predicted resonant line profiles were derived from these fundamental considerations. In this initial step of analysis, several assumptions were introduced. The next step in analysis was the translation of predicted line profiles into measurement system performance requirements. These initial instrument requirements were then used as the foundation for initiating the instrument design study.

The critical nature of certain assumptions introduced in the derivation of predicted resonant line profile characteristics suggested the formulation of a plan for verification. This plan called for direct measurement to verify the ozone resonant line shape and intensity characteristics, and further to verify the anticipated performance of instrument techniques and components at short millimeter wavelengths. The key features of the measurement plan are shown in Figure 2-2.

The need for verification of both theoretical predictions and instrument performance characteristics was introduced in the instrument design portion of the effort. As shown in Figure 2-1, the system performance requirements, derived from predicted line profile characteristics, were translated into performance requirements imposed on earth based, balloon, and satellite measurement instruments. The design approach for each observing platform was influenced primarily by the environment imposed on the sensor.

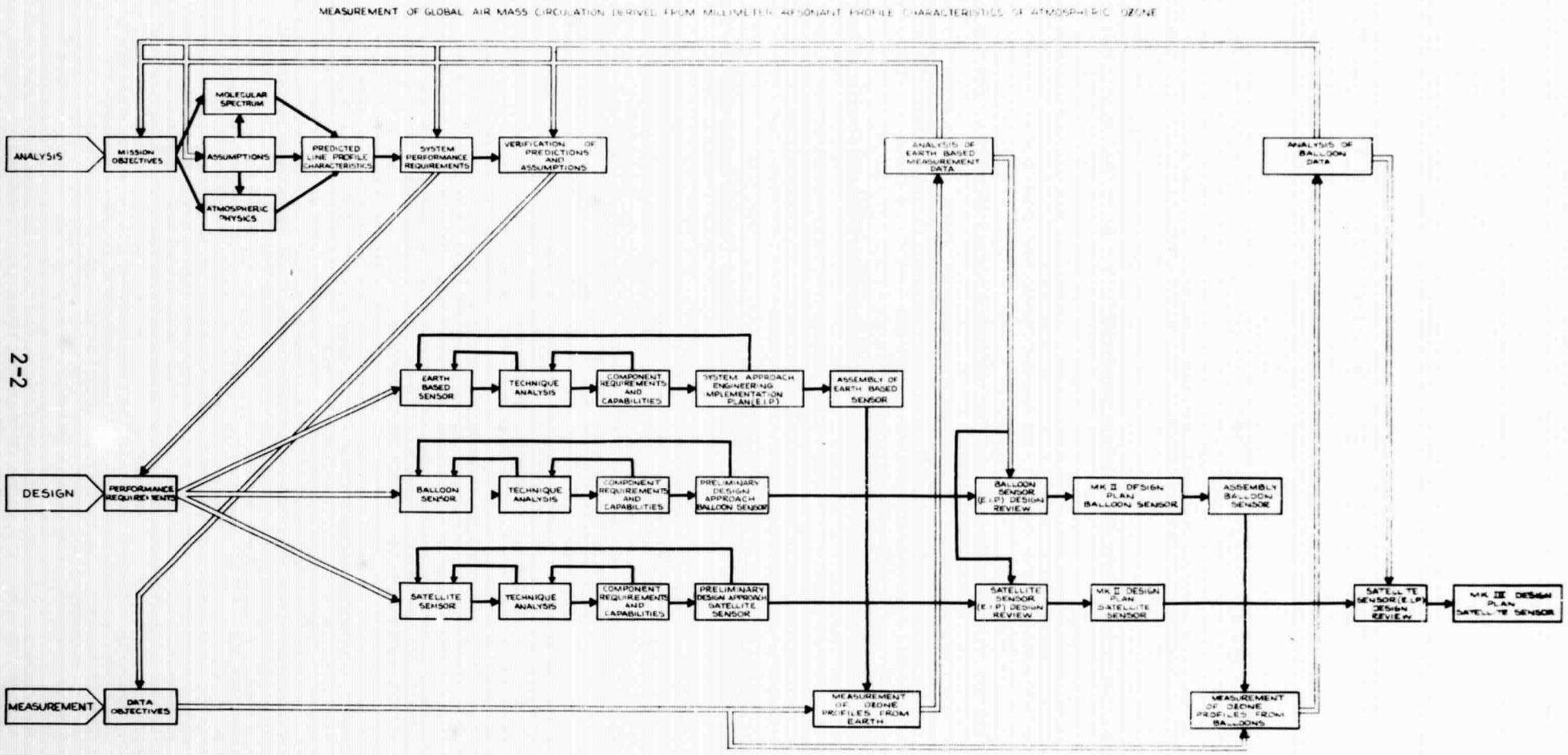

OVERALL PROGRAM SCHEDULE

FIGURE 2-1

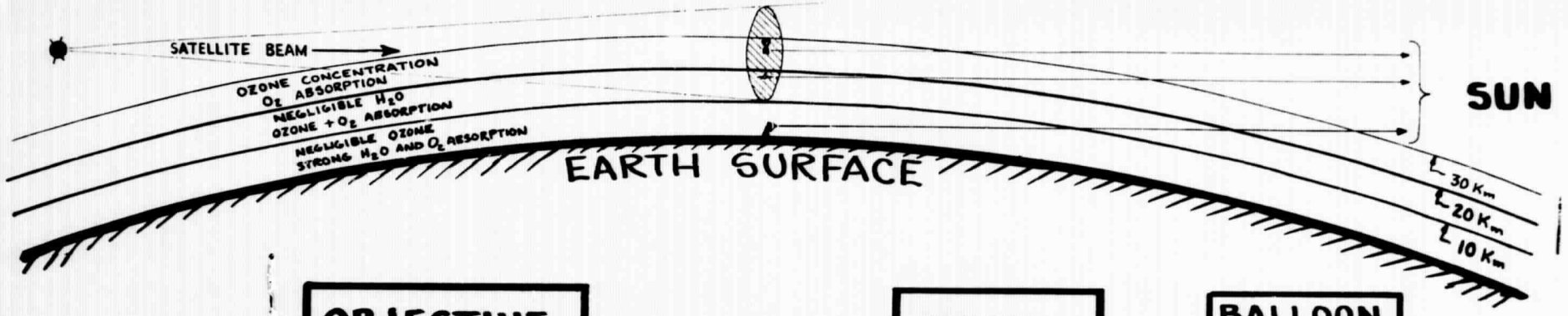

OBJECTIVE	EARTH	BALLOON AND/OR AIRCRAFT
● GENERAL VERIFICATION OF LINE SHAPE AND INTENSITY.	★	
● EXPERIMENTAL VERIFICATION OF PROFILE ABOVE 15-20 Km, LINE WIDTH AND SHAPE.		★
● STATUS OF INSTRUMENT TECHNOLOGY.		★

MEASUREMENTS LEADING TO SATELLITE SENSOR DEFINITION.

FIGURE 2-2

The earth based sensor design was given top-priority during the early phases of the program. The immediate objective of earth based measurements was to verify the general shape and intensity of that resonant line selected as the most likely candidate for achievement of program objectives. The plan included assembly of the earth based measurement instrument, followed by accumulation of observational data. The data was then scheduled for analysis to provide significant program inputs to the analytical portion of the effort in the areas of:

Mission objectives

Assumptions

System performance requirements

Verification of predictions and assumptions

A very significant additional product of this analysis was an instrument design review to establish the suitability of instrument design approaches for future balloon and satellite measurement instruments.

Referring again to Figure 2-1, the next scheduled step in the program plan was to update the balloon instrument design plan, based on the measured performance characteristics of the earth based instrument. The balloon instrument was then scheduled for assembly and accumulation of data from a balloon observing platform. The final step in the original program plan was analysis of the data obtained from the balloon observing platform to provide program inputs to overall mission objectives, and satellite instrument requirements in a manner similar to that scheduled for the analysis of earth based measurements.

The reasonable assumption was introduced at the time the plan was formulated that measurements obtained from an earth based instrument, when combined with observational data obtained from a balloon platform, would be sufficient to define the design approach to the satellite instrument.

All portions of the program plan, as outlined above, were successfully accomplished under the contract, with the one exception that the Balloon Flight Program was not included.

As a reasonable alternative, the earth based measurement instrument was modified to provide more detailed knowledge of the resonant profile characteristics of atmospheric ozone than could be obtained by the instrument in its initial configuration.

The ozone line resonant selected for this application was the $4_{0,4} \longrightarrow 4_{1,3}$ transition at 101.737 GHz.

In this section of the Final Report, more detailed information is provided concerning: the various phases of the program as they were actually implemented, the predicted and measured characteristics of the atmospheric ozone line at 101.7 GHz, and the design of the earth based measurement instrument.

2.1 Program Phases

The implementation of this study and investigation during the three-year period from April of 1966 through April of 1969, closely followed the projected plan developed in the early months of the investigation, as shown in Figure 2-1. The total program effort is describable in three phases:

Phase I - Analysis leading to the approach definition, and the selection of the resonant line frequency.

Phase II - Development of measurement objectives and partial assembly of an earth based measurement instrument to verify instrument performance characteristics as well as analytical predictions concerning the millimeter characteristics of atmospheric ozone.

Phase III - Definition of the satellite instrument design approach based on the measured characteristics of atmospheric ozone emission and absorption at 101.7 GHz obtained through earth based observations.

The scope of effort and the accomplishments during the first phase of the program are shown in Figure 2-3. This initial portion of the study and investigation included:

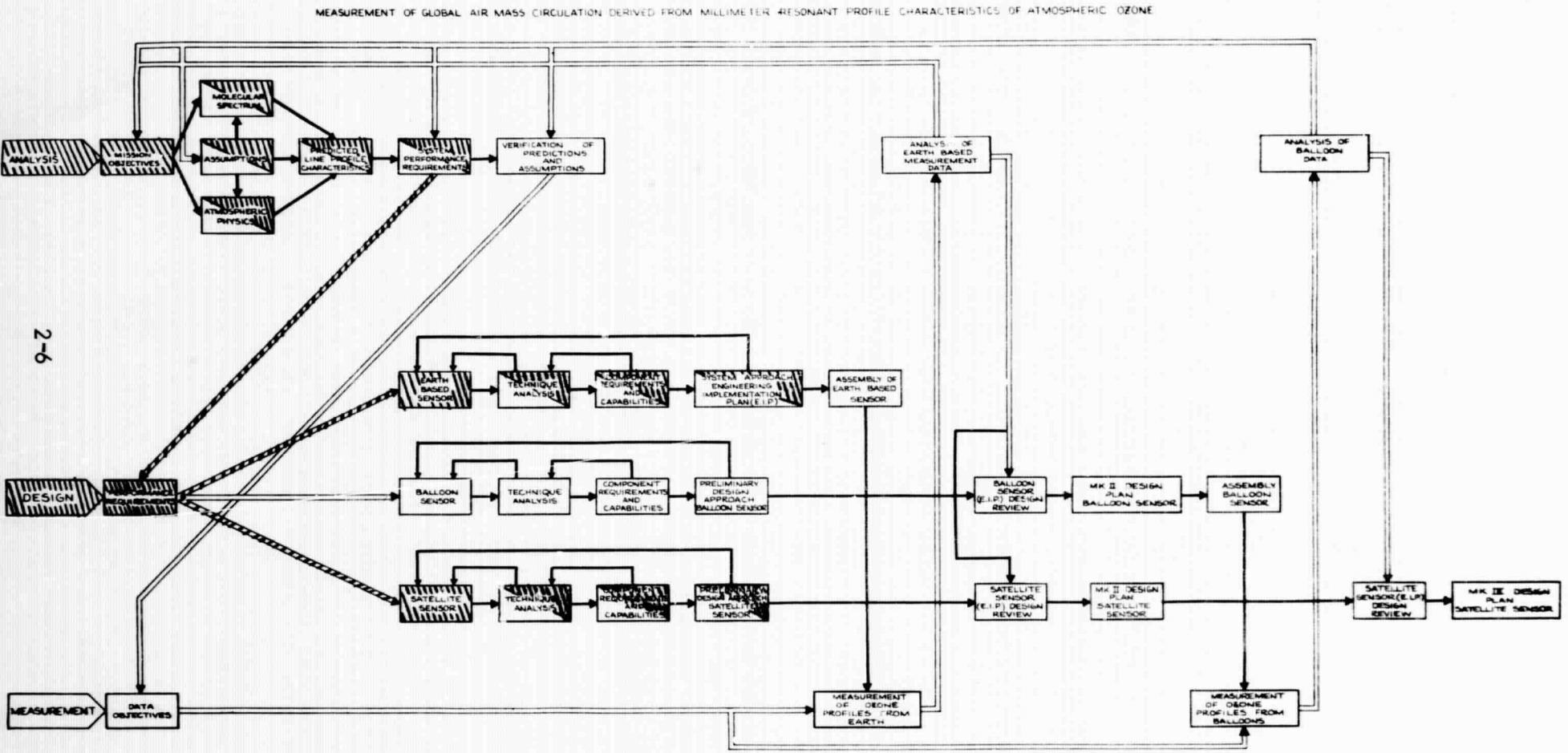

PROGRAM SCHEDULE PHASE I

FIGURE 2-3

(a) Investigation of atmospheric ozone emission and absorption profile characteristics in the vicinity of selected resonant lines as viewed from various observing platforms.

(b) Analysis of atmospheric ozone line profile data in terms of the meteorological significance of obtaining a detailed global time-function of the concentration and motion of atmospheric ozone when viewed from various observing platforms.

(c) Development of measurement instrument performance requirements based on the anticipated ozone line profile emission and absorption characteristics.

(d) Analysis and development of competitive sensor system design approaches to meet the performance requirements imposed on earth based and satellite instruments.

As a direct result of this initial phase of the investigation, it became apparent that verification of several critical analytical assumptions introduced in the derivation of anticipated resonant line profile characteristics would be required. Direct experimental measurement was considered the most conclusive approach. A laboratory measurement program was considered , however, measurements of this type would provide useful knowledge concerning resonant profile shape (bandwidth) characteristics only under simulated atmospheric conditions. The important fact was that we would be unable to directly simulate atmospheric measurements. The selection of direct, rather than laboratory measurements, was based on the immediate need to assure the validity of critical assumptions, including anticipated instrument performance capabilities. Though the knowledge gained from laboratory measurements would not be as encompassing in the scope of its impact, it would provide very important supporting information concerning the physical constants associated with the molecular transitions of interest. These laboratory measurements are included in our recommended

Implementation Plan for the satellite system. This plan is described in Section 3.4.

Phase II of the program effort was primarily concerned with defining the most appropriate methods for verification of the predicted millimeter characteristics of the ozone line resonance at 101.7 GHz. The scope of the program effort during this phase and the related progress is shown in Figure 2-4. This second phase of the study and investigation included:

(a) Extension of the investigation of atmospheric ozone emission and absorption profile characteristics initiated under the first phase of the program. A computer program was developed to aid in the analysis of resonant profile characteristics.

A discussion of the computer program and the associated predictions concerning resonant profile characteristics, in both absorption and emission for earth based, aircraft, balloon, and satellite observing platforms, is included in Section 2.2 of this report.

(b) The preliminary design plan for the earth based measurement instrument was refined to an Engineering Implementation Plan status. Selected portions of the instrument considered most critical to overall performance were assembled and evaluated. These sub-functional units included the antenna system, portions of the RF calibration circuitry and the multi-channel intermediate frequency subsystems required for the detection of ozone resonant profile line characteristics at a frequency of 101.7 GHz. The design and measured performance characteristics of the earth based measurement instrument is described in Section 2.3 of this report.

(c) Though the earth based instrument design was only partially

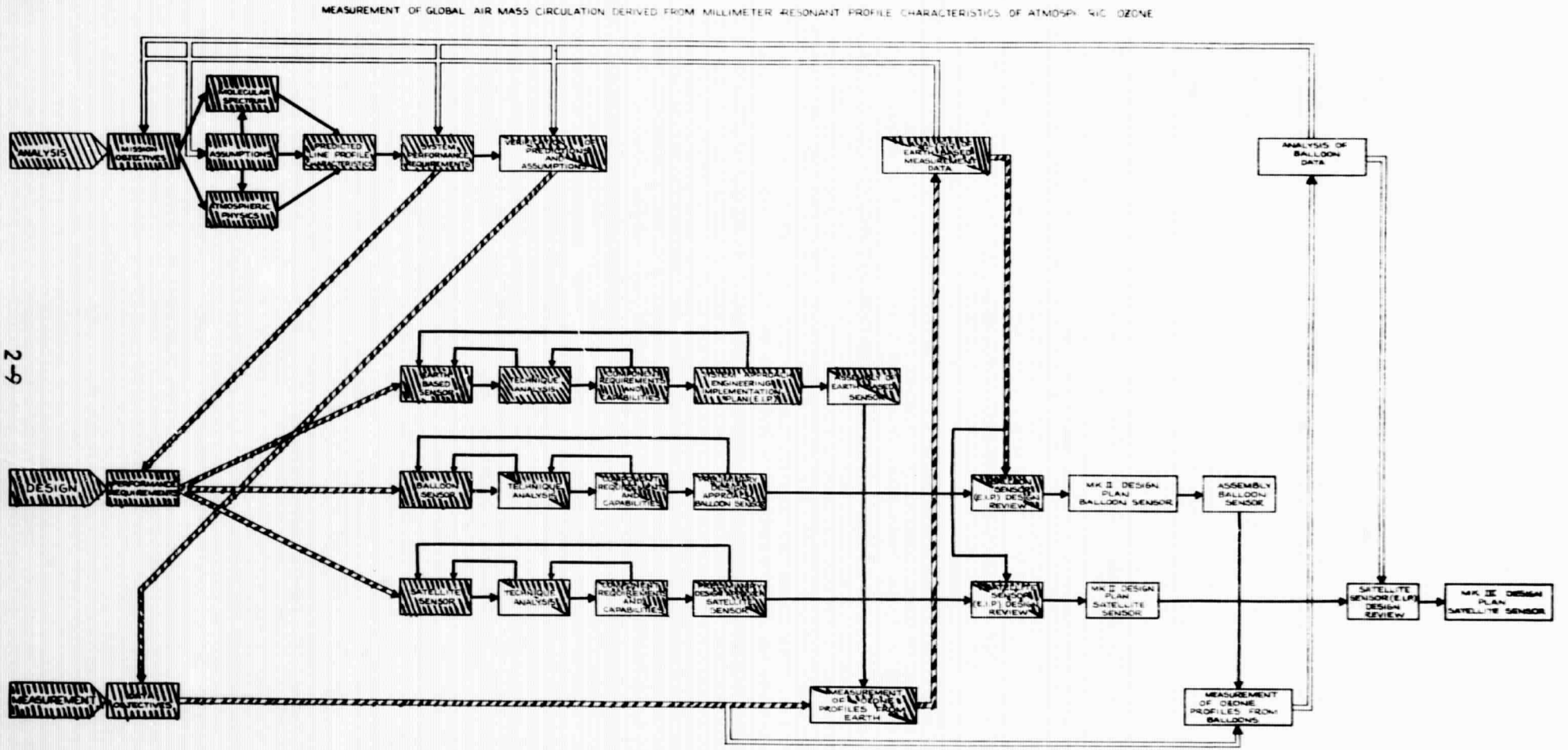

PROGRAM SCHEDULE PHASE II

FIGURE 2-4

implemented through the assembly phase, an adequate number of functional subsystems were available to perform an initial series of observational measurements. The objective of these measurements was to accumulate preliminary observational data sufficient to demonstrate the ability to detect and measure the absorption profile resonant characteristics of atmospheric ozone. We were unsuccessful in this attempt; however, considerable knowledge was gained concerning instrument performance characteristics.

(d) The measured performance characteristics of the earth based instrument in its partially assembled form were included in a design review of the balloon and satellite instrument approaches.

The third phase of this study and investigation included several significant milestones. The scope of the program effort and the related accomplishments during this final phase are shown in Figure 2-5. This phase of the effort included:

(a) The earth based instrument which was partially assembled under Phase II was fully implemented in accord with the design approach initiated under Phase I.

(b) Observational measurements were performed with the earth based instrument in its fully implemented form. The ozone resonant line at 101.7 GHz was detected in absorption, using the sun as a background source, and the profile in the vicinity of the line center frequency was partially resolved.

(c) The performance capability of the earth based instrument was extended to provide 16 separate channel outputs, 15 of which were designed to provide a simultaneous profile resolution of contiguous frequency segments over a 170 MHz band centered

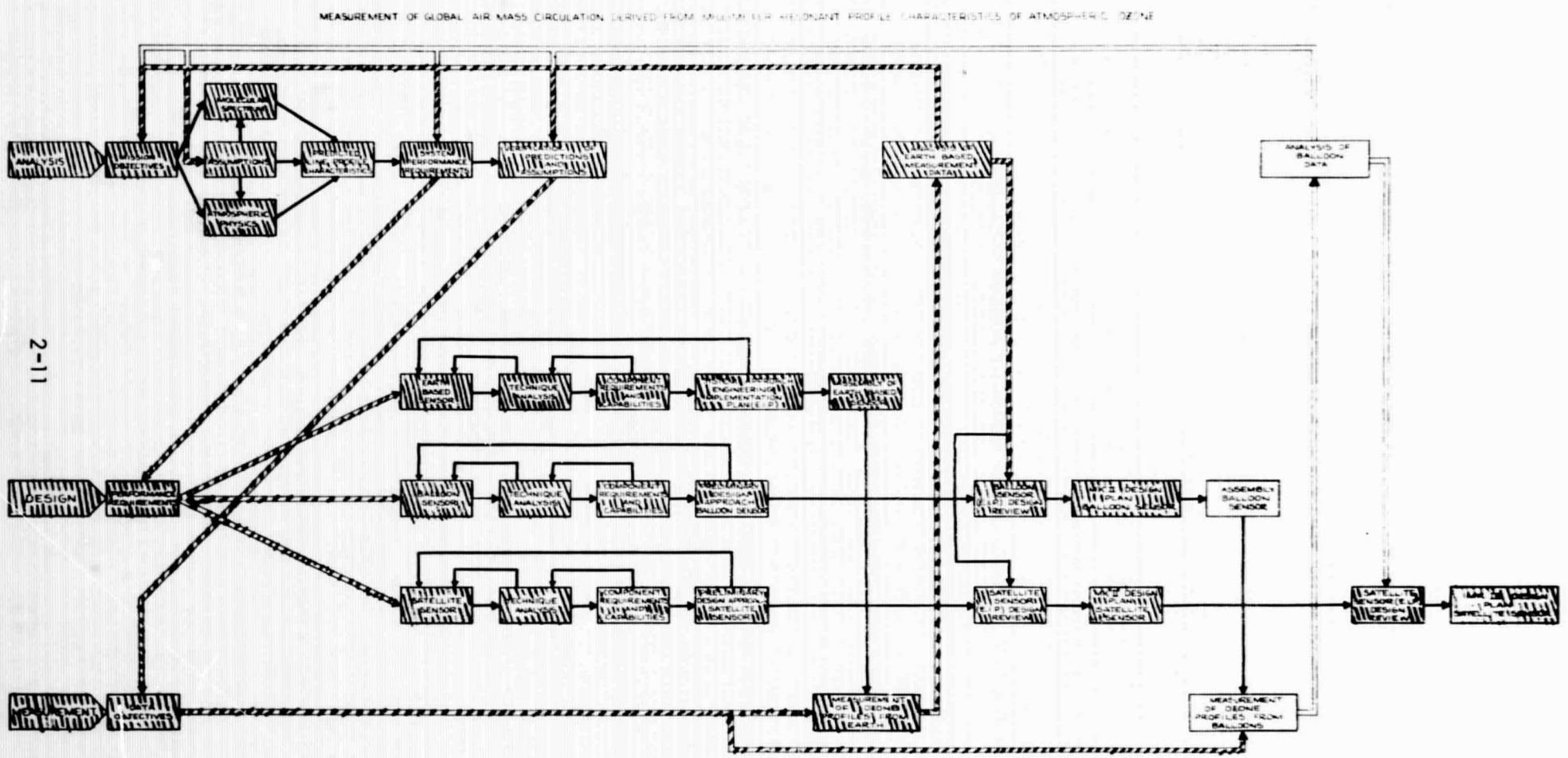

PROGRAM SCHEDULE PHASE III

FIGURE 2-5

on the line frequency. The 16th channel was designed to provide a base-band response covering 750 MHz centered on the line frequency.

(d) The performance characteristics of the modified earth based instrument were evaluated to assure that the performance achieved was consistent with that anticipated. Observational data accumulated with the instrument in its modified form confirmed the potential capability of the instrument to accumulate useful data from an earth based platform in a reliable manner using routine observational procedures.

(e) The recommended electrical and mechanical design approach for the satellite instrument and an implementation plan for its assembly was completed.

During this final phase of the study and investigation, an unanticipated frequency resonance was detected in the radiometer system. By isolating each of the functional subsystems we were able through a series of tests to identify that the effect was associated with the geometry of the antenna structure. The characteristics of this effect and the method used to reduce its distortion of the observational data to an undetectable level is discussed in Addenda C.

2.2 Predicted Atmospheric Ozone Profiles at 101.7 GHz

The performance characteristics and design approach for any measurement instrument are predicated on the anticipated characteristics of the input signal. For the application investigated under this program, the anticipated resonant line profile characteristics of atmospheric ozone observed in both emission and absorption from various observing

platforms were required to establish the performance requirements that would be imposed on the design of the radiometric measurement instrument. At the time that the program was initiated, observational data was not available; hence, the resonant profile characteristics, in particular, the line intensity and shape were derived from analysis of available data concerning the physics of molecular transitions and the composition of the atmosphere. The number of critical assumptions necessarily introduced in this analysis suggested the development of a computer program, capable of accommodating the anticipated dynamic range of several significant parameters which contribute to the intensity and shape of the profile.

The analytical portion of the effort, leading to the development of the predicted line profile characteristics, was undertaken by Dr. W. M. Caton during the first and second phase of the program. Two computer programs were developed to calculate atmospheric ozone absorption and emission characteristics. These computer programs were also adapted to the calculation of the background emission and absorption contributed by molecular oxygen and water vapor. One of the programs provides the calculation of the anticipated profile obtained by an observer looking up through the atmosphere, either from the earth's surface or from an observing platform within the earth's atmosphere. The second program computes the profile that would be observed by a downward looking observer located in either the earth's atmosphere or above the atmosphere. The related geometries for these computer programs are illustrated in Figures 2-6 and 2-7, respectively.

The calculations performed with either program are based on a model atmosphere of 100 layers, each of arbitrary thickness. The absorption coefficient for each layer is calculated for the temperature, pressure, water vapor content and ozone contents introduced in the program. The fundamental expression used in the program is:

$$A = e^{-\Sigma_i \alpha_i l_i} \qquad (2\text{-}1)$$

where: α_i is the absorption coefficient at a point in the i^{th} layer;

l_i is the path length through the layer;

A is the total absorption of the atmosphere.

GEOMETRY ASSOCIATED WITH THE "EARTH" PROGRAM

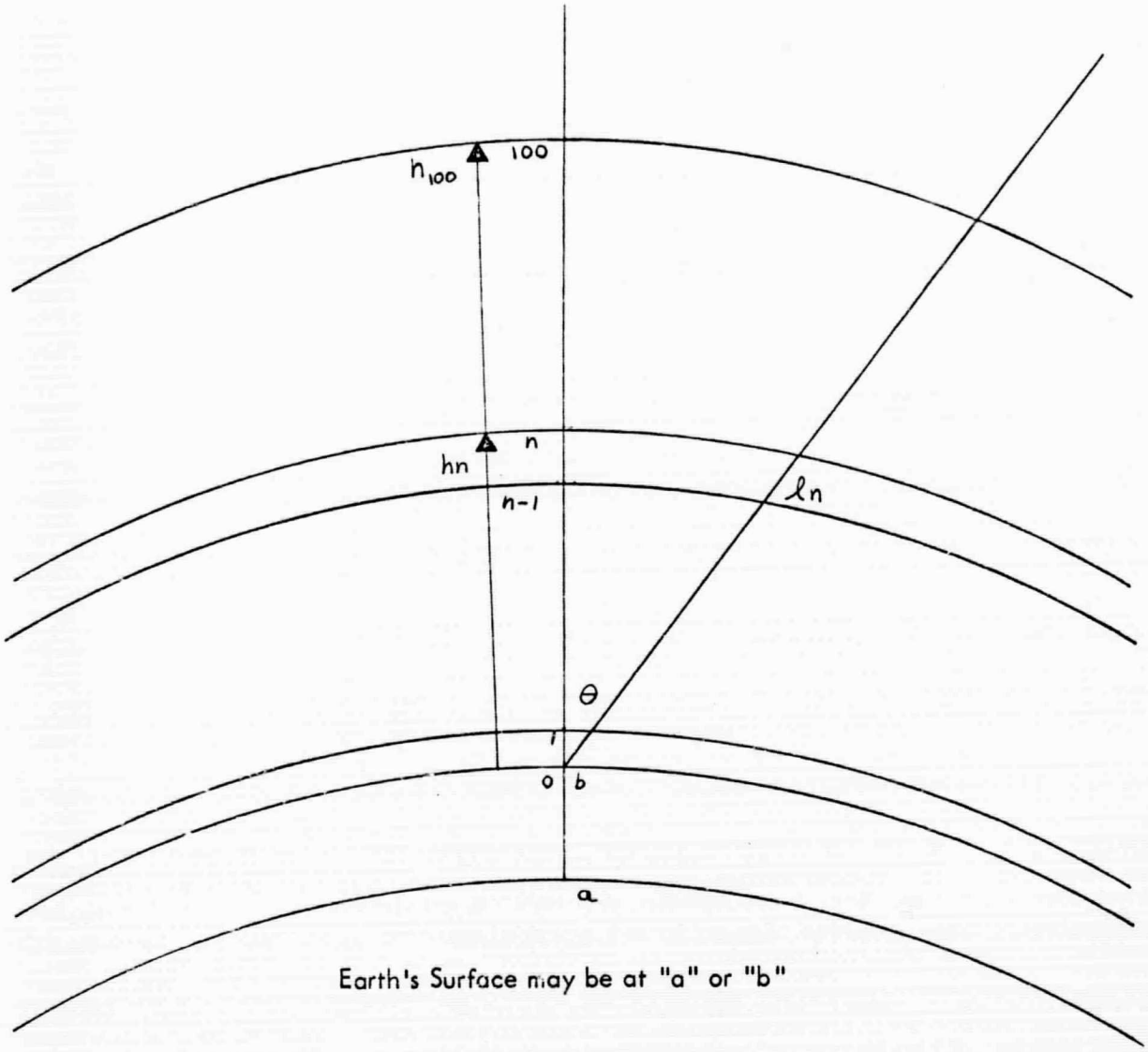

Earth's Surface may be at "a" or "b"

FIGURE 2-6

GEOMETRY ASSOCIATED WITH THE "SATELLITE" PROGRAM

h_{100} may be less than or greater than H

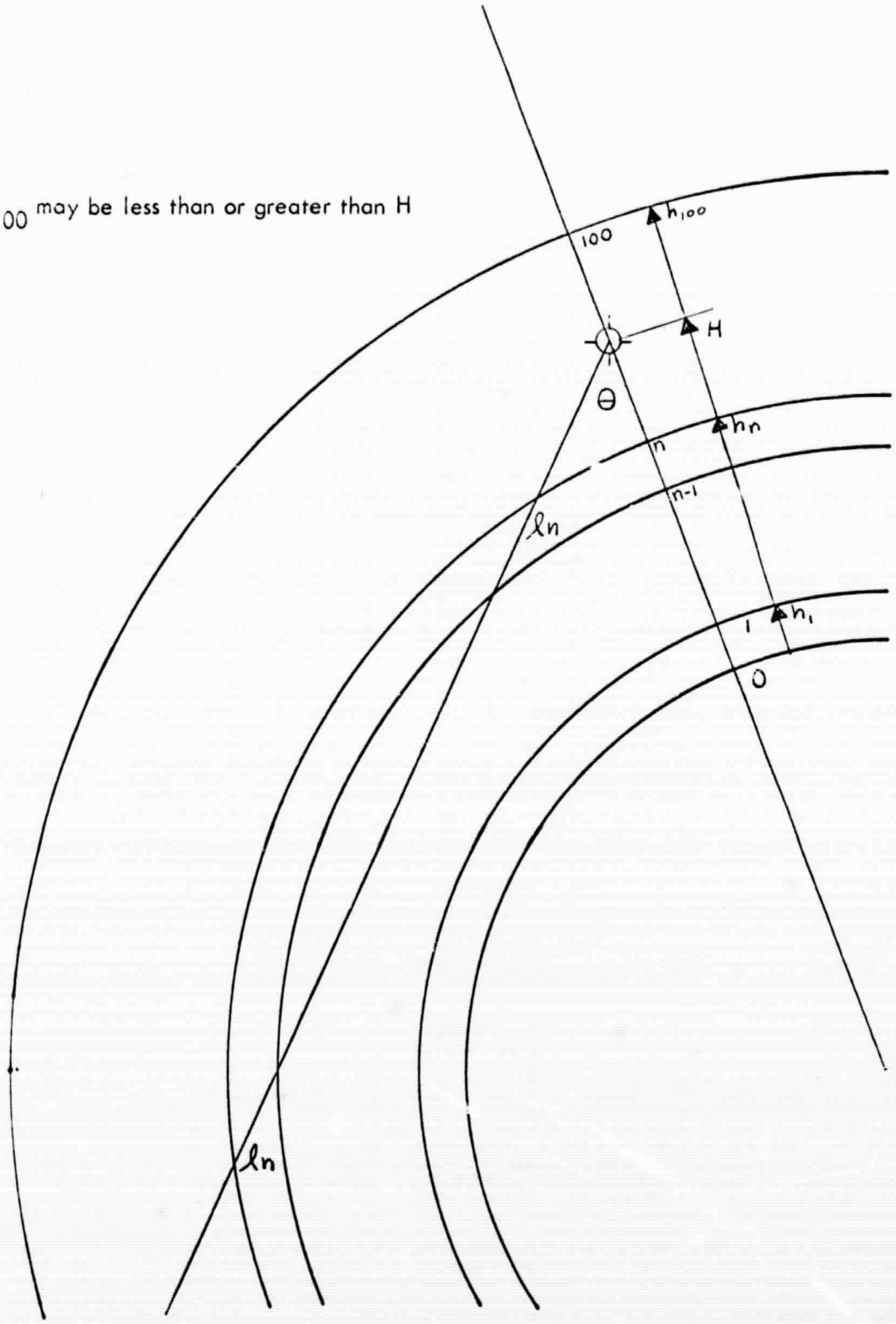

FIGURE 2-7

The program computes the apparent emission temperature of the atmosphere, T, from the expression:

$$T = \sum_i T_i \, e^{-\sum_{R=1}^{i-1} \alpha_R \ell_R} \qquad (2\text{-}2)$$

where: T_i is the temperature of the i^{th} layer. The program also computes, ΔA, the increment in the atmospheric attenuation, and ΔT, the increment in the atmosphere's apparent temperature produced by the presence of the atmospheric ozone.

The computer program prints out the quantities A, ΔA, T, and ΔT for 25 frequencies and 15 zenith angles as specified in the program input. In addition, the absorption and the emission of each layer, as measured by the observer, can be printed out for the first of the frequencies and angles specified, or for all frequencies and angles.

Since the absorption coefficient of ozone is given by the expression:

$$\alpha_{O_3} = A_1 \frac{e^{-A_2/T}}{T^{5/2}} N_{O_3} \nu^2 \left[\frac{\Delta\nu}{(\nu - A_3)^2 + (\Delta\nu)^2} + \frac{\Delta\nu}{(\nu + A_3)^2 + (\Delta\nu)^2} \right] \qquad (2\text{-}3)$$

where:

$$\Delta\nu = \left[(A_4 P T^{-1/2})^2 + (A_5 T^{1/2})^2 \right]^{1/2} \qquad (2\text{-}4)$$

the values for the coefficients A_1 through A_6 must be included in the program input. These constants specify the ozone transition to be included in the calculations. For the 101 GHz transition, the values of these coefficients are:

$$A_1 = 1.2 \times 10^{-24} \text{ km}^{-1}$$

$$A_2 = 13.1^{\circ}\text{K}$$

$$A_3 = 10.17368 \times 10^{10} \text{ Hz}$$

$$A_4 = 5.28 \times 10^{7} \ (^{\circ}\text{K}^{1/2}) \text{ mm}^{-1}$$

$$A_5 = 7.31 \times 10^{3} \ (^{\circ}\text{K})^{-1/2}$$

The magnitudes of these coefficients were obtained from:

E.K. Gora, "The Rotational Spectrum of Ozone,"
J.Mol. Spectroscopy 3, 78-99, (1959).

C.H. Townes and A.L. Schawlow, "Microwave Spectroscopy,"
McGraw Hill, New York, 1955.

The computer calculated resonant line profile characteristics for the 101.7 GHz transition, for satellite earth based platforms, are shown in Figures 2-8 through 2-10. The assumptions introduced in these particular profile calculations were standard atmospheric conditions with an atmospheric ozone distribution with height as shown in Figure 2-11.

The performance requirements for the earth based measurement instrument were derived directly from the anticipated absorption profile characteristics as shown in Figure 2-8.

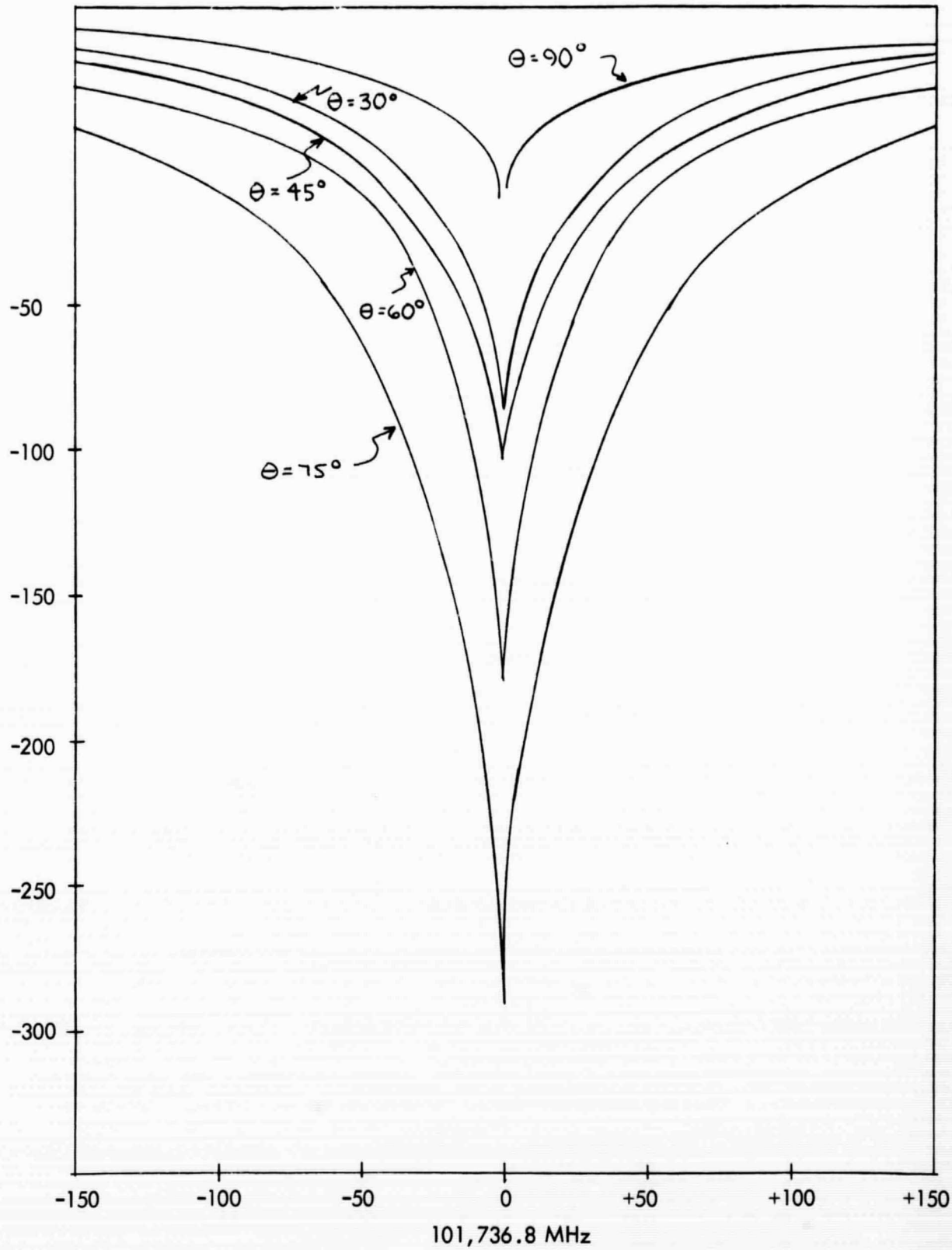

CHANGE IN THE SUN'S APPARENT TEMPERATURE AS VIEWED FROM THE EARTH'S SURFACE

FIGURE 2-8

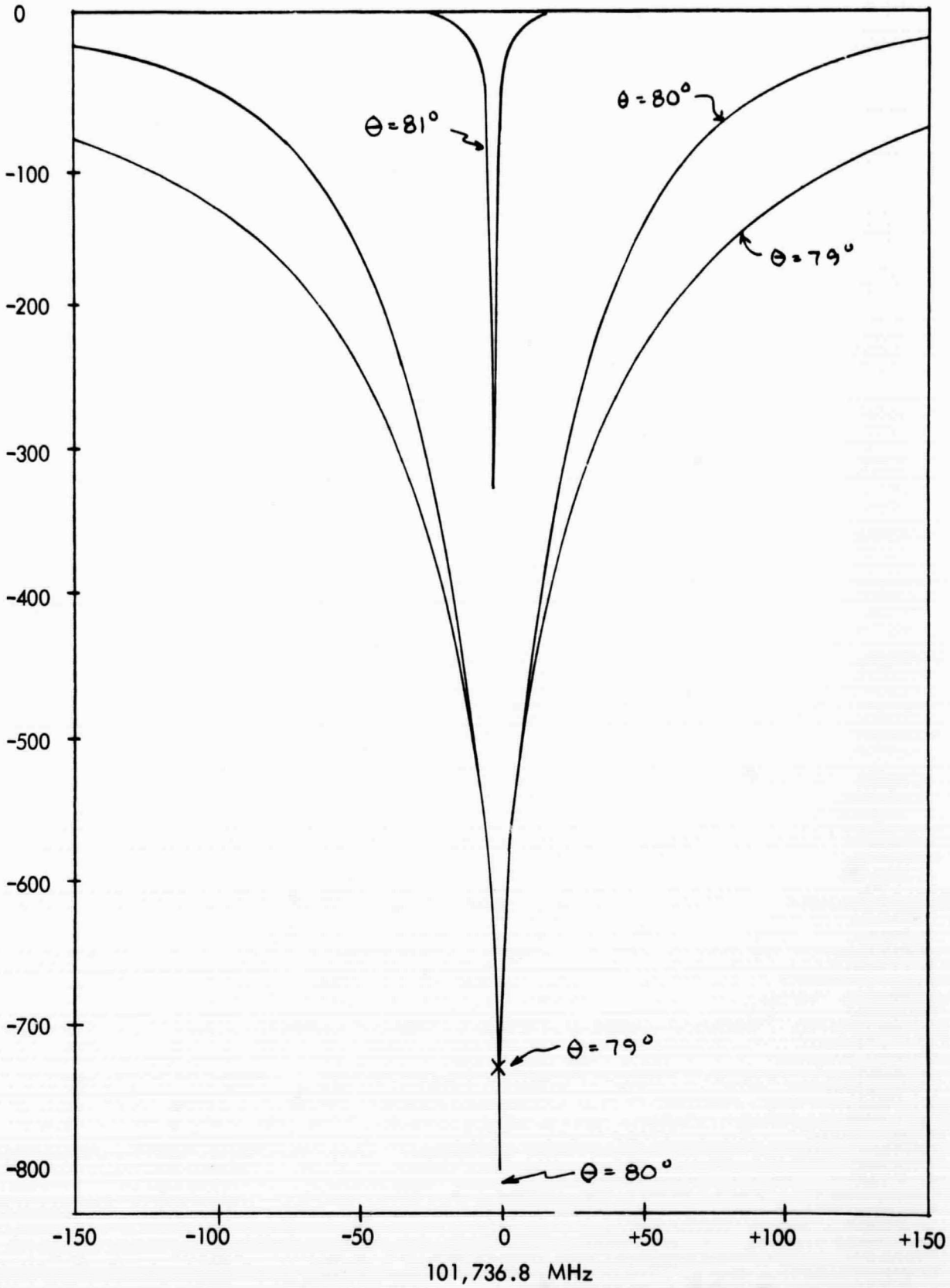

CHANGE IN THE SUN'S APPARENT TEMPERATURE AS VIEWED FROM A SATELLITE 125 KM ABOVE THE EARTH'S SURFACE

FIGURE 2-9

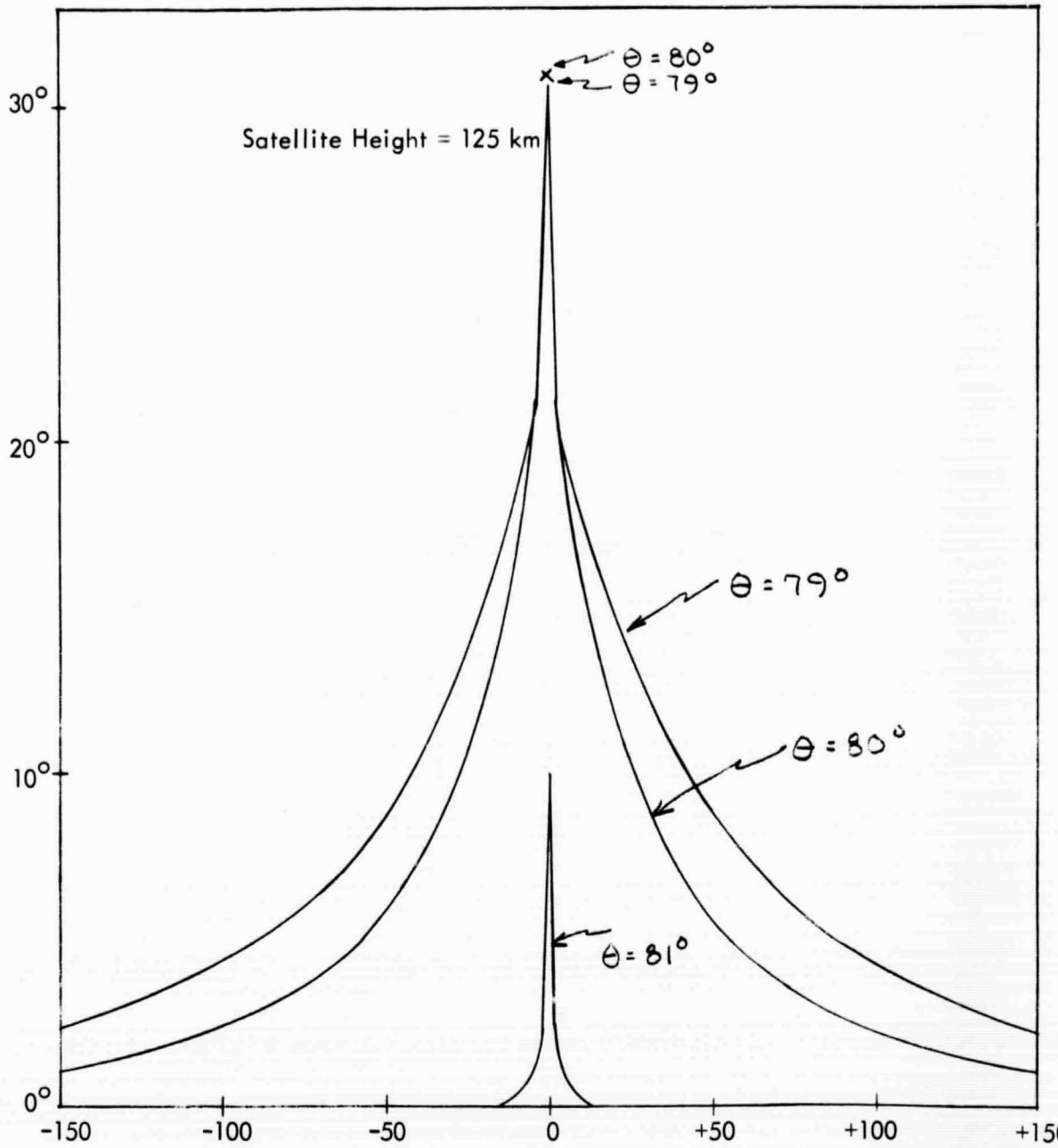

APPARENT TEMPERATURE OF THE EARTH'S ATMOSPHERE AS VIEWED FROM A SATELLITE

FIGURE 2-10

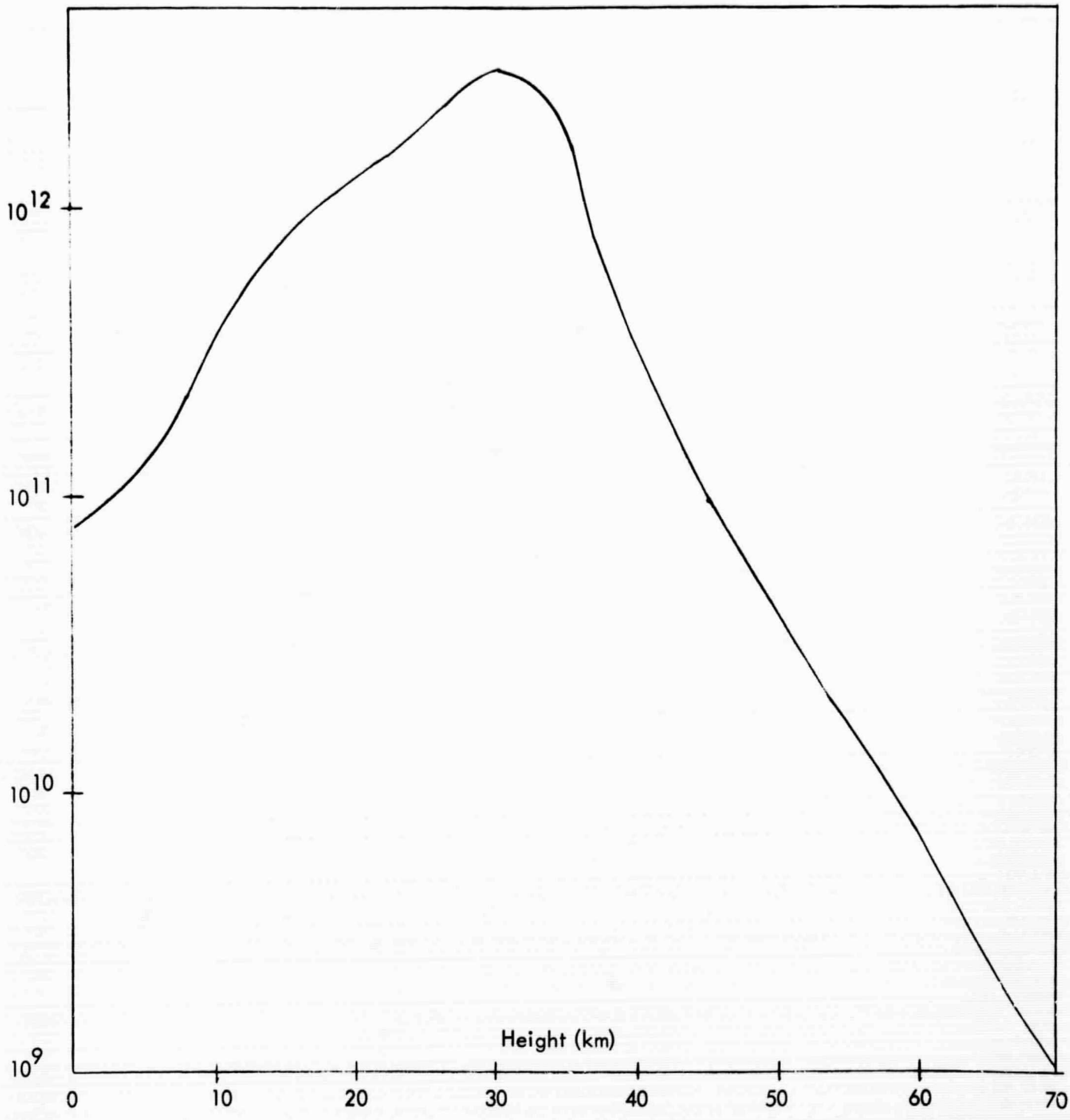

OZONE CONCENTRATION VS HEIGHT ABOVE THE EARTH'S SURFACE

FIGURE 2-11

2.3 Design of the Earth Based Measurement Instrument

Requirements

The performance requirements for a radiometric receiving system capable of detecting and resolving the atmospheric ozone resonant line profile at 101.7 GHz can be derived directly from the anticipated intensity and bandwidth characteristics of the input signal. At the time the investigation was initiated, no direct observational data was available concerning these characteristics. A computer program analysis, based on reasonable assumptions, was developed to obtain predicted profile characteristics, as described in a prior section of this report.

The predicted profile that would be observed in absorption by an earth based instrument when viewing the sun at a zenith angle of 60°, as shown in Figure 2-8, was used in the definition of measurement instrument performance requirements. In developing the measurement system specifications, the following reasonable assumptions were made concerning the nature of the absorption spectrum at 101.7 GHz:

(1) An exo-atmospheric brightness temperature of the sun of 6,000°K.

(2) Attenuation due to atmospheric water vapor and oxygen under clear dry observing conditions of 1 db at a zenith angle of observation of 60°.

(3) A peak attenuation due to ozone of 3% in a 10 MHz band centered on the line frequency when observed at a zenith angle of 60° under clear dry observing conditions.

(4) An exponential shape for the absorption profile with a "half-power" bandwidth of 50 MHz.

From the foregoing:

(a) The brightness temperature of the sun at a 60° zenith observing angle would be 4,700°K.

(b) A 3% absorption in a 10 MHz band would provide a temperature difference of 140°K relative to the observed sun temperature.

(c) The temperature difference relative to the sun temperature observed in a 50 MHz band would be approximately 90°K.

(d) The temperature difference observed between a 10 MHz and a 50 MHz filter centered on the line frequency would be approximately 50°K.

For an antenna diameter larger than two feet, the main beam angle would be well-within the subtended angle of the solar disk as viewed from the earth. Assuming an effective aperture efficiency of 50%, the received signal characteristics at the antenna output would be one-half those listed above; in particular, the sun temperature would be 2,350°K.

For a radiometric receiver operating in a superheterodyne mode without image rejection, the values noted above would be further reduced by another factor of two (if we wish to compare the required sensitivity with that obtained by radiometer systems in 1966, near the frequency of operation).

From this analysis, the input signal to the radiometer when converted to an IF frequency should provide a temperature difference of 22.5°K between the sun level and the observed level in a 50 MHz band centered on the line. The difference temperature between 50 MHz and 10 MHz filters centered on the line should be 12.5°K.

Assuming that the rms sensitivity of the radiometer should be one-tenth the anticipated signal level to qualify for detection, and further that a reasonable integration time is 80 seconds, then:

(a) The rms sensitivity, $\overline{\Delta T_N}$, in a 10 MHz band should be 1.25°K.

(b) The rms sensitivity in the 50 MHz band should be 2.25°K.

The reported state-of-the-art in 1966, based on radiometer performance obtained at 95 GHz at the Aerospace Corporation, was 1.5°K rms for a post detection integration time constant of 1 second with a "bandwidth" of 1 GHz. The conversion of this reported sensitivity to other bandwidths and integration time constants is shown in Table 2-1.

TABLE 2-1

STATE OF THE ART IN 1966 AT 95 GHz

$\Delta\nu$ (MHz)	Time Constant(s)	$\overline{\Delta T_N}$(°K)	Remarks
1000	1	1.5	Aerospace Corp.
10	1	15	
10	80	1.7	1.25°K required
50	80	0.75	2.25°K required
10	20	3.4	

From Table 2-1, it is apparent that the requirement for detection is not quite met by the anticipated sensitivity in a 10 MHz band; however, it is easily met by the anticipated sensitivity in the 50 MHz band.

Initial Approach

The design of the system for the initial detection was based on the above analysis. The frequency response was provided by seven filters, as shown in Figure 2-12.

(a) Five contiguous filters, each with a bandwidth of 10 MHz.

(b) A 50 MHz filter covering the entire band of the five contiguous filters.

(c) A 2 GHz filter to provide a broad band response to the sun temperature level.

Detection was predicated on comparison of the 50 MHz response to the 2 GHz response. It was anticipated that a comparison of the central 10 MHz filter response with the

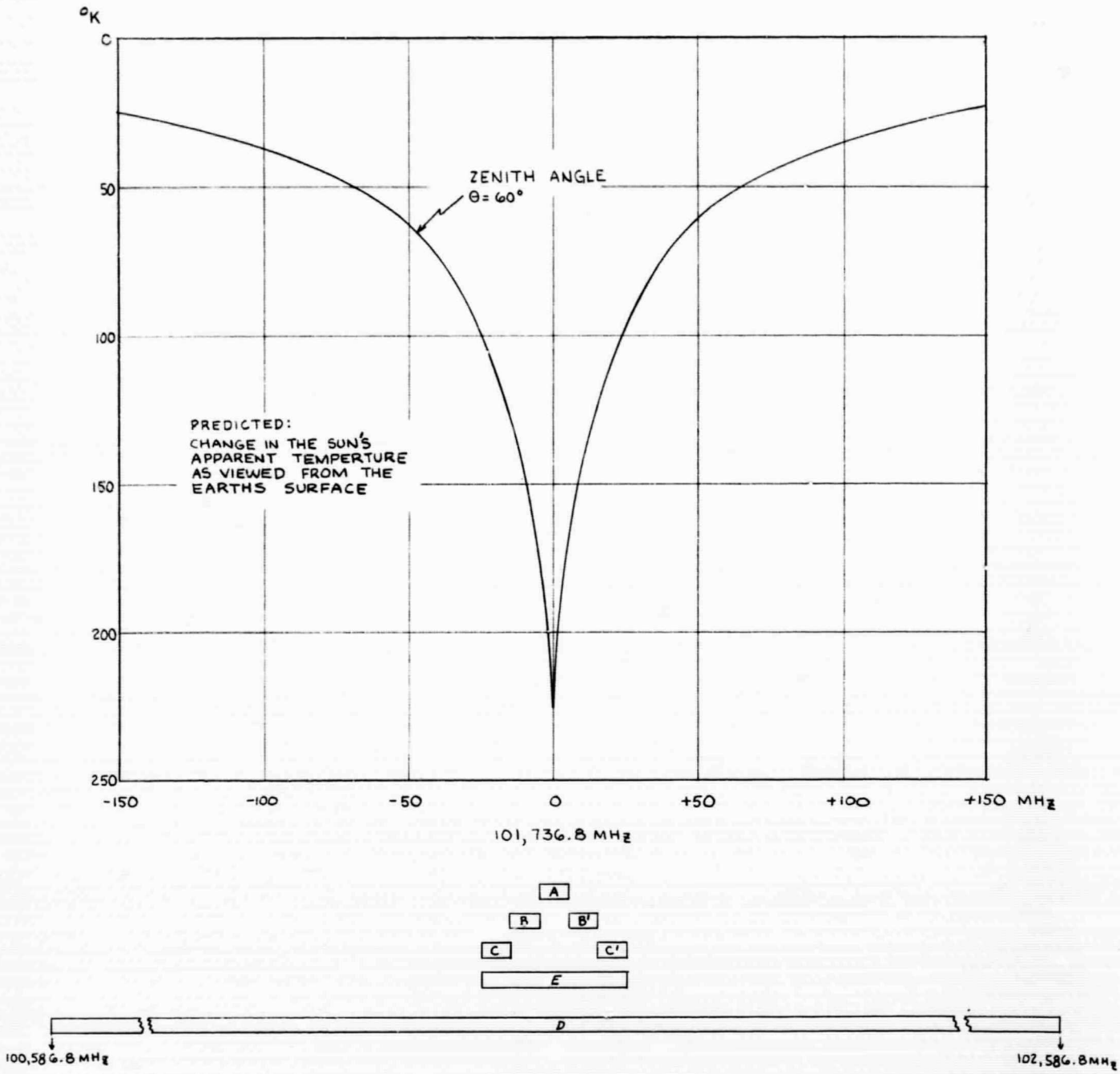

MULTI-CHANNEL FREQUENCY RESPONSE
EARTH BASED ATMOSPHERIC OZONE MEASUREMENT INSTRUMENT
(INITIAL APPROACH)

FIGURE 2-12

50 MHz response would represent a borderline detection; however, lack of detailed knowledge concerning atmospheric ozone concentration in the mesosphere suggested that this narrower band comparison be attempted.

The performance specifications for the earth based measurement instrument were based on this analysis of performance requirements. The measurement instrument consists of an antenna and multi-channel radiometric receiver. The significant performance specifications for these two subsystems derivable directly from the measuremenr requirements, as described above, are:

For the antenna:

(a) The antenna temperature of the sun measured at the output of the antenna should be a minimum of 2,000°K at a zenith angle of 60° under clear weather conditions, typical of a standard atmosphere.

(b) The antenna should be capable of tracking the sun for a minimum period of 30 minutes, during which the reduction in the observed sun antenna temperature under clear weather conditions, due to mechanical mis-alignment of the antenna structure, should not be greater than 10% of the peak value.

(c) Mechanical effects due to changes in the antenna structure, and in particular, the motion of the feed relative to the reflector during normal operation should not induce a differential frequency response across the observing band greater than the rms fluctuation level.

For the receiver:

(a) Provision should be included for setting, measuring, and monitoring the frequency of the first local oscillator (free-running klystron), in order to determine the central frequency response of all channels to within $\pm$ 0.5 MHz.

(b) The base line zero stability for all channels should be such that the maximum change in the output of any channel from the pre-set zero value should not exceed 1° Kelvin in a period of 30 minutes when the signal and comparison ports of the radiometer are terminated in gas discharge noise sources with their effective noise inputs adjusted to the nominal value of the sun antenna temperature.

(c) With a post detection integration time no greater than 80 seconds, the minimum detectable signal sensitivity in a channel bandwidth of 10 MHz should, at minimum, be equivalent to an input noise (signal) change of 1.5°K rms.

(d) The gain of all channels during any 30-minute observing period should not change by more than 2%.

(e) The receiver should include circuitry which automatically discriminates against broadband noise changes of up to $\pm$ 100°K in such a manner that the zero base line value of any and all channels, as measured at the output recorder, will be re-adjusted to its pre-set value within a period of 5 seconds. This automatic zero adjustment should be better than 1° Kelvin over the full dynamic range of a $\pm$ 100°K unbalance to discriminate against the passage of fair weather clouds through the antenna beam.

(f) A separate output should be provided to allow continuous recording of the sun antenna temperature during normal operation.

A functional block diagram of the multi-channel earth based measurement instrument in its initial configuration is shown in Figure 2-13. The dual conversion superheterodyne translation of the input signal frequencies to their corresponding first and second intermediate frequencies is shown in Figure 2-14. Photographs of the antenna subsystem and the operator control console in the initial system configuration are shown in Figures 2-15 and 2-16.

The system design included, as an integral part, all of the calibration and monitoring circuitry required to measure and evaluate all critical performance characteristics. The measured performance characteristics were as follows:

For the antenna:

(a) The antenna temperature of the sun referred to the antenna output terminal is 2,200°K, $\pm$ 200°K, at a nominal zenith angle of 60° under clear weather conditions.

(b) When the antenna main beam is boresighted on the sun and the mount control placed in an automatic track mode, the maximum observed reduction in the peak value during a 30-minute period is less than $\overline{\Delta T}_N$ (rms).

(c) Mechanical effects due to changes in the antenna structure are not detectable within the rms fluctuation level. The evaluation of this system performance parameter was made after absorbing material was introduced in the antenna structure. (See Addenda C).

For the receiver:

(a) Provision for setting, measuring, and monitoring the frequency of the first local oscillator is included as a part of the system. The accuracy of measurement is determined

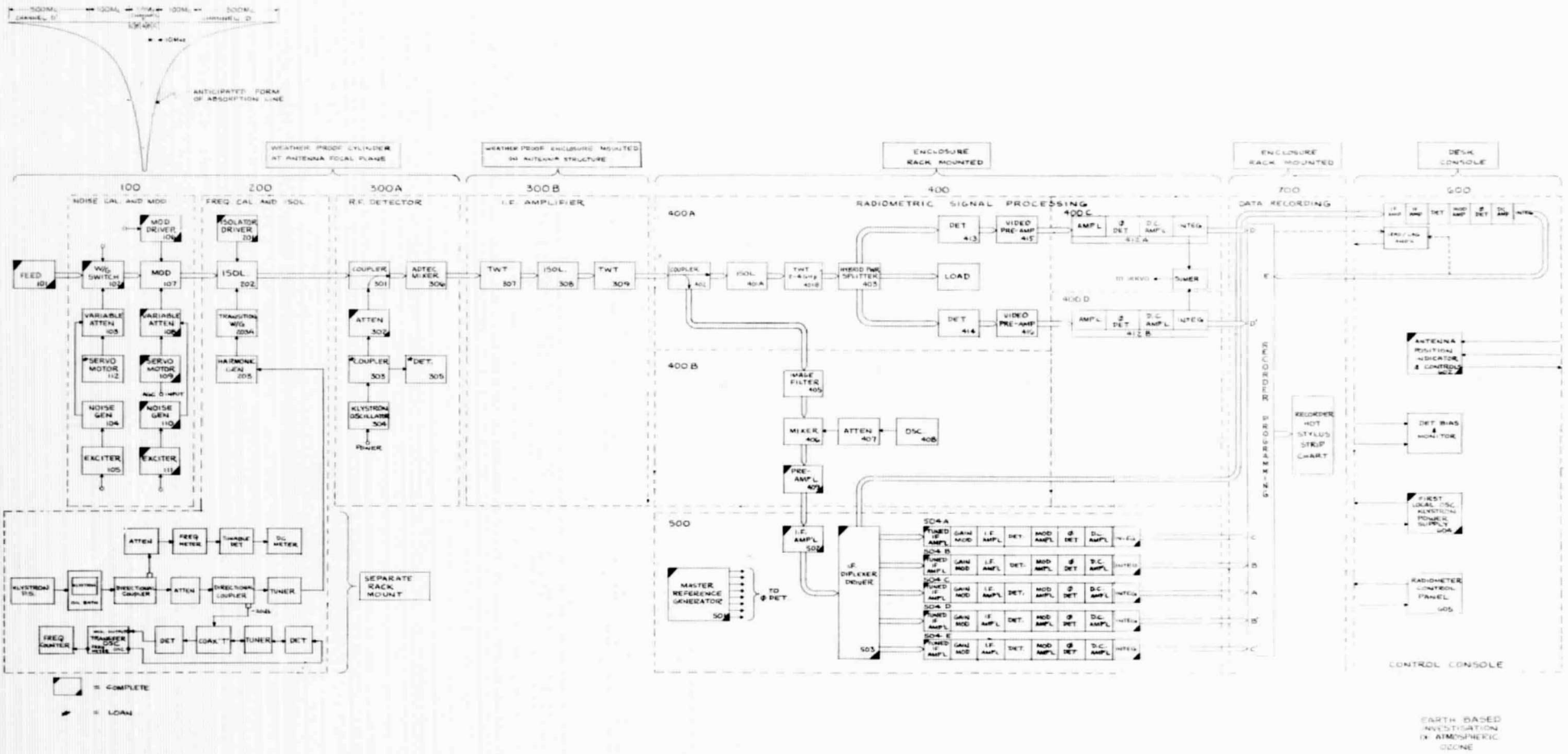

BLOCK DIAGRAM -- MULTI-CHANNEL EARTH BASED ATMOSPHERIC MEASUREMENT INSTRUMENT
(INITIAL APPROACH)
FIGURE 2-13

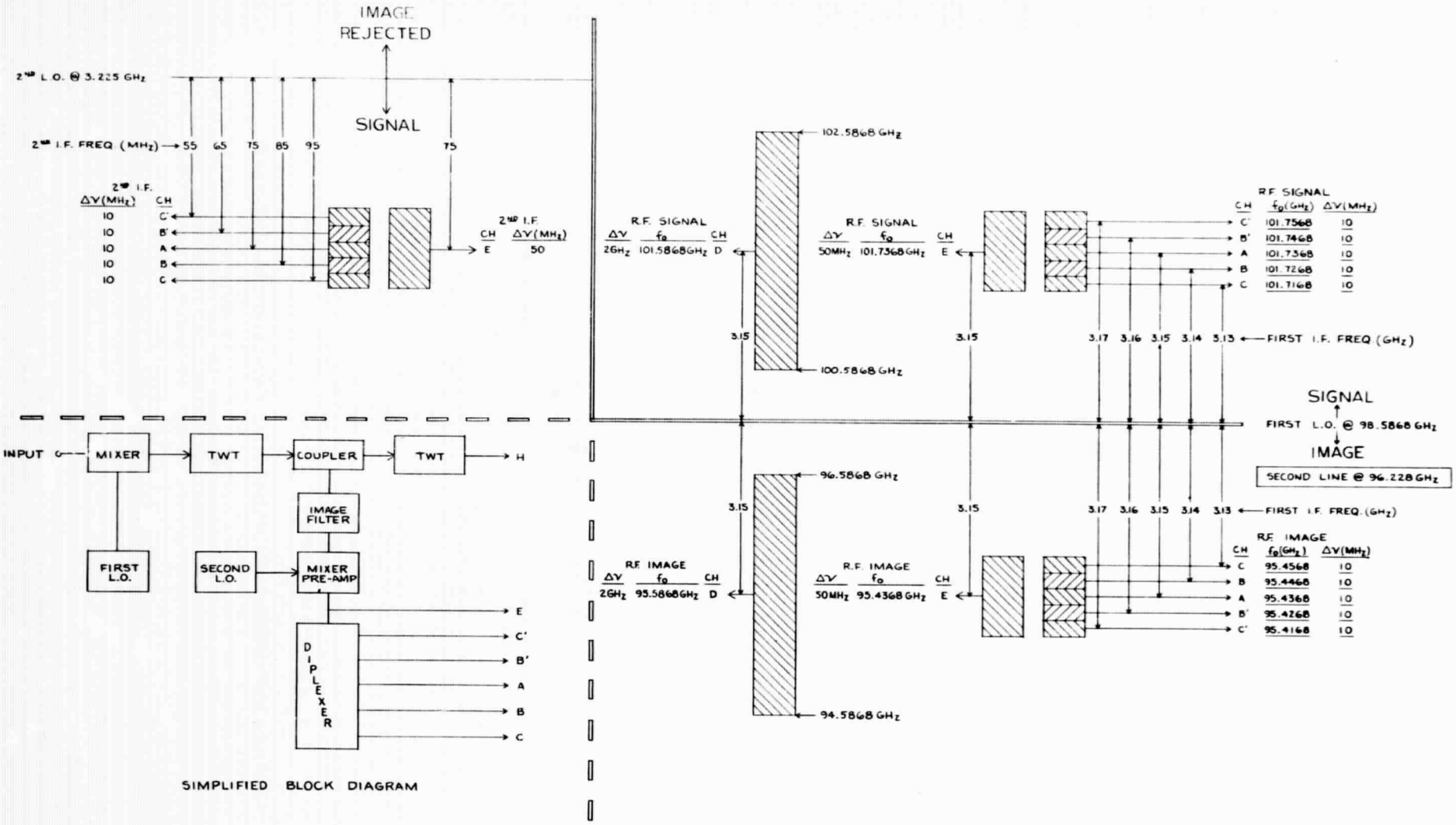

FREQUENCY RESPONSE

EARTH BASED OZONE SENSOR
(INITIAL APPROACH)

FIGURE 2-14

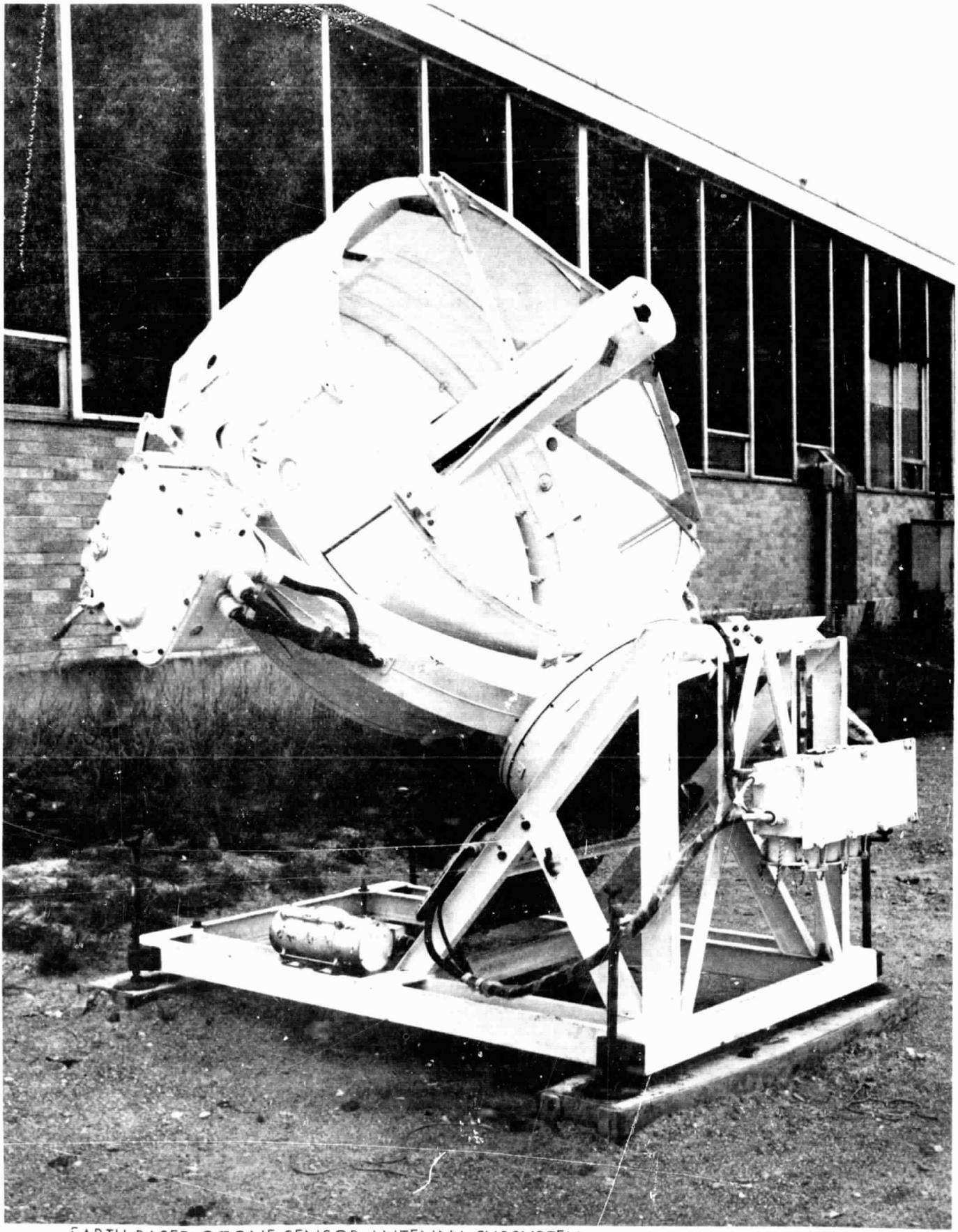

EARTH BASED OZONE SENSOR ANTENNA SUBSYSTEM (INITIAL APPROACH)

A266

FIGURE 2-15

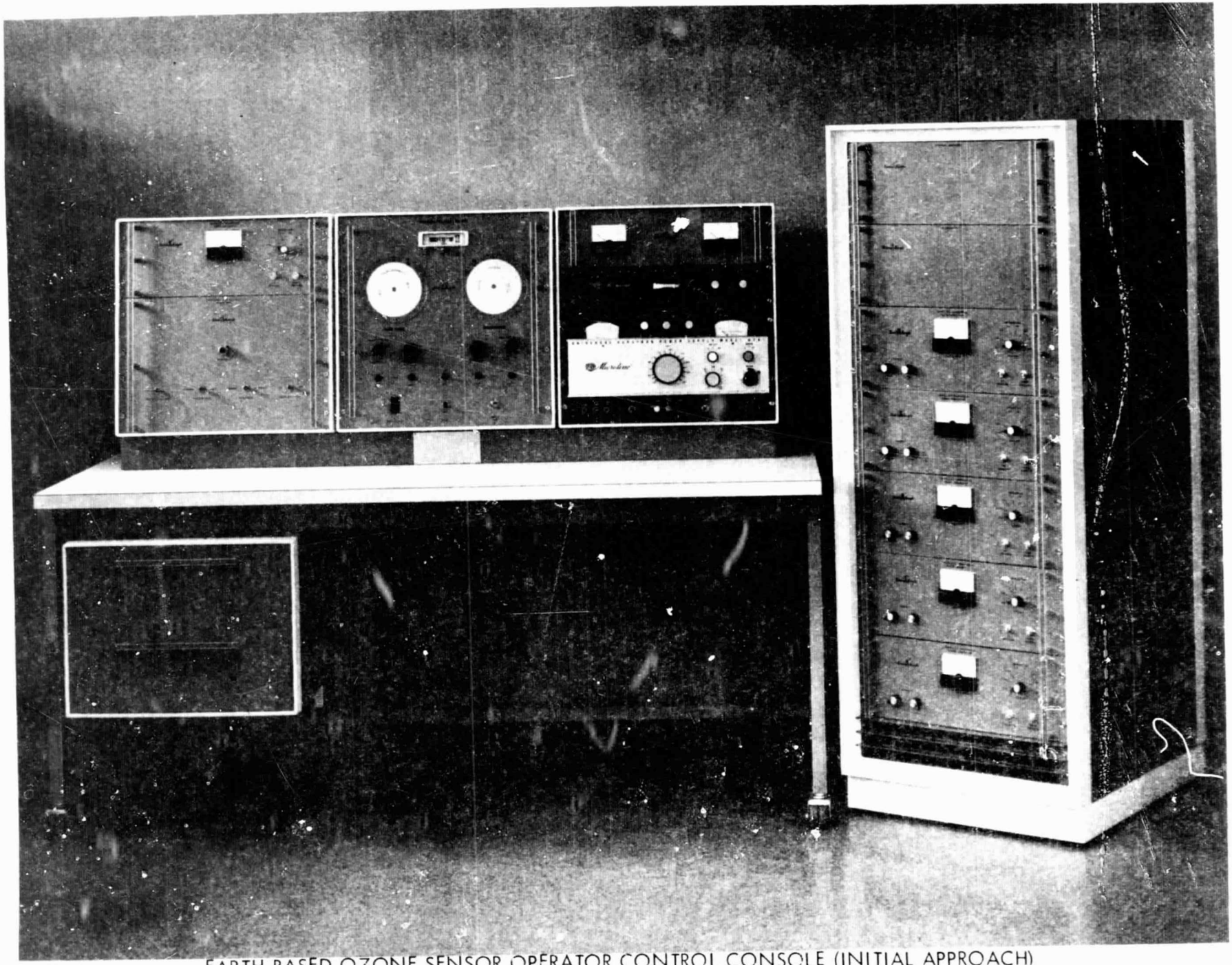

EARTH BASED OZONE SENSOR OPERATOR CONTROL CONSOLE (INITIAL APPROACH)

A265

by the frequency stability of the oscillator which, of course, varies from tube to tube. The inherent accuracy of the frequency measurement technique, however, is $\pm$ 1 MHz.

(b) The base line stability of the system is 1°K (maximum) for 30 minutes with the input terminated at the normal value of the sun antenna temperature.

(c) The sensitivity of the system for a channel bandwidth of 10 MHz is 2.0°K, $\pm$ 0.15°K rms, with a post detection integration time constant of 20 seconds.

(d) The gain stability of all channels during an arbitrary 30-minute observing period was measured to be within $\pm$ 1.25%.

(e) With the signal and comparison input ports terminated in gas discharge noise sources, at an effective input temperature (referenced to the input ports) adjusted to the typically observed value of the sun antenna temperature, variations of $\pm$ 100°K introduced at the signal port are effectively discriminated against by the action of the internal noise feedback servo loop. The loop time constant is 5 seconds. There is no detectable change in the output record of the various signal channels for a differential $\pm$ 100°K impulse function, typically induced by clouds passing through the main antenna beam.

(f) An output recording of the sun antenna temperature is provided for continuous strip chart recording. This

signal is derived from a calibrated potentiometer coupled to the shaft of the servo motor contained within the noise feedback servo loop.

Modifications Introduced after Ozone Detection

The frequency response of the earth based measurement instrument, in its initial configuration, was predicated on a design approach that would optimize the possibility of detection. Only a small segment of the line profile in the vicinity of the line center frequency was included in the frequency response. Following the detection of the line, which also verified the ability to measure the line profile shape, the frequency response of the instrument was extended to provide a more comprehensive view of the profile. In the initial approach, the profile resolution was confined to a 50 MHz band centered on the line frequency, as shown in Figure 2-12. In the modified form, the bandwidth was extended to 170 MHz centered on the line frequency. This was accomplished by introducing three filters on either side of the original 50 MHz band. Three narrow band contiguous filter channels, each 3.3 MHz wide, were also introduced within the 10 MHz band centered on the line frequency. By driving the noise servo from the 170 MHz channel, which spans all of the contiguous filters, the differential temperature response, between this base band and the channels on and immediately adjacent to the line frequency, is enhanced by nearly a factor of two.

The narrow band channels (3.3 MHz) were introduced to obtain a measure of the peak response of the absorption profile associated with ozone concentration in the upper atmosphere (approaching the lower portions of the mesosphere). The design approach for these narrow band channels included provision for reduction of bandwidth to values as small as 0.5 MHz. The 3.3 MHz value was selected on the basis of the known frequency drift characteristics of the klystron local oscillator. The drift characteristics of the klystron used in this system varies from tube to tube; however, the best tube performance observed during the program showed frequency drifts of up to 3 MHz in a period of one to two hours. One solution to this problem is phase-locking of the klystron oscillator. The feasibility of implementing a phase-lock

circuit of the type required was investigated in November of 1968. Commercially available units required for this circuit were obtained on a loan basis. Laboratory tests verified the simplicity with which phase-locking could be achieved, using commercially available equipments. The phase-lock circuit was not implemented during the period of this investigation; however, this item is included in the recommended implementation plan for the satellite instrument, in that portion of the total effort which suggests supporting measurements be continued, using the Earth Based Instrument.

The addition of three filter channels on either side of the original 50 MHz channel and three contained within the 10 MHz channel response centered on the line frequency increased the total number of channels from the original seven to sixteen. The filter channel frequencies and bandwidths in their modified form referenced to the predicted ozone absorption profile that would be obtained at a zenith angle of observation of 60° is shown in Figure 2-17.

A functional block diagram of the multi-channel radiometer system in its modified form is shown in Figure 2-18. The conversion of the input signal frequencies by a dual heterodyning action to their corresponding first and second intermediate frequency filter bandwidths is shown in Figure 2-19.

During the final phase of the program effort, the Earth Based Measurement Instrument was relocated to an area that would provide improved horizon coverage for the antenna system and additional space for the operator control console. A photograph of the instrument in its modified form, after relocation, is shown in Figure 2-20.

2.4 Observational Data

The ozone resonant line at 101.7 GHz was first detected in December 1967. The measured line shape was in excellent agreement with that predicted by the computer program analysis performed by Dr. Caton. The intensity of the line, as measured in absorption, was slightly higher than anticipated. This was not considered particularly significant since yearly variations, and possibly even diurnal variations as great as a factor of 2 or 3, were anticipated. A comparison of the measured absorption profile with the predicted profile is shown in

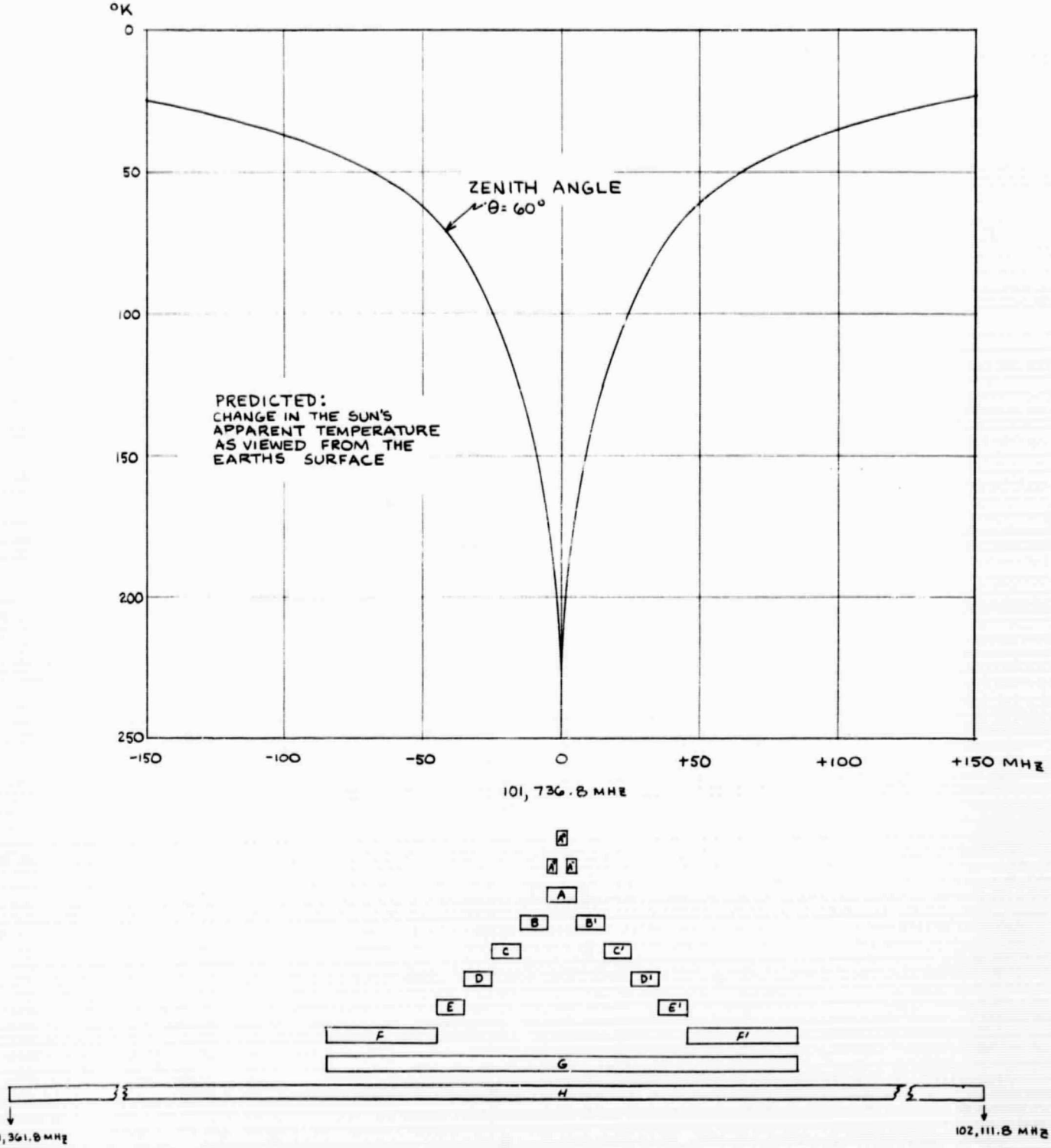

FIGURE 2-17

MULTI-CHANNEL FREQUENCY RESPONSE
EARTH BASED ATMOSPHERIC OZONE MEASUREMENT INSTRUMENT
(16 CHANNELS)

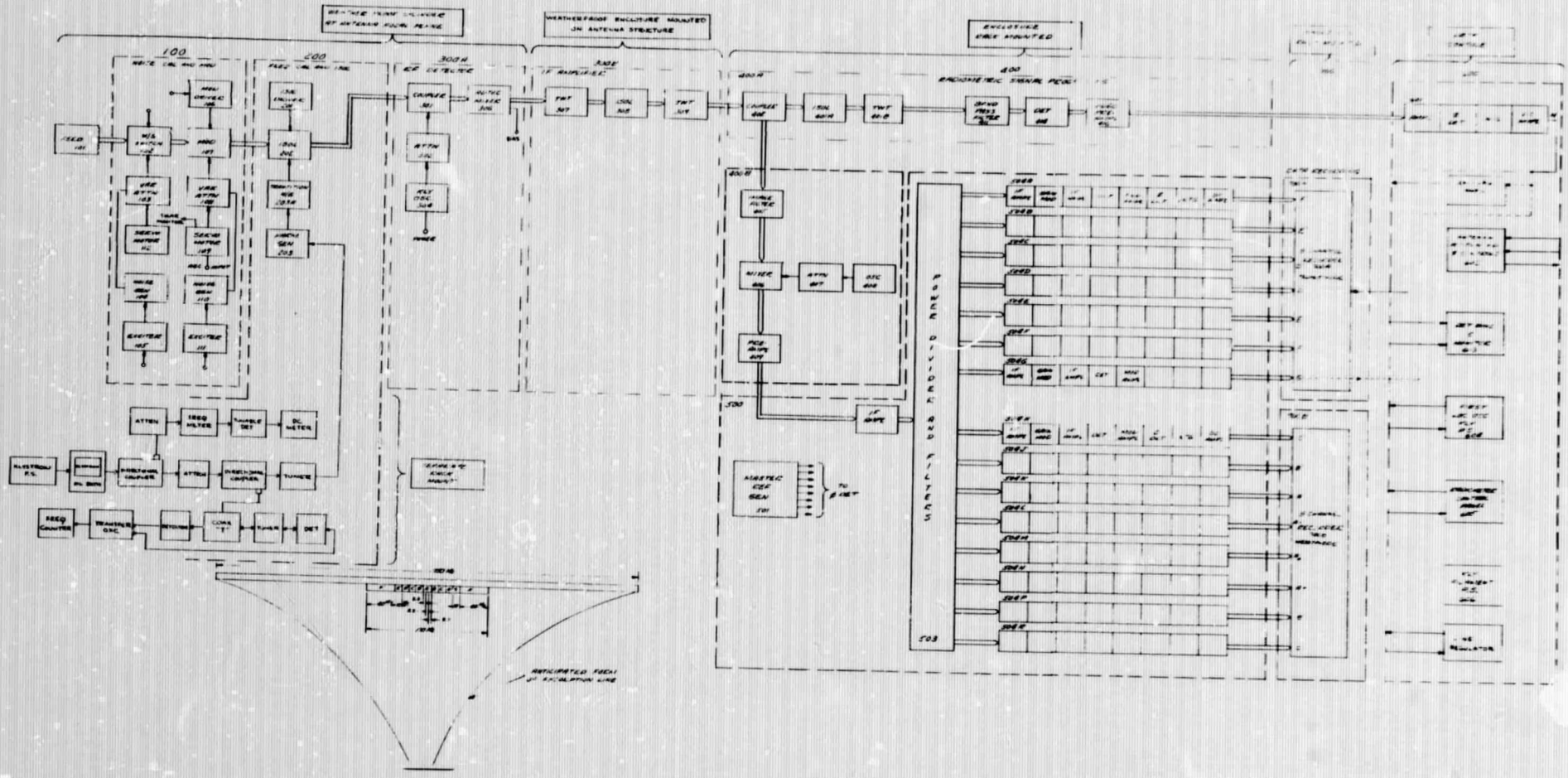

BLOCK DIAGRAM -- MULTI-CHANNEL EARTH BASED ATMOSPHERIC MEASUREMENT INSTRUMENT

(16 CHANNELS)

FIGURE 2-18

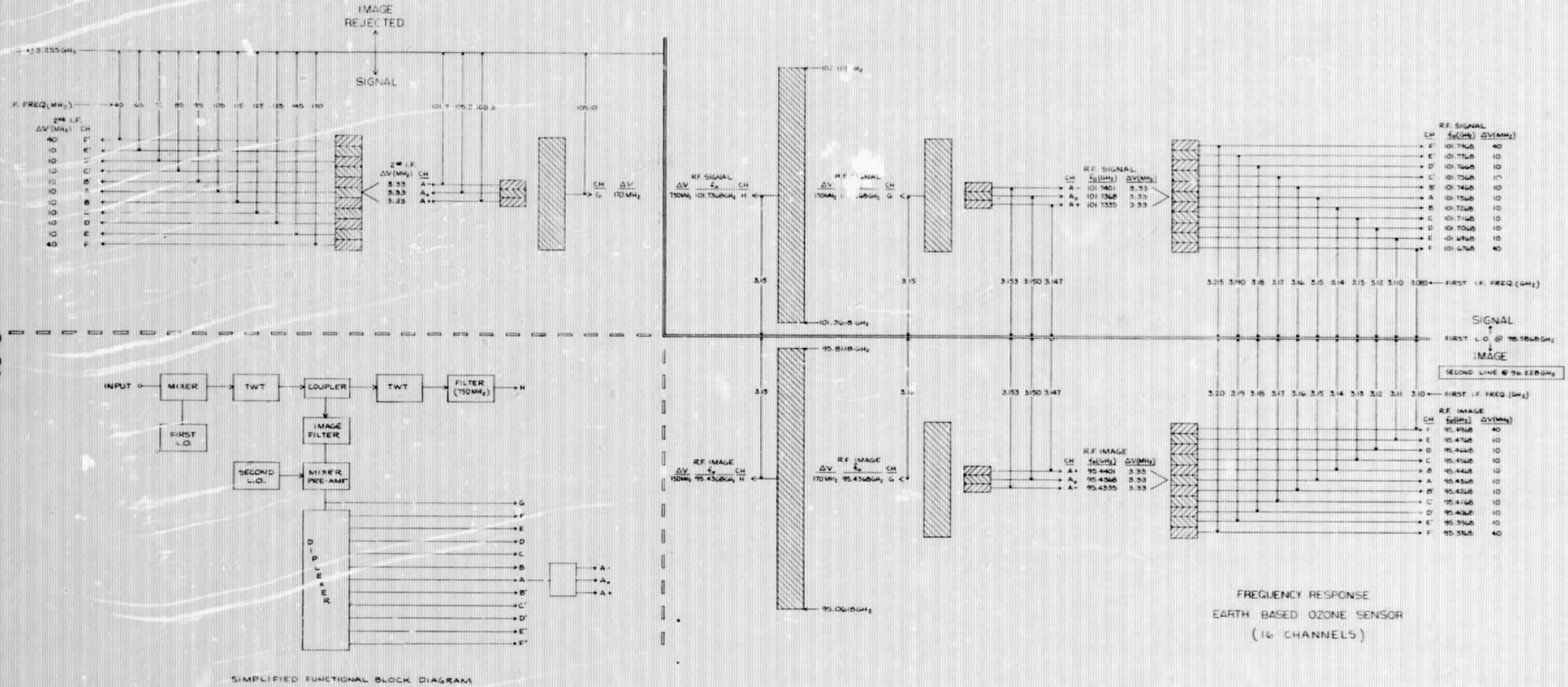
IMAGE REJECTED
SIGNAL
INPUT
MIXER
TWT
COUPLER
TWT
FILTER (750MHz)
FIRST L.O.
IMAGE FILTER
SECOND L.O.
MIXER PRE-AMP
DIPLEXER
SIMPLIFIED FUNCTIONAL BLOCK DIAGRAM
SIGNAL
IMAGE
FREQUENCY RESPONSE
EARTH BASED OZONE SENSOR
(16 CHANNELS)

FIGURE 2-19

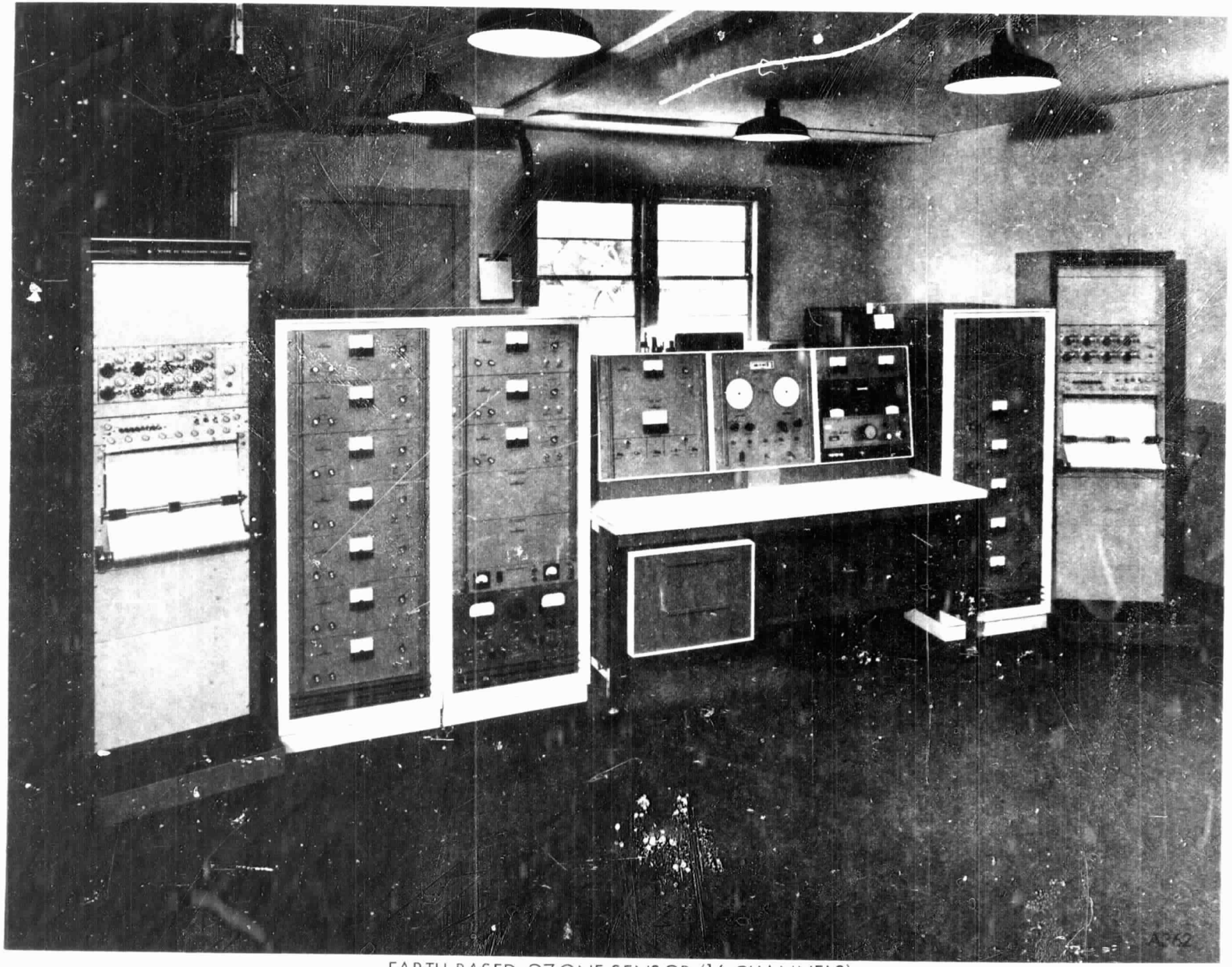

EARTH BASED OZONE SENSOR (16 CHANNELS)

Figure 2-21. These initial observations were the subject of a publication in the March 1969 issue of the Astrophysical Journal. A copy of this publication is included as Addenda B to this report.

The decision was made in January of 1968 to proceed with modification of the instrument to extend the frequency response to a total of 16 channels, as described in the prior section of this report. The assembly of the various units required nearly six months of design and assembly time. During this period, the Earth Based Measurement Instrument was operated in its initial configuration to accumulate observational data for further analysis. This data which was accumulated during the Spring of 1968 exhibited a systematic diurnal effect in the form of a "base line tilt." It appeared that the broadband background noise level would tilt in one direction during the period of morning observations, become essentially flat near noon, and then tilt in the opposite direction during afternoon observations. Attempts to explain this "base line tilt" effect, in terms of a natural atmospheric phenomena, were unfruitful. It was not until August of 1968 that this effect was isolated as an instrument effect and identified with the antenna. A discussion of this effect and its remedy is included as Addenda C to this report. As a consequence of this instrument induced distortion of the observational data obtained during the Spring of 1968, this data was not considered useful for reduction and inversion. Though the ozone line could easily be identified as super-imposed on this instrument effect, the magnitude of the latter precluded the usefulness of the data for inversion.

Analysis of the antenna effect and development of suitable corrective measures was accomplished during the three-month period from August through October of 1968. The instrument was inoperative from November 1968 through mid-February 1969, due to the unavailability of klystron first local oscillator tubes. Observational data was obtained during the thirty-day period from mid-February through mid-March 1969. This observing series was again terminated by a klystron tube failure. During this thirty-day observing period, however, excellent records of the atmospheric absorption profile were obtained. No diurnal

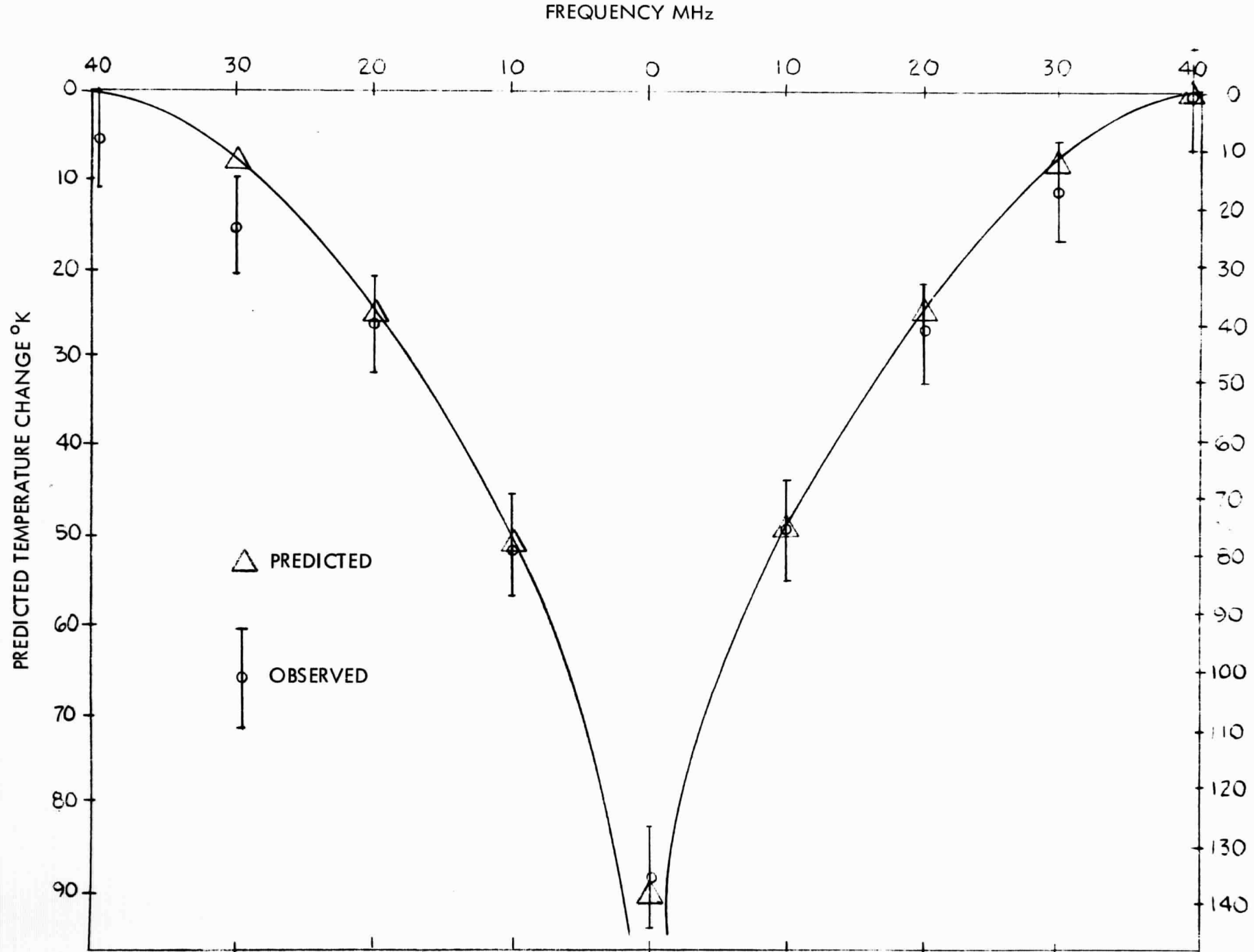

MEASURED VS PREDICTED OZONE PROFILE
FIGURE 2-21

base line tilt was observed, and the system performance evidenced considerable stability and reliability. This was the first opportunity that we had to observe the performance of the instrument in its modified form. A typical ozone profile data record obtained during this observing period is shown in Figure 2-22. The measured data points are shown in this Figure with reference to the computer predicted absorption profile. Comparison of the shape and intensity of the ozone absorption profile obtained during this observing period was that obtained at the time of the initial detection (Figure 2-22) shows again the marked similarity between the measured profile shape and the predicted shape. The intensity, however, as before was greater than predicted.

The klystron used during this thirty-day period of observation exhibited excessive frequency drift characteristics, in comparison with the performance of other tubes of this type previously used in the system. These frequency drift characteristics precluded the opportunity to extend the integration time to obtain a precise measure of the peak response of the narrow band (3.3 MHz) channels centered on the line frequency. Only on rare occasions was the klystron frequency stability adequate to provide a significant charge period for the output integrator. On these limited occasions, there was a pronounced enhancement (factor of 1.5) in the narrow band channel response. This series of observations definitely emphasized the observational data value of narrow band contiguous filters centered on the line frequency, with equal emphasis on the need for klystron phase-locking to make these channels useful.

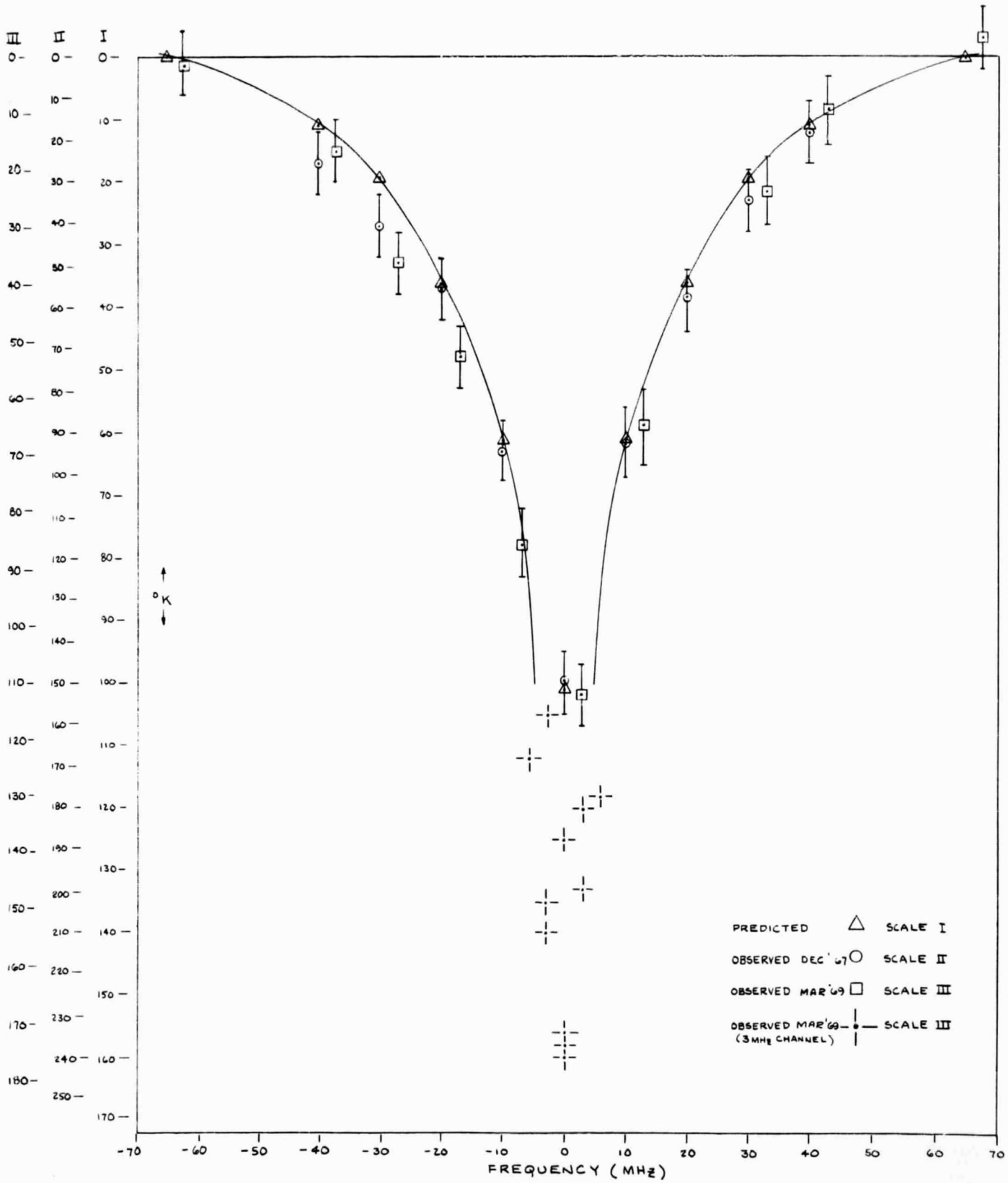

FIGURE 2-22

PREDICTED AND MEASURED ATMOSPHERIC OZONE PROFILES
ABSORPTION SPECTRUM AT 101.7 GHZ

The recommended implementation plan prepared in support of the satellite instrument design approach was completed in November of 1968. An abstract of the key features of this planning document is included in Section 3.4.

3.1 Analysis of Instrument Requirements and the Experiment Approach

The derivation of instrument requirements will be aided by a brief review of the methods that will be used in the analysis of the data obtained from orbit, to determine the percentage of ozone concentration relative to the total air content at various altitudes. Certain disciplinary relationships are significant since there is a common use of terminology in the concept of "weighting functions." The proposed method for analysis of ozone data provides a simplification in measurement instrument requirements in the sense that an absolute temperature measurement is not required at a single frequency in order to deduce the ozone concentration. The difference temperature between measurements made at two frequencies is used to infer the concentration in an atmospheric layer. A precise measure of the temperature difference between the two frequencies is required; however, the absolute value of either is not required. The relationship between the ozone absorption coefficient α and significant variable parameters may be expressed in the form:

$$\alpha(\nu) \propto T^{-5/2} \frac{N_{O3}}{\Delta\nu} \left[\frac{(\Delta\nu)^2}{(\nu-\nu_0)^2 + (\Delta\nu)^2}\right] \qquad (3\text{-}1)$$

where N_{O3} is the ozone concentration, $\Delta\nu$ is the line half-width, ν is the frequency of observation, and ν_0 the line frequency. The line width is proportional to pressure which is in turn proportional to the product of the total number of air molecules N_T and a temperature term $T_{EXP}^{-(5/2+\beta)}$, where β is in the range 0.5 to 1.0. The absorption coefficient can, therefore, be rewritten in the form:

$$\alpha(\nu) = DT^{-(5/2+\beta)} \frac{N_{O3}}{N_T} \left[\frac{(\Delta\nu)^2}{(\nu-\nu_0)^2 + (\Delta\nu)^2}\right] \qquad (3\text{-}2)$$

The constant of proportionality D includes molecular constants and geometrical factors associated with the path of observation through the atmosphere. The term in brackets is defined as a "single frequency weighting function", W_ν. We now define a "difference weighting function", $W_{\nu_1 - \nu_2}$ in the form:

$$W_{\nu_1 - \nu_2} = \beta \left[\frac{(\Delta\nu)^2}{(\nu_1 - \nu_0)^2 + (\Delta\nu)^2} - \frac{(\Delta\nu)^2}{(\nu_2 - \nu_0)^2 + (\Delta\nu)^2} \right] \qquad (3\text{-}3)$$

where β is a constant which normalizes the difference frequency weighting function to unity. Inspection of Equation 3-3 indicates that the maximum value of $W_{\nu_1 - \nu_2}$ occurs when:

$$(\nu_1 - \nu_0)(\nu_2 - \nu_0) = (\Delta\nu)^2 \qquad (3\text{-}4)$$

Since the observed brightness temperature at any single frequency of observation is proportional to the integration of the absorption coefficient along the path through the atmosphere, the ozone concentration can be derived from a difference temperature measurement at two frequencies which define the altitude limits of the observed layer. A graphical plot of six single frequency weighting functions is shown in Figure 3-1 (a). The corresponding difference weighting functions are shown in Figure 3-1 (b). The three difference weighting functions shown in solid lines are obtained from the differences of the paired sets of the four single frequency weighting functions, also shown in solid lines in Figure 3-1 (a).

The single frequency weighting functions at 2 and 20 MHz (shown dotted) which combine to form the difference frequency weighting function at 6.3 MHz (dotted) show the degree to which difference frequency weighting functions at 2, 6.3, and 20 MHz tend to overlap and thereby provide inter-dependent samples of the atmosphere. The development of the weighting functions in Figure 3-1 (solid lines) is predicated on the dual use of data obtained at intermediate observing frequencies; i.e., observational data obtained at 6.3 MHz would be used for both the upper and middle weighting functions, and at 63 MHz

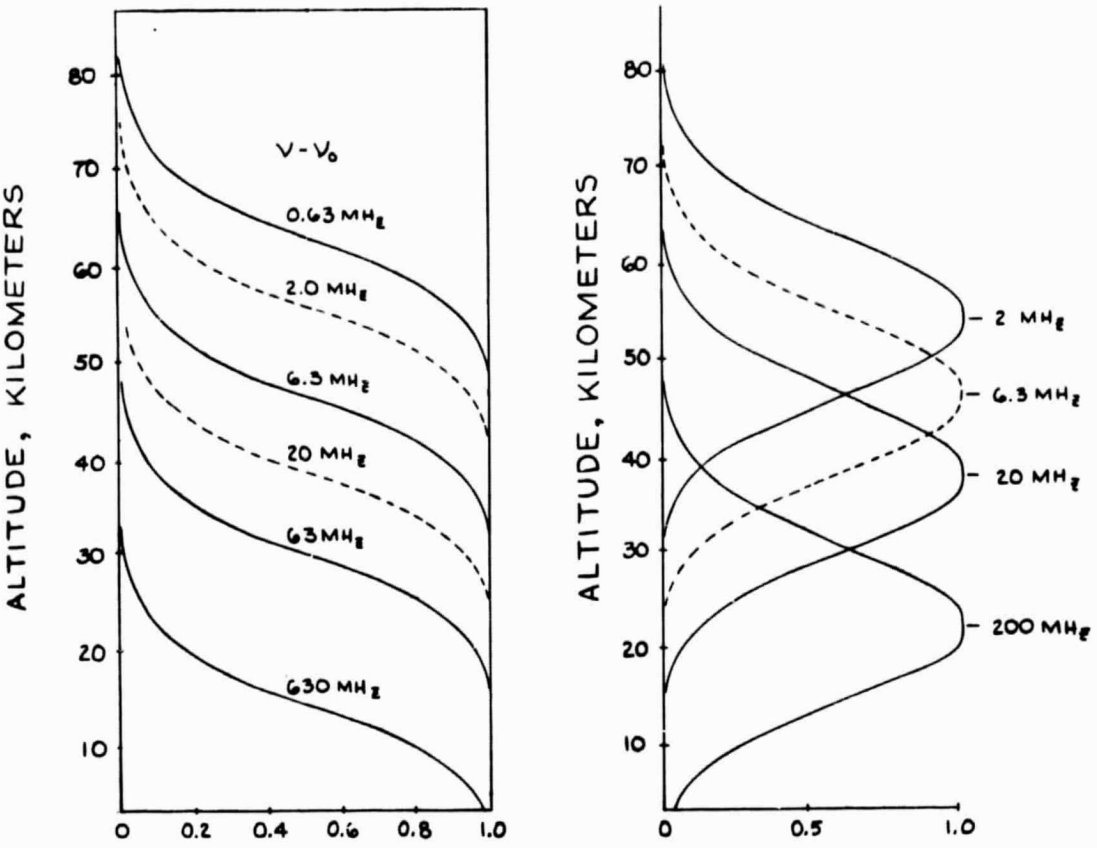

(a) NORMALIZED SINGLE FREQUENCY WEIGHTING FUNCTIONS W_V vs FREQUENCY DISPLACEMENT FROM THE LINE FREQUENCY

(b) NORMALIZED DIFFERENCE FREQUENCY WEIGHTING FUNCTIONS $W_{V_1 - V_2}$ vs FREQUENCY AND ALTITUDE.

WEIGHTING FUNCTIONS OF ATMOSPHERIC OZONE

FIGURE 3-1

for both the middle and lower difference frequency weighting functions.

The natural limit in the difference weighting function half-width is not immediately apparent from the example of atmospheric ozone weighting functions shown in Figure 3-1. The natural limit is shown graphically in Figure 3-2. Recalling that the observed temperature at any frequency of observation is proportional to the integral of the absorption coefficient over the ray path of observation, a factor C (h), representing all terms in the integrand other than those in the weighting function, takes the typical form shown in Figure 3-2 (a) for standard ARDC model atmospheric temperatures and pressures, and for values of atmospheric ozone concentration as calculated by Hunt*. The form of C (h) is primarily determined by the factors outside the bracket in Equation 3-1. From Equation 3-3, it is apparent that the width of the weighting function $W_{\nu_1-\nu_2}$ is determined by the ratio $(\nu_1-\nu_0)/(\nu_2-\nu_0)$. The width of $W_{\nu_1-\nu_2}$ is constant for constant values of this ratio. A plot of this ratio versus the width of the difference frequency weighting function decreases to a minimum of about 14.5 km as the difference $(\nu_2-\nu_1)$ decreases to zero. This indicates that as the two frequencies of observation required to define a difference frequency weighting function approach the corresponding "frequency of the weighting function", the minimum half-width of the weighting function becomes 14.5 km. The minimum width of the difference frequency weighting functions for useful data can also be seen directly if one plots the value of the factor B in Equation 3-3 as a function of the width of the difference frequency weighting function, since this normalizing factor is directly indicative of the energy contained under the area of the weighting function when plotted as a function of altitude and amplitude. The graph of B versus the width of $W_{\nu_1-\nu_2}$ is shown in Figure 3-2 (c). It is evident

---

* Hunt, B.G., 1966: "Photochemistry of Ozone in a Moist Atmosphere," J. Geophys. Res., 71, 1385.

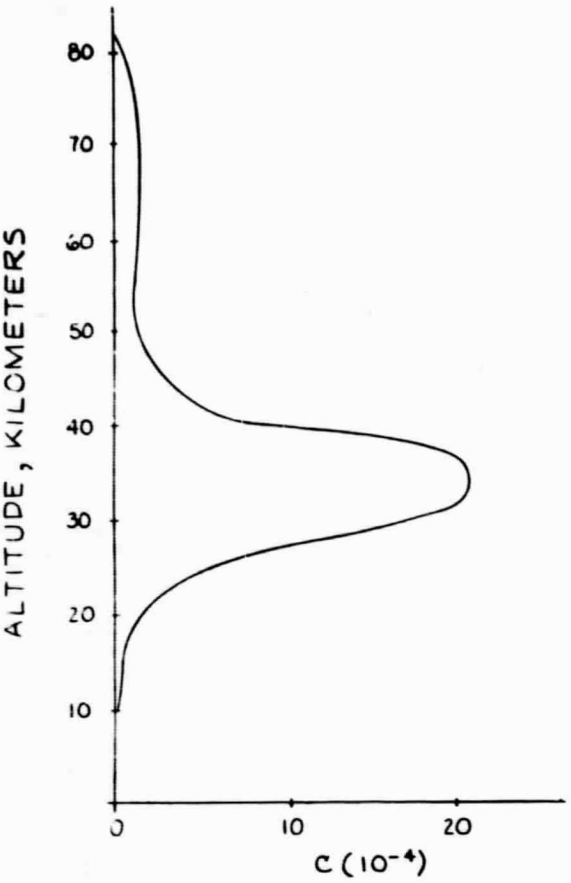

(a) C(h) vs HEIGHT (h) IN KM FOR STANDARD ARDC MODEL ATMOSPHERE AND O_3 CONCENTRATION AFTER HUNT( )

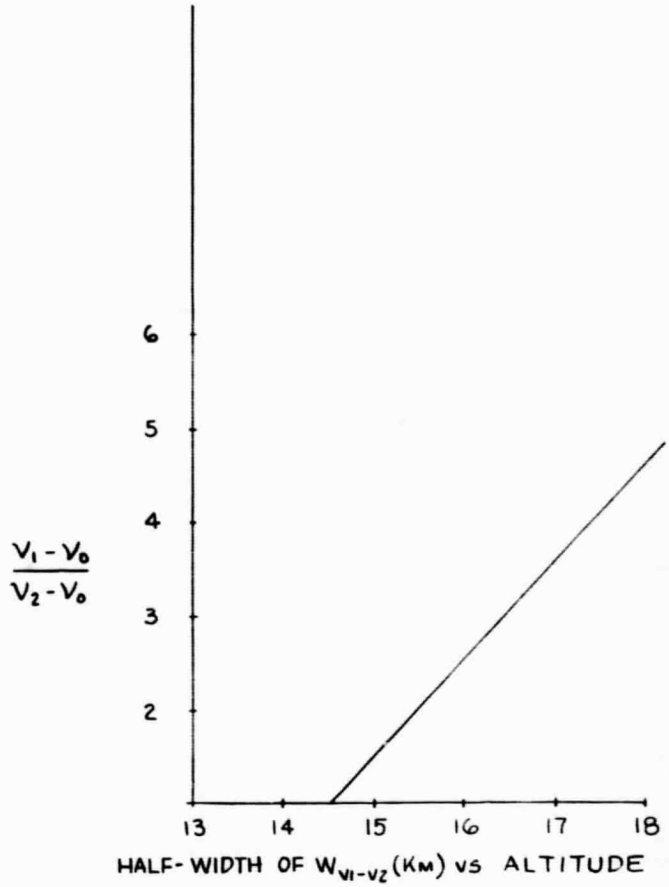

(b) WIDTH OF DIFFERENCE FREQUENCY OZONE WEIGHTING FUNCTION VS $(V_1 - V_0)/(V_2 - V_0)$

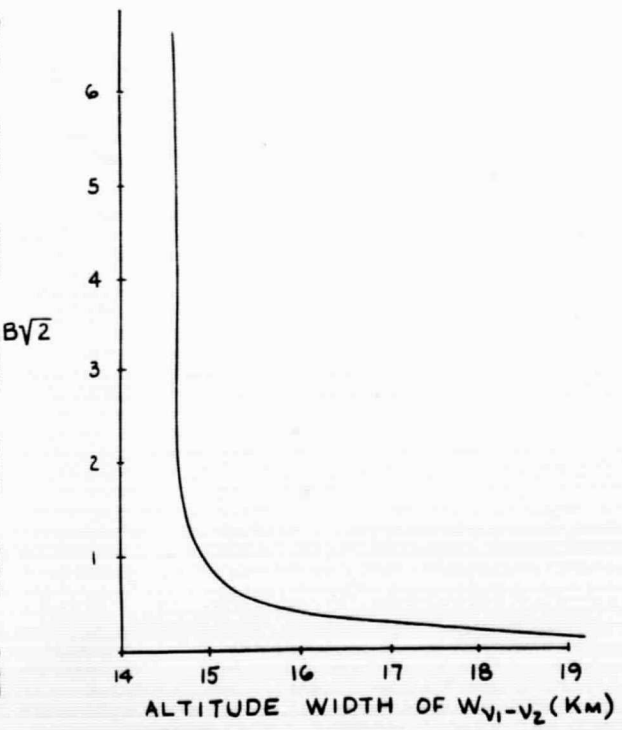

(c) NORMALIZING FACTOR B vs WIDTH OF THE DIFFERENCE FREQUENCY WEIGHTING FUNCTION W_{V1-V2}

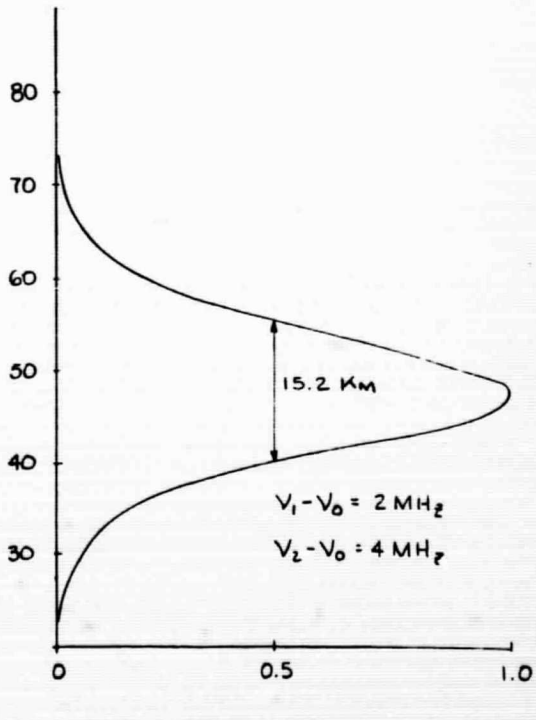

(d) WEIGHTING FUNCTION $W_{V_1-V_2}$ VS ALTITUDE (WHERE $2V_0$ = LINE WIDTH DETERMINED BY THE ATMOSPHERIC PRESSURE AT THE ALTITUDE OF THE PEAK RESPONSE)

HALF WIDTH LIMITS
OZONE DIFFERENCE FREQUENCY WEIGHTING FUNCTIONS
FIGURE 3-2

from this graph that the minimum usable width of a difference frequency weighting function is approximately 15 km. A graph of a difference frequency weighting function near this optimum width of 15 km is shown in Figure 3-2 (d). The corresponding frequencies of observation for the single-frequency weighting functions are displaced from the line frequency by 2 and 4 MHz, respectively. Comparison of the shape and width of this weighting function (Figure 3-2(d)) with the weighting function shown graphically by the dotted line in Figure 3-1 (b) indicates that a weighting function developed from observing frequencies displaced 2 MHz and 20 MHz from the line frequency provides nearly the same definition of the atmospheric layer as that provided by the combination of 2 MHz and 4 MHz measurements. This tends to suggest the value of using intermediate frequencies of observation to perform a dual role in the derivation of ozone concentration for adjacent weighting functions.

The experiment approach and associated ozone sensor performance characteristics are based on the foregoing analysis.

The ozone sensor would view the horizon continuously with a nominal one angular degree resolution. The boresight axis of the antenna power pattern would be stabilized along a line tangent, to a 35 km altitude, above the earth's surface. Stabilization of the antenna boresight would be provided by a molecular atmospheric oxygen horizon sensor included as part of the measurement instrument. Stabilization capability should be at least 15 arc minutes.

The instrument will measure the thermal radiation at 8 wavelengths in four paired sets displaced about the ozone resonant line frequency of 101.7 GHz. The observing frequencies and corresponding weighting function altitudes are given in Table 3-1. The observed temperature difference between adjacent paired sets at these frequencies provides a measure of the ozone concentration in three atmospheric layers defined by the corresponding "difference frequency" weighting functions. The altitude profiles of these weighting

functions were previously described and graphically shown in Figure 3-1 (b).

TABLE 3-1
FREQUENCIES OF OBSERVATION

Frequency MHz	Weighting Function Peak Height h_o (km)
101,737. $\pm$ 0.63	50
101,737. $\pm$ 6.3	33
101,737. $\pm$ 63	18
101,737. $\pm$ 630	

By observing in the horizon direction, the effects of telluric radiation from the surface are negligible. The emission profile of the 101.7 GHz line resonance, as viewed from a 600 nautical mile orbit by a nominal one arc degree antenna power pattern pointing toward the horizon, is shown in Figure 3-3. The frequencies of observation occur as paired sets as a consequence of the superheterodyne mode of operation. The local oscillator is tuned to the center frequency of the line. The observed brightness temperature difference between adjacent "paired signals" is represented in the form of an integral along the path through the atmosphere, determined by the antenna power pattern and the geometry along the direction of observation. The integrand includes the product of the temperature dependent term $\left(T_{EXP}^{-(5/2+\beta)}\right)$ and the ozone mixing ratio (N_{O_3}/N_T) weighted by the altitude profile of the corresponding difference frequency weighting function which selects the atmospheric layer under observation by spatial filtering in the frequency domain.

The four signal outputs from the ozone sensor would be sampled every second and recorded for later telemetry to ground. The telemetered data, including vehicle orbit characteristics on a common time-base with the signal data, would be transferred to digital magnetic tapes. The data obtained on the magnetic tapes would then be transformed into records of brightness temperature at each observing frequency as a function of time and

PREDICTED 101.7 GHz OZONE EMISSION PROFILE

AS VIEWED FROM NIMBUS ORBIT

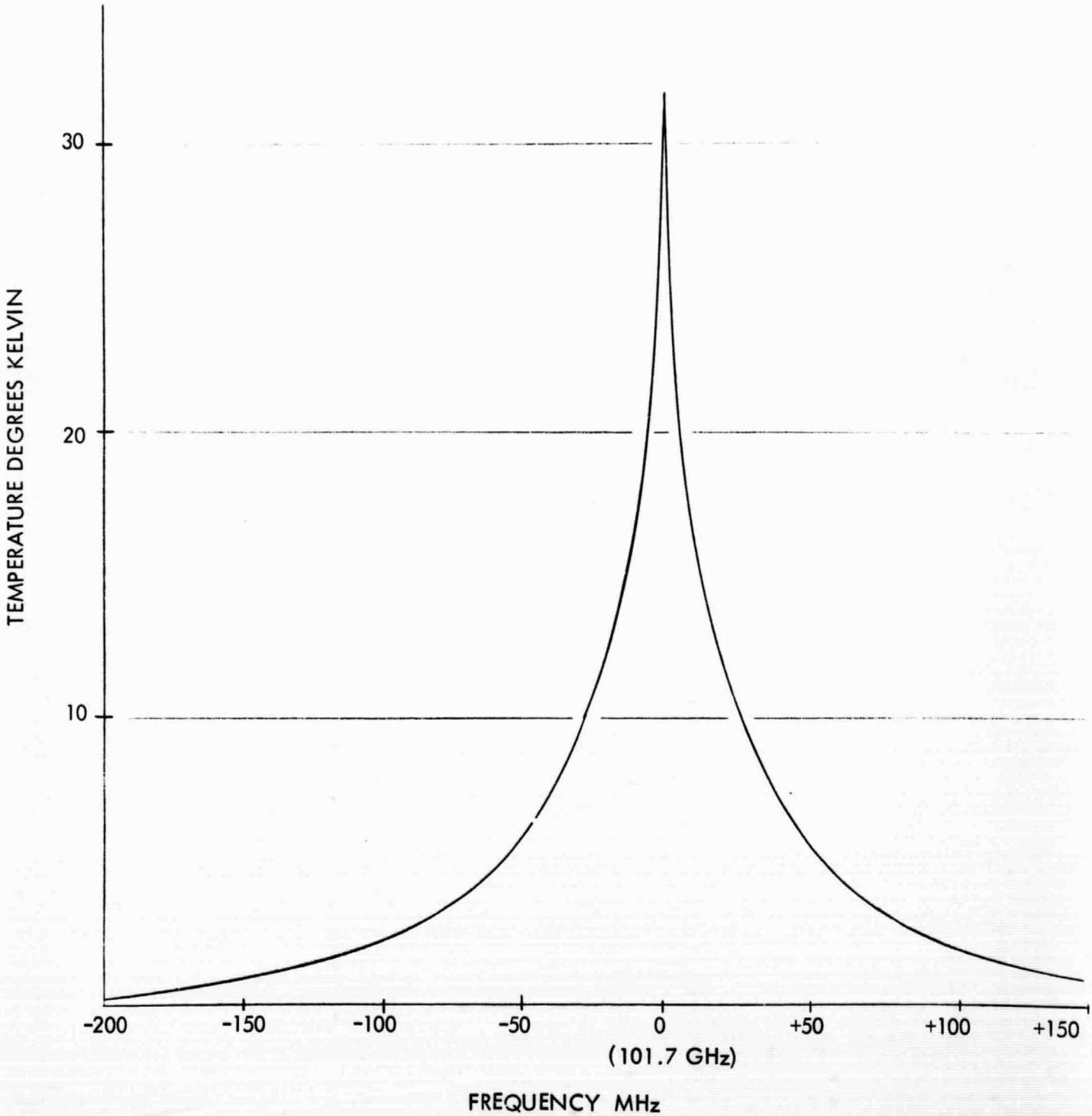

FIGURE 3-3

terrestrial coordinates. The data would then be inverted by the difference frequency method to obtain three data point profiles of the ozone concentration derived as weighted values at the mean altitudes of 18, 33, and 50 km. The profiles obtained along the ground track for each orbit would then be compared with earth-based, balloon, and rocket measurements, depending upon their availability.

The flight data would be compared with data from other instruments aboard the spacecraft; in particular, any sensors which may provide a measure of the vertical temperature profile of the atmosphere over the altitude range from 15 to 60 km. The line profile is weakly temperature dependent. In the region of the atmosphere from 15 to 60 km, the characteristic range of temperatures is 220 to 270° K. A large percentage change in temperature at any altitude would not be anticipated. Knowledge of any anomalous high-altitude temperature variations, however, would aid in data interpretation. In addition, the time function of any appreciable rotation of the vehicle about the yaw axis would be required in order to define the horizon point of the ozone sensor antenna beam throughout the flight. In the event that rotation about the yaw axis is stabilized within 5 to 10 arc degrees about some arbitrary direction, yaw angle data would not be required; however, the nominal pointing position of the antenna beam, relative to the orbital plane, is required. Data measurement requirements are summarized in Table 3-2.

TABLE 3-2

DATA MEASUREMENT REQUIREMENTS

Expected Values of Parameter	Antenna Temp. ^{o}K	T_A ^{o}K
	Average	$50^{o}K$
	Range	0 - $400^{o}K$ in $100^{o}K$ steps
Measurement Characteristics	Times per day	continuous
	Duration of each	continuous
	Total number in mission	maximum possible
Output Signal of Instrument	Type (Digital, Analogue)	Analogue
	Frequency Range	0 - 100 Hz
	Amplitude Range	0 - 5 volts
	Instrument Resolution (% Total Scale)	0.1%
Read-out Requirements	No. of Channels	4 signal, 10 dng. data analogue
	Sampling Rate	200/sec. (max.)
	Telemetry	needed
	Recorder	needed
Time Identification Method	Spacecraft clock or other	needed

3.2 Recommended Satellite Instrument Design

The Satellite Measurement Instrument would be a four-channel microwave radiometer system operating at a nominal frequency of 101.7 GHz. A second microwave radiometer operating at 60 GHz in a horizon sensor mode is also required. The 60 GHz unit would be equipped with two antennas directed to opposing horizons. The boresight of one of these antenna beams would be coincident with the boresight of the four-channel ozone radiometer antenna. Both radiometers would be of Correlation Type as described in Addenda A of this report. Both would use solid state components throughout. The Correlation Mode negates the need for the typical Dicke modulator and isolator used in power comparison radiometers. As a result, radiometers of this type are small in size and weight and require a small amount of input power. The measurement instrument would be designed for rigid mounting on the lower surface of the Satellite with a clear view toward opposing horizons in the orbital plane. System calibration would be self-contained. No "sky horn antennas" or other devices would be used.

A block diagram of the recommended sensor system configuration is shown in Figure 3-4. The four ozone signal channels share a common conical horn antenna. The single channel oxygen radiometer operating at a frequency of 60.8 GHz would provide a power comparison between the brightness temperature of the earth oxygen mantle as observed toward opposing horizons. The difference signal when synchronously detected by the radiometer provides an output error voltage in the form of an odd function about a null which is coincident with the nadir direction. This voltage is fed as an error signal via a servo amplifier to a DC torque motor integral with the yoke support member, to position the boresight of the ozone sensor antenna at a nominal 35 km altitude above the horizon.

A functional block diagram of the four-channel ozone radiometer is shown in Figure 3-5. The sensitivity of the individual channels is expected to be better than $1^{\circ}K$ rms. The absolute temperature measurement accuracy between channels would be better than $1^{\circ}K$ rms. The input temperature dynamic range is $0 - 400^{\circ}K$. The linearity of the system would be

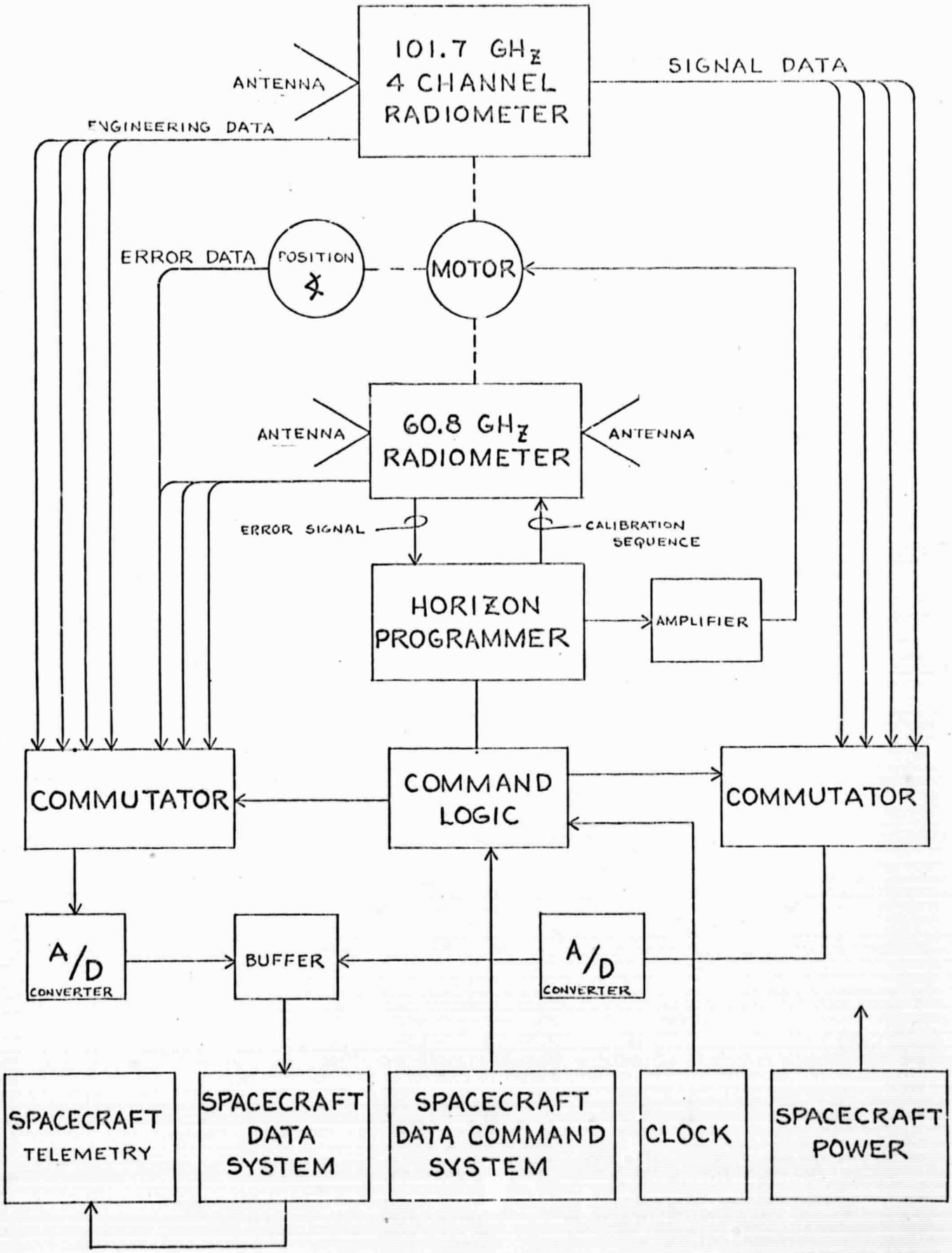

SYSTEM BLOCK DIAGRAM -- SATELLITE MEASUREMENT INSTRUMENT
FIGURE 3-4

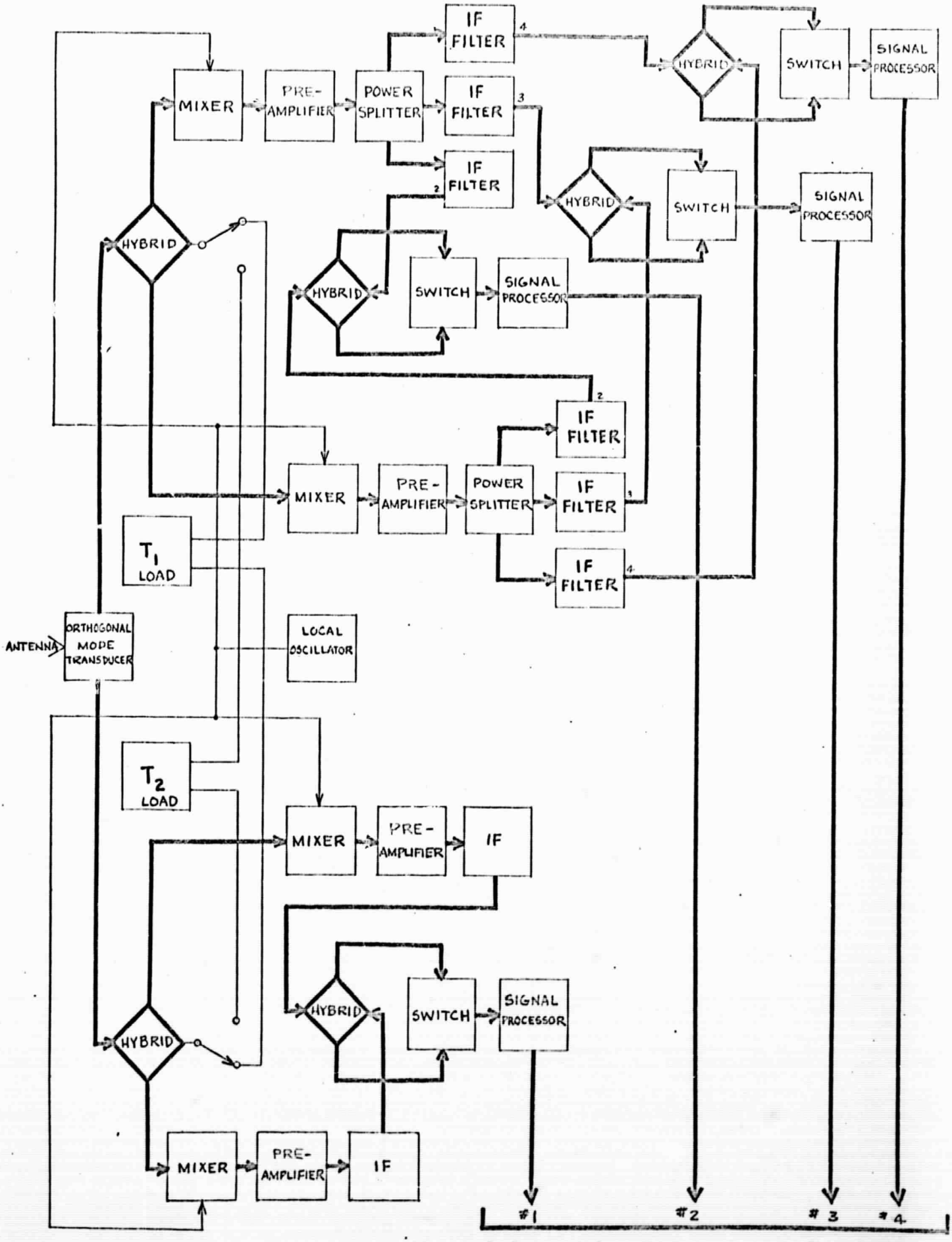

FIGURE 3-5 -- BLOCK DIAGRAM - OZONE RADIOMETER

$\pm$ 0.1%. System performance monitoring in the form of engineering data as well as signal data outputs would be in analog form, 0 - 5 volts DC.

A functional block diagram of the oxygen horizon sensor is shown in Figure 3-6. The null output value is calibrated by internal switching of the radiometer inputs to a black body load.

The Satellite Measurement Instrument would consist of a single rectangular package symmetrically truncated at a nominal 60° angle on either end. The instrument package is 14-3/8 inches long, 10-3/4 inches high, and 10 inches deep. The instrument package is attached to a yoke frame at the elevation axis trunnions. The DC torque motor and elevation axis angle position indicator are integral parts of the yoke frame. The yoke will mount directly to the lower portion of the Satellite as shown in Figure 3-7.

The weight, size, power requirements and environmental tolerance limits for the Satellite Measurement Instrument are summarized in Tables 3-3 through 3-5.

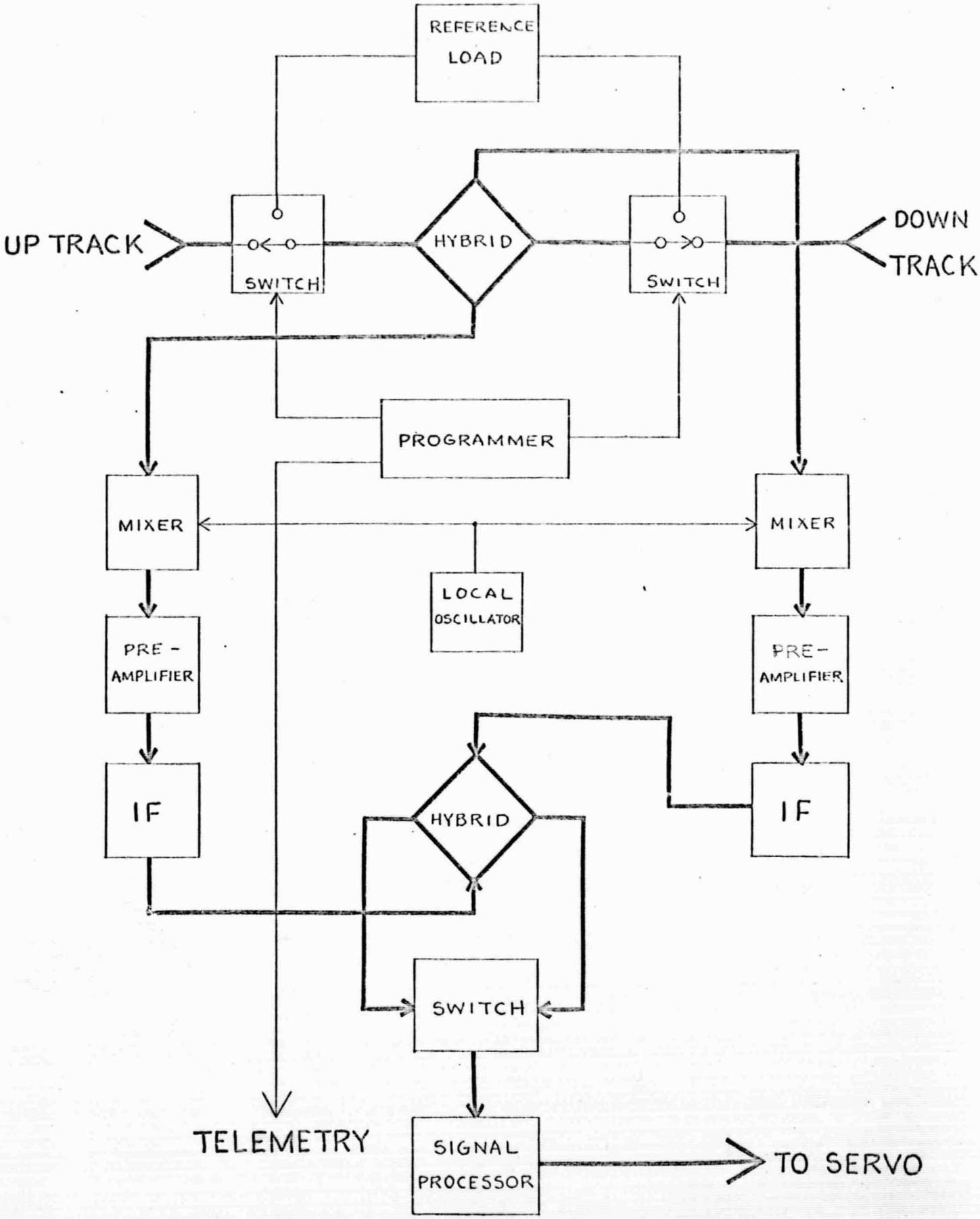

BLOCK DIAGRAM - O_2 HORIZON SENSING RADIOMETER
FIGURE 3-6

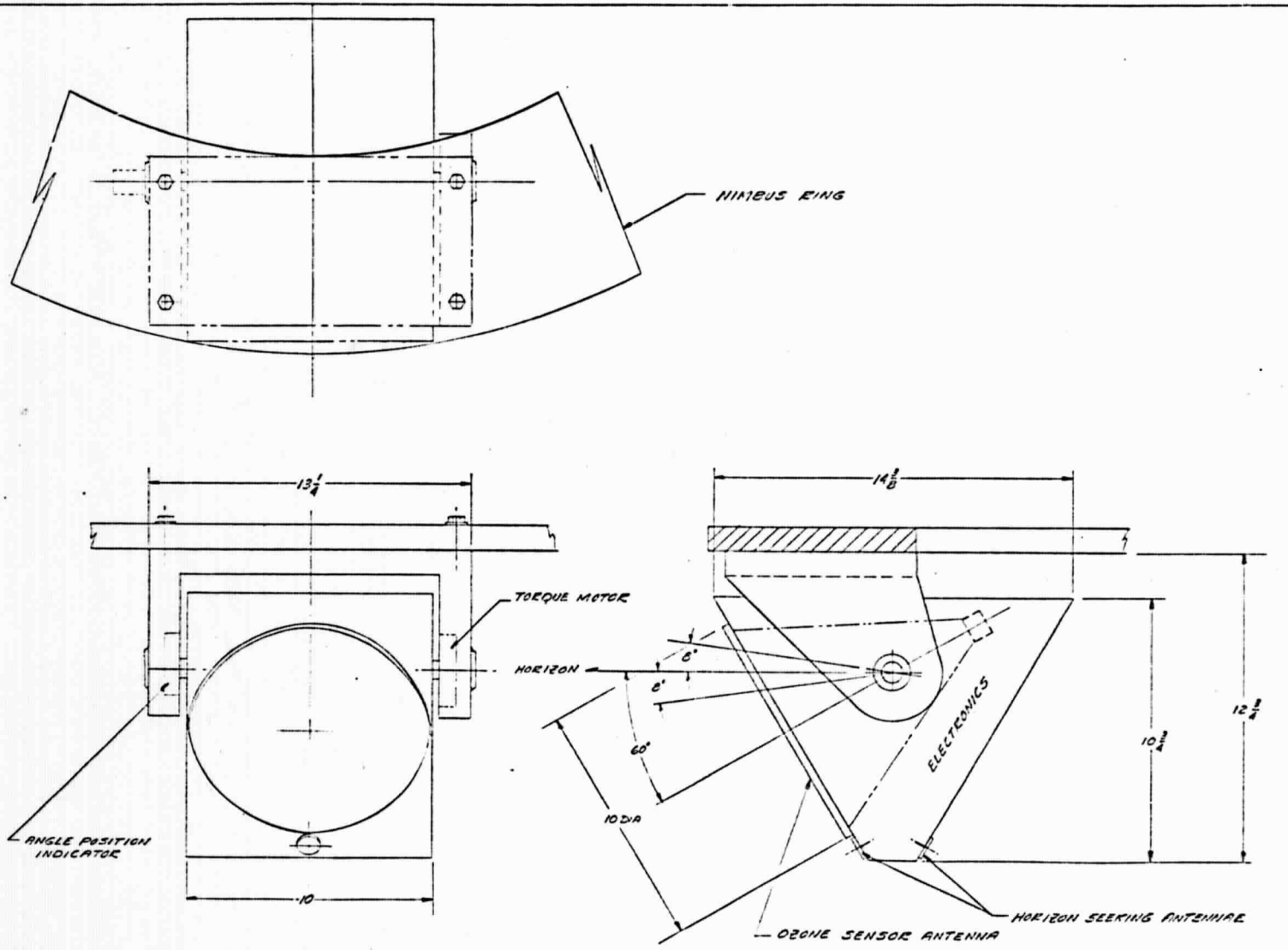

ENVELOPE -- SATELLITE MEASUREMENT INSTRUMENT

FIGURE 3-7

TABLE 3-3

WEIGHT AND SIZE OF SATELLITE MEASUREMENT INSTRUMENT

Weight	Volume	Dimensions	Shape
35 lb	1600 in^3	14-3/8" x 10-3/4" x 10" (See Figure 1-10 for yoke)	Rectangular Truncated at either end

TABLE 3-4

INPUT POWER REQUIREMENTS OF MEASUREMENT INSTRUMENT

POWER

	Standby	Average	Maximum
Total Power:	None	25 watts	35 watts

POWER CONSUMED BY SEPARATE ASSEMBLIES

	Standby	Average	Maximum
Meas. Inst.	None	20 watts	25 watts
Yoke	None	5 watts	10 watts

TABLE 3-5

ENVIRONMENT CONSTRAINTS FOR THE SATELLITE MEASUREMENT INSTRUMENT

Constraint	Tolerance Limits
Thermal	
Stored	-35 to +65°C
Operational	-10 to +55°C
Atmospheric Pressure	0 to 30,000 ft. or vacuum
Relative Humidity	0 - 80%
Air Movement Rate	0 - 60 mph
Atmospheric Composition	standard
Contaminants	no dust or salt spray
Acceleration (Storage)	
Positive	2 g
Negative	2 g
Transverse	2 g
Acceleration (Operation)	
Positive	Typical of Nimbus environment
Negative	Typical of Nimbus environment
Transverse	Typical of Nimbus environment
Vibration (Storage)	
Random	0.2 g
Sinusoidal	0.1 g
Vibration (Operation)	
Random	Typical of Nimbus environment
Sinusoidal	Typical of Nimbus environment

TABLE 3-5 (Continued)

Constraint	Tolerance Limits
Noise	Typical of Nimbus environment
Light Tolerance	
Intensity	Any
Wave Length	Any
Radiation Tolerance	Typical of Nimbus environment
RFI	Sensitive
EMI	Sensitive

CONTAMINANTS	OUTPUT RANGE
Vibration	
Random	None
Sinusoidal	None
Noise	None
Light	None
Radiation	None
RFI	60.8 GHz and 101.7 GHz oscillators
EMI	DC-DC inverters and DC torque motor

3.3 Critical Areas

The most critical performance characteristic of the Satellite Measurement Instrument which effects the design approach is the required sensitivity. To resolve the emission profile of atmospheric ozone, the Satellite Instrument must be approximately one order of magnitude more sensitive than the Earth Based Measurement Instrument. Radiometer sensitivity is normally improved by:

Reducing the receiver noise temperature;

Increasing the receiver bandwidth;

Increasing the post detection integration time constant.

The measurement of line profiles precludes the possibility of increasing the receiver bandwidth since the bandwidth of the individual channels is determined by the frequency resolution intervals needed to resolve the line profile. The maximum available time constant for satellite observations is determined by the motion of the antenna beam through the atmosphere as the satellite moves in its orbit about the earth. As a consequence of these restraints imposed on bandwidth and post detection integration time constant, improvement in sensitivity can be accomplished only by reducing the system noise temperature.

The major contributors to system noise temperature are:

RF losses in the signal path between the antenna output and the first converter (mixer) input.

The mixer conversion efficiency and effective noise temperature of the crystals.

A conservative estimate of the anticipated improvement in mixer performance at a wavelength of 3 mm during the next one to two years is 3 db. This falls far short of the required factor of ten improvement in sensitivity. The remaining alternative to achieve the required improvement is to minimize all RF losses in the signal path between the antenna output terminal and the mixer input. The major contributors to RF losses are the ferrite modulator and isolator which perform the Dicke switching function for the radiometer in the Earth Based

Measurement Instrument. Other sources of RF loss are the couplers associated with the calibration circuitry. The ferrite devices and couplers located in the input signal path of the Earth Based Instrument contribute approximately 5 db (factor of 3) of loss. If these devices could, by some technique, be removed from the signal path, then the corresponding improvement in sensitivity, when combined with the anticipated 3 db improvement in mixer performance, would provide a total improvement of a factor of 6 -- still short of our goal of 10.

Early in 1968, we initiated an in-house supported investigation of radiometric techniques which would perform the function of the Dicke type radiometric mode without requiring the typical Dicke switch forward of the mixer. The concept was predicated on a prior study of radiometric modes for monopulse radar receiving systems. A breadboard model of this new radiometric mode was assembled and evaluated at a wavelength of 5 mm. The test results confirmed the validity of the technique, and further confirmed an anticipated additional 2 db improvement in sensitivity over that obtained by the Dicke mode, independent of RF losses and mixer performance. The design of the Satellite Instrument is based on the preliminary test results performed on the breadboard model.

In summary, the recommended design approach anticipates an improvement of one order of magnitude in the presently achieved sensitivity of the Earth Based Instrument. This will be obtained by using the "Taylor Radiometric Mode"* which eliminates the need for ferrite devices and couplers in the input signal transmission line at a saving of 5 db in loss, and provides an additional 2 db improvement in sensitivity over that achieved by the Dicke mode. This 7 db improvement, when combined with the anticipated 3 db improvement in crystal performance characteristics, leads to the desired overall improvement of 10 db in sensitivity.

The Taylor Radiometric Mode is a form of correlation mode. The zero base line stability of this mode is enhanced by the unique introduction of a switching device at the intermediate frequency, following the mixer, which eliminates the differential response characteristics of

*Hugh Taylor, the inventor, is the Area Leader for Advanced Techniques at the Ewen Knight Laboratory.

diode sum and difference networks which perform this function in radar circuits. A more detailed discussion of this radiometric mode is included in Addenda A to this report.

Improvement in sensitivity is the most significant feature of the Taylor Mode. The following additional features, however, are worthy of note:

(a) The pulsating magnetic field radiated by a Dicke type ferrite modulator is eliminated completely. Though this radiation has received little attention in the literature, it is of considerable significance in satellite instrument applications. The reason is that only two microwave radiometric systems have been flown in space; one to the planet Venus in 1962, and the other in earth orbit in 1967. The effect of the pulsating magnetic field of the modulator was detected by the magnetometer on the Venus flight. Though the magnetometer was located several feet from the radiometric system, the pulsating magnetic field of the modulator was easily detected. Though considered a possible contaminating influence on solar wind measurements, the radiometer was occasionally turned "on" during the flight to the planet to provide a calibration signal for the magnetometer, this fortuitous circumstance is less likely to be repeated in future satellite measurement programs.

(b) The deletion of the ferrite devices eliminates the need for the associated driving circuitry, with the result that the instrument is smaller in size and weight, and requires less input power. These, of course, are more important considerations for satellite instrumentation, than for earth based or balloon instruments.

The second most critical performance requirement, effecting the design approach of the Satellite Instrument, is the need to stabilize the ozone antenna beam in the direction of the horizon. The ozone antenna beam must be pointed tangent to the horizon at an altitude approximately 30 km above the horizon. The half-power beamwidth of the ozone antenna is 1°. The boresight axis must be maintained within $\pm 0.25^{\circ}$. Most satellite observing platforms are not adequately stabilized to meet this requirement. The recommended approach, as described in Section 3.2, is to support the entire ozone sensor unit on a gimbal, whose motion is controlled by a molecular atmospheric oxygen horizon sensor. The anticipated performance capability of the oxygen horizon sensor is well-within the required $\pm 0.25^{\circ}$. Though considerable research and instrument development has been accomplished during the past six years, since the initial concept of an oxygen horizon sensor was suggested, the validity of the concept has not, as yet, been established through direct measurement. This is a critical consideration for the ozone sensor program, since the entire satellite experiment depends on either improvement in stabilization of available satellite observing platforms or the verification of advanced horizon sensor techniques, typical of the oxygen sensor concept. It would be inappropriate to include, within the first ozone satellite experiment, the evaluation of the horizon sensor.

The third area in which the required performance characteristics effect the design of the Satellite Instrument is associated with the need for a long-term reliable operation in the space environment, which requires that the system be assembled from completely solid state units. In this category is the first local oscillator. At the present time, solid state oscillators operating at a wavelength of 3 mm are not available commercially. Several research groups have, however, reported operation of solid state devices at shorter wavelengths. The development of a reliable device of this type for the Satellite Instrument appears feasible; however, further development is required to assure the translation of these devices from a laboratory research status to a qualified space flight status.

A less critical component is the balanced mixer. This unit qualifies as a critical item

primarily because of the limited number of active research and development programs now underway or planned for the near-future. To assure the desired improvement of a factor of 2 in the present performance of these crystal devices, additional development support may be required.

In the foregoing, discussion of critical program areas was confined solely to the technique and component considerations associated with the development of the Satellite Instrument. Other areas of equal significance, in terms of an overall satellite experiment program, include analysis and measurements in support of the experiment. In the area of analysis, a more detailed computer program for the prediction of ozone profiles, than accomplished under this investigation, is suggested. In addition, laboratory measurements of millimeter ozone transition intensities and profiles would provide valuable knowledge concerning the inter-action of the physical processes associated with these transitions.

A continuation of direct measurements of atmospheric ozone resonant profile characteristics to include data obtained from balloons, as well as from the Earth Based Instrument, would provide a significant contribution to knowledge concerning diurnal and seasonal variations. In addition, continued operation of the Earth Based Instrument would assure the availability of a complete sensor system for evaluation of functional developmental units as they become available in the early phases of satellite instrument development. The performance characteristics of functional units, such as solid state oscillators and balanced mixer preamplifiers, can be determined in greater detail when introduced in the existing system. This provides a simple vehicle for obtaining a direct comparative measure of performance improvement relative to present day capabilities.

As previously noted in the comments on observational data, the value of observational data would be enhanced considerably by the introduction of a phase-lock circuit for the klystron local oscillator. Though the immediate objective would be to improve the usefulness of the observed data, obtained on a day-to-day basis, the same circuitry would be applicable to investigating the techniques for phase-locking solid state oscillators.

3.4 Recommended Implementation Plan

The satellite instrument design approach as described in Section 3.2 is based on the feasibility of accomplishing certain technological advancements in the current state-of-the-art, some of which require advanced technological research. The time schedule required for successful achievement in each of these areas as imposed by a satellite flight program was investigated. The objective was to establish the inter-relationship between areas of potential risk and the time available to reduce the level of risk to assure that a satellite flight program schedule would not be jeopardized. For this analysis, a time period of four and one-half years was arbitrarily selected as a reasonable interval from the time of initiating the program to the time of satellite launch.

In developing the Implementation Plan, the Satellite Flight Program was divided into two major areas of effort:

Support Program

End Item Hardware

All technical efforts associated with advanced development in the previously defined critical areas were assigned to the Support Program. The End Item Hardware effort included only those engineering steps normally required in the development of a Satellite Flight Instrument, after technological areas of risk are removed.

A flow diagram was prepared showing all major milestone efforts for both the Support Program and the End Item Hardware Program to identify the interrelationship of milestones in each of these major program areas. This flow diagram is shown in Figure 3-8.

The next step in development of the Implementation Plan was preparation of a master time schedule for all program milestones as shown in Figure 3-9. The program time period required during the Support Program milestone accomplishments was determined by noting the relationship of each Support Program milestone to an End Item Hardware milestone. Though the time available for Support Program milestone

RECOMMENDED IMPLEMENTATION PLAN
SATELLITE MEASUREMENT INSTRUMENT

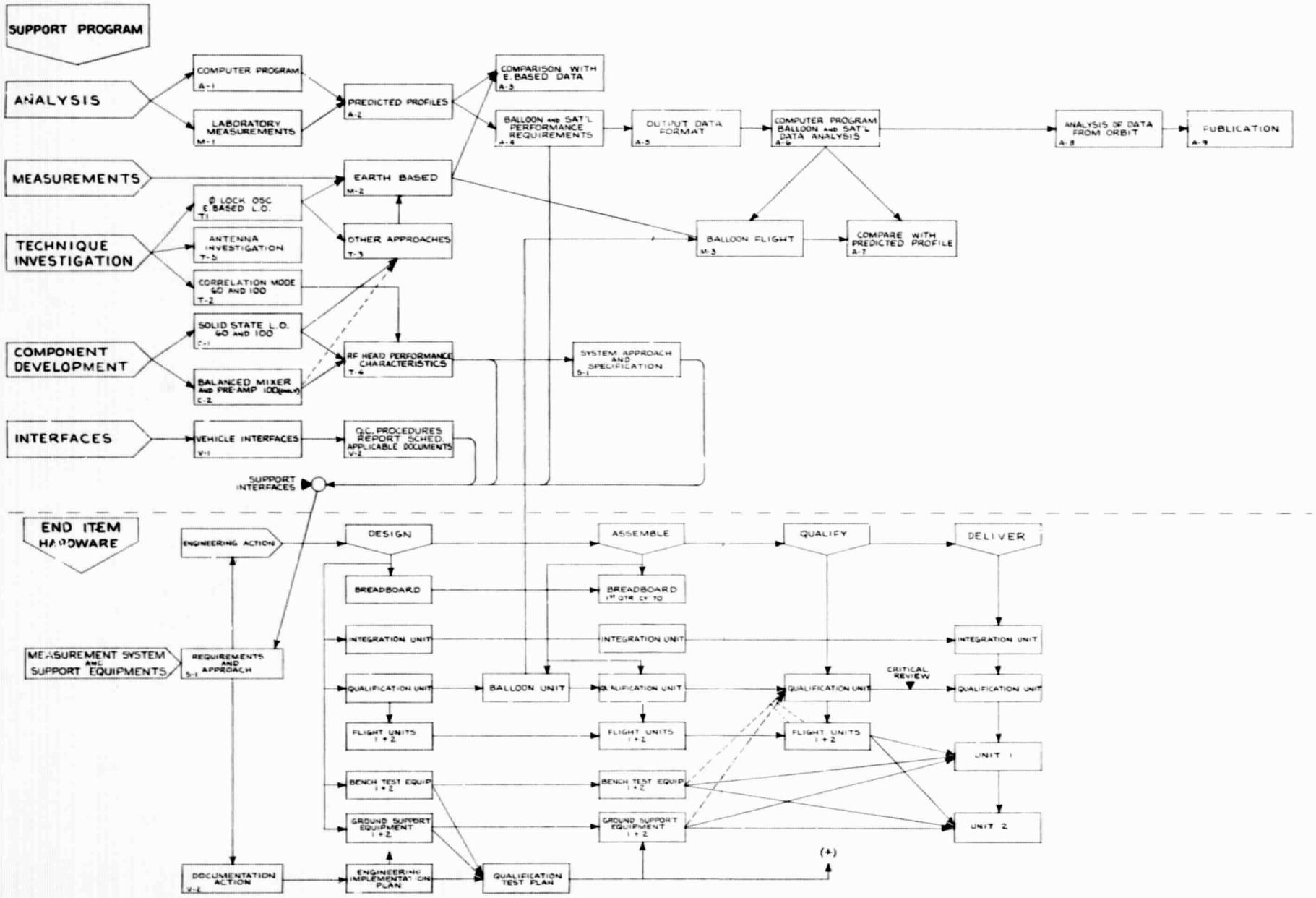

FIGURE 3-8

SATELLITE FLIGHT PROGRAM

RECOMMENDED IMPLEMENTATION PLAN

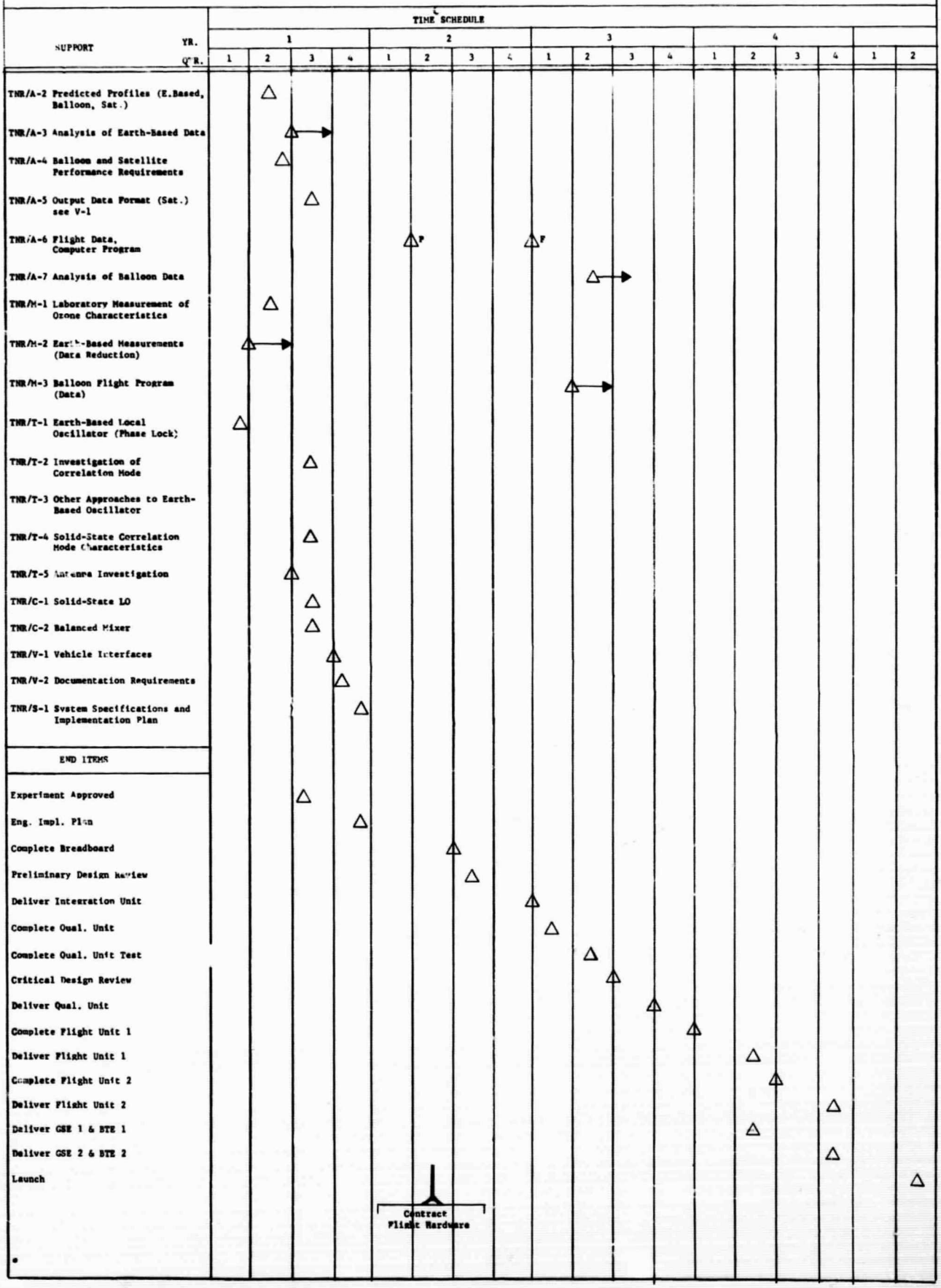

FIGURE 3-9

accomplishments appeared reasonable in most cases, the schedule was considered somewhat optimistic for:

(1) Technique investigation of the Correlation Mode at 60 and 100 GHz.

(2) Component developments associated with solid state local oscillators at 60 and 100 GHz, and a balanced mixer preamplifier at 100 GHz.

Each task identified with a Support Program milestone was further described to provide additional written detail concerning: objectives, significance, technical approach, and time schedule. This technical information was compiled in a separate document and forwarded to the Electronics Research Center in November of 1968, to support the feasibility of implementing the recommended design approach for the Satellite Instrument.

It should be noted that the Implementation Plan makes no reference to the critical need for a horizon stabilization system for the ozone sensor. It was assumed that this capability would become available through technological advancements in the field of satellite navigation and guidance.

ADDENDA "A"

ADDENDA "A"

CORRELATION RADIOMETER

(TAYLOR MODE)

In a dual channel correlation receiver* (Figure 1), the input signal is divided between two channels and then recombined at the output by means of a multiplier to obtain a DC output with a mean value ideally not biased by receiver noise.

Each input component is separately amplified and the receiver noise is added to each channel through a power summation process. The amplifier outputs are recombined in a second hybrid. The operation of the hybrid combiner is such that the signal components, which are phase coherent with respect to themselves, will sum vectorially; while the noise components, which are phase incoherent, will combine power-wise. The result will be two outputs from the combiner as follows.

$$P_1 = \frac{V_A^2}{2}\left[G_1 + 2\sqrt{G_1 G_2} + G_2\right] + \frac{V_R^2}{2}\left[G_1 - 2\sqrt{G_1 G_2} + G_2\right] + \frac{V_N^2}{2}\left[G_1^2 + G_2^2\right]^{1/2} \quad (1a)$$

$$P_2 = \frac{V_A^2}{2}\left[G_1 - 2\sqrt{G_1 G_2} + G_2\right] + \frac{V_R^2}{2}\left[G_1 - 2\sqrt{G_1 G_2} + G_2\right] + \frac{V_N^2}{2}\left[G_1^2 + G_2^2\right]^{1/2} \quad (1b)$$

These two signals are applied to oppositely polarized square-law detectors to obtain voltage output proportional to:

$$E_{DC} \equiv P_1 - P_2$$

$$\sim 2\left(V_A^2 - V_R^2\right)\left(G_1 G_2\right)^{1/2} + V_N^2\left[G_1^2 + G_2^2\right]^{1/2} \quad (2)$$

*The correlation function is defined as the integral of the product of two signals, or their envelopes, as a function delay. If the two waveforms are the same except for the delay, we obtain the auto-correlation; if they are different, we obtain the cross-correlation. In the receiver configuration shown, the delay is introduced by motion of the antenna and the multiplication process by first taking the voltage sum and difference of the two inputs, and then taking the difference of the squares of the resulting waveforms; i.e., $(V_A + V_R)^2 - (V_A - V_R)^2 = 4V_A V_R$ where V_A^2 and V_R^2 are proportional to $KT_A B$ and $KT_R B$, respectively.

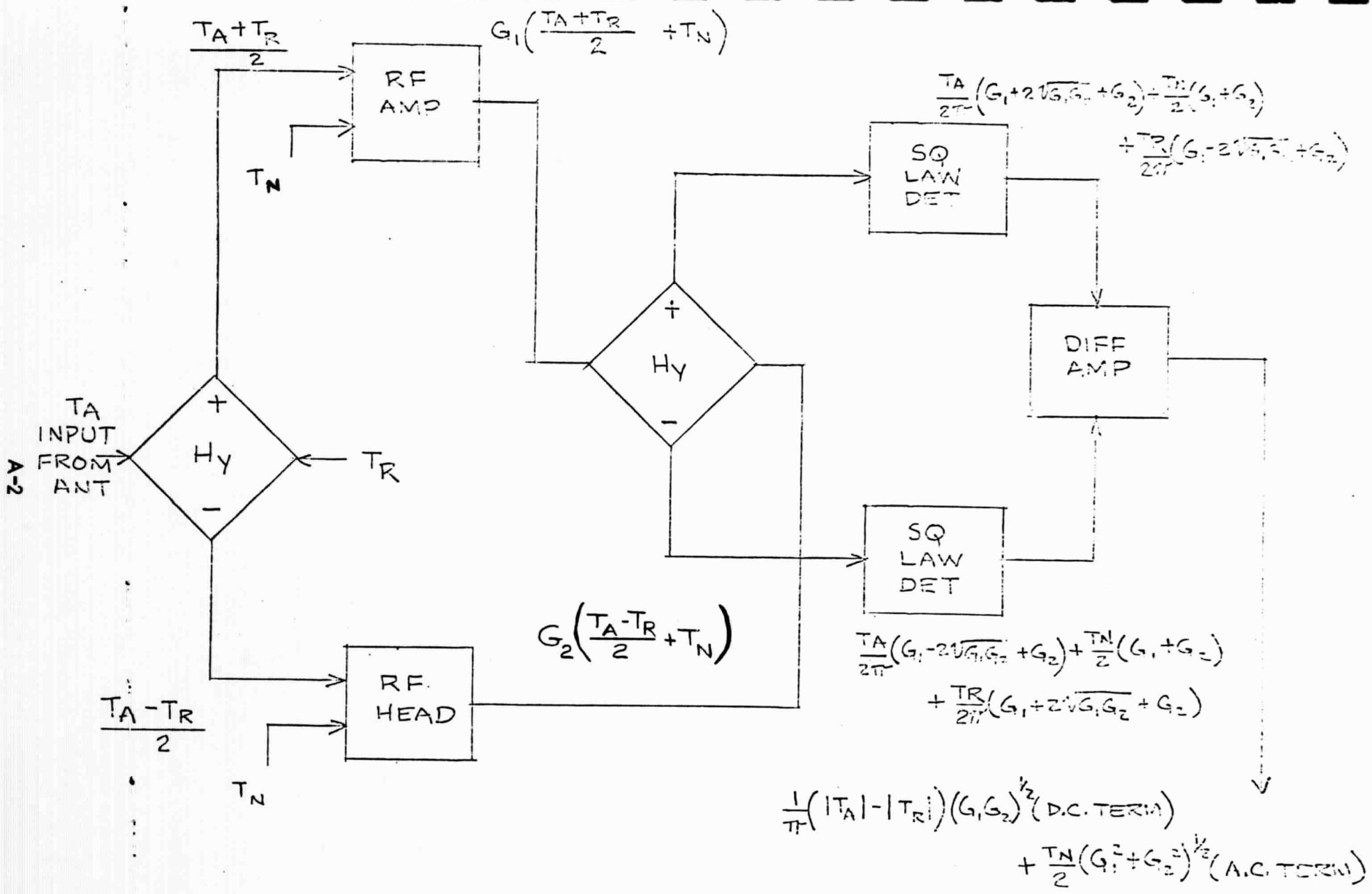

FIGURE 1
DUAL CHANNEL CORRELATION RADIOMETER

Considering V_A, V_R, and V_N to be randomly distributed, the average value of the square of a Gaussian amplitude distribution is $1/2\sqrt{1}$ of the mean square value of the input signal. The peak AC noise output is reduced by one-half, due to the rectification action of the detectors, hence;

$$\mathcal{L}_d = \left(\frac{1}{\pi}\right)\left(V_A^2 - V_R^2\right)\left(G_1 G_2\right)^{1/2} + \frac{V_N^2}{2}\left[G_1^2 + G_2^2\right]^{1/2} \tag{3}$$

(DC term) (AC term)

The signal-to-noise ratio is then:

$$\frac{S}{N} = \left(\frac{2}{\pi}\right)\left(\frac{V_A^2 - V_R^2}{V_N^2}\right)\left[\frac{G_1 G_2}{G_1^2 + G_2^2}\right]^{1/2} \tag{4}$$

Letting $G_2 = G_1 + \Delta G$ gives:

$$\frac{S}{N} = \left(\frac{2}{\pi}\right)\left(\frac{V_A^2 - V_R^2}{V_N^2}\right)\left[\frac{1 + \frac{\Delta G}{G_1}}{2 + \frac{2\Delta G}{G_1} + \left(\frac{\Delta G}{G_1}\right)^2}\right]^{1/2} \tag{5}$$

For $\Delta G = 0$, this reduces to:

$$\frac{S}{N} = \left(\frac{\sqrt{2}}{\pi}\right)\left(\frac{V_A^2 - V_R^2}{V_N^2}\right) \tag{6}$$

The resultant signal-to-noise ratio is thus a factor of $1/\sqrt{2}$ less than the maximum value obtained with a total power radiometer.*

Overall performance is based on the use of a balanced set of detector elements and the sensitivity expression is now written:

$$\Delta T_{(MIN)} = \left[\frac{\pi^2}{4\beta\tau} + \left(1 - \frac{\Delta G}{G_0}\right)_{AV}^2 \Delta G_{dET}^2\right]^{1/2}\left[F + \frac{T_A}{T_0} - 1\right] T_0 \tag{7}$$

where ΔG_{dET} is the change in the slopes of the balanced detector diodes as a function of drive level, i.e.:

$$\Delta G_{dET} = G_{diode_1} - G_{diode_2} \tag{8}$$

*The detected signal is described in terms of the squared mean and the detected noise in terms of one-half the mean square value of their respective distributions. The squared mean of a normal distribution is equal to $\frac{1}{2\pi}$ and the mean square is 1/2. The additional loss of one-half is a result of the central limit theorem of statistics which states that the fluctuations will assume a normal distribution about the mean with the uncertainity in the filtered mean considered to be equal to one-half the standard deviation of the filtered distribution.

where:

G_{diode_1} = slope of the square-law detector transfer characteristic in millivolts/milliwatt measured at the actual operating point;

$\left(\frac{\Delta G}{G_o}\right)_{AV}$ = the fractional gain variation occurring in both channels of the pre-detection amplifiers.

Thus, for a $\pm (\Delta G/G_o)_{AV}$ fractional gain variation, the drive level to the detector diodes will be $(1 \pm \Delta G/G_o)_{AV} P_o$ where P_o is the nominal value of drive power for which the detector is balanced. Further, assume that for this $(\Delta G/G_o)_{AV} P_o$ change in drive level, the respective diode slopes change by ΔG_{dET}. This will introduce a DC bias error voltage at the multiplier output equal to:

$$\Delta E_{dc} = \pm \left(1 - \frac{\Delta G}{G_o}\right)_{AV} P_o \Delta G_{dET} \qquad (9)$$

The fractional bias error due to gain variations is thus:

$$\frac{\Delta E_{dc}}{P_o} = \left(1 - \frac{\Delta G}{G_o}\right)_{AV} \Delta G_{dET} \qquad (10)$$

The bias error (Equation 10) provides a measure of the degree to which the zero base line can be established. Hence, the ability to match the slopes of the diode characteristics can become the limiting parameter with respect to the accuracy that can be achieved in the presence of a varying drive level to the multiplier. This is avoided in the switched load configuration by the use of a single detector element. This same advantage can be achieved with the correlation radiometer by driving a switch input amplifier from the outputs from the second hybrid, as indicated in Figure 2. The switched input amplifier then drives a single detector element without introducing any additional loss in signal-to-noise ratio due to the switching.(1)

(1) Taylor, H.P., Zulch, D.I., "Radiometric Monopulse Receiver Systems," Patent Application.

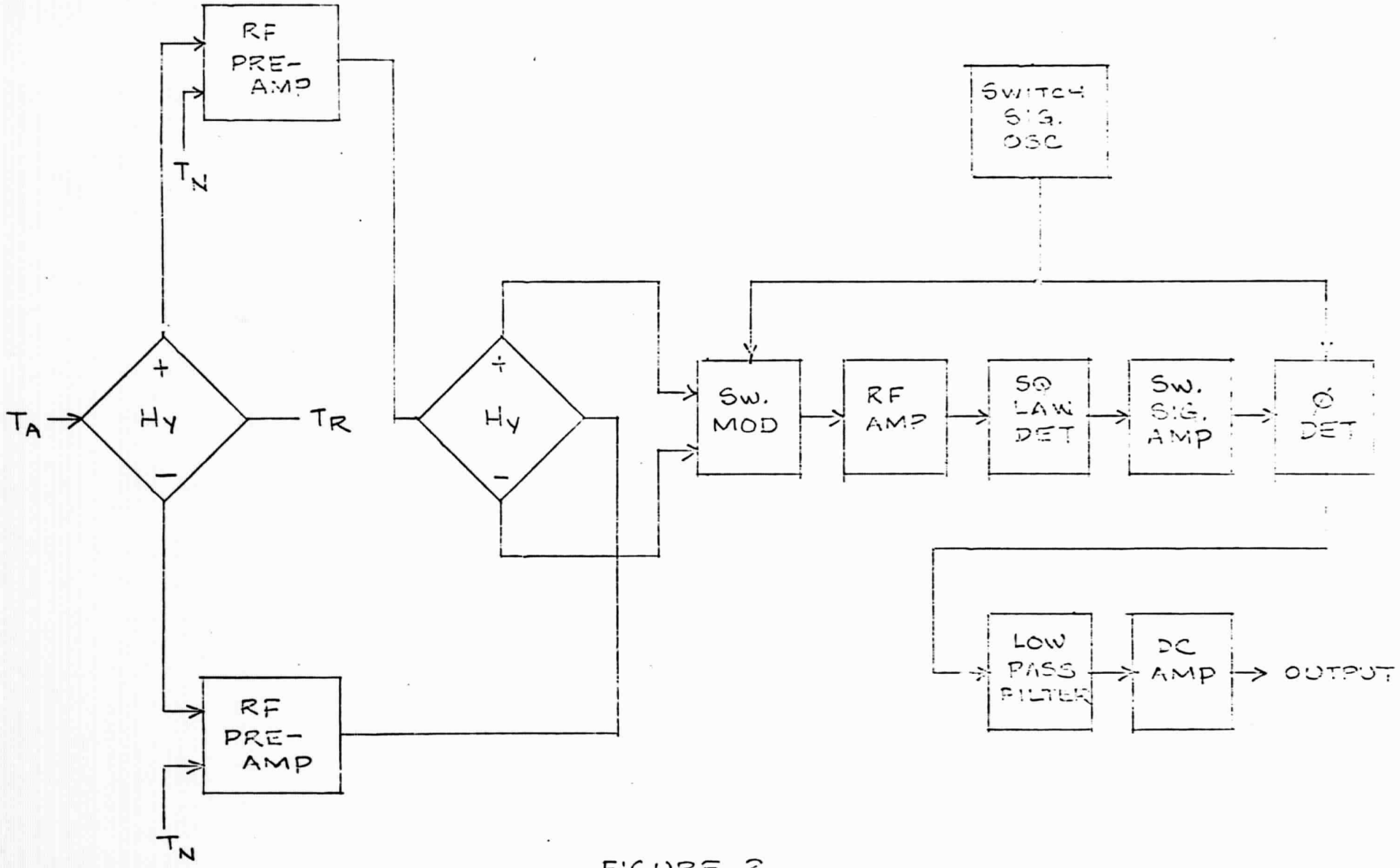

FIGURE 2

IMPROVED VERSION OF DUAL

CHANNEL CORRELATION RADIOMETER

ADDENDA "B"

THE ASTROPHYSICAL JOURNAL, Vol. 151, March 1968

RADIO MEASUREMENT OF THE ATMOSPHERIC OZONE TRANSITION AT 101.7 GHz

W. M. CATON
Chico State College Physics Department, California

G. G. MANNELLA
NASA, Instrumentation Laboratory, Electronics Research Center

P. M. KALAGHAN
Air Force Cambridge Research Laboratories, Prospect Hill Observatory

A. E. BARRINGTON
NASA, Instrumentation Laboratory, Electronics Research Center

H. I. EWEN
Ewen Knight Corporation
Received February 12, 1968

The first experimental detection of the $22_{3,19} \rightarrow 23_{2,22}$ transition of molecular atmospheric ozone in the absorption spectrum of the Sun at 36.025 GHz was obtained by Mouw and Silver (1960). In 1966, Caton (see Caton, Welch, and Silver 1967) detected the 37.836 GHz, $17_{3,15} \rightarrow 18_{2,16}$ transition in absorption and, in the same year, the $16_{2,11} \rightarrow 15_{3,13}$ transition at 30.056 GHz in emission. Barrett, Neal, Staelin, and Weigand (1967) announced the detection of the $19_{2,18} \rightarrow 18_{3,15}$ transition at 23.86 GHz in emission. The line intensities associated with each of these observations were so weak in comparison to receiver sensitivity that it was necessary to integrate several hours and, in one case, days of data in order to confirm detection.

In this communication, we wish to report the successful detection and preliminary line-profile resolution of the $4_{0,4} \rightarrow 4_{1,3}$ atmospheric ozone transition at 101.737 GHz in both absorption and emission. The search for this particular line resonance was prompted by the anticipated higher intensity (Gora 1959) relative to previously detected lines, leading to a shorter integration time and ability to resolve the line profile. All observations were conducted during the period from November 30 through December 20, using an equatorially mounted 5-foot searchlight reflector as the parabolic antenna.

The receiver is a double-conversion superheterodyne. First-intermediate-frequency amplification is provided by three traveling wavetubes in cascade with an instantaneous band width of 2 GHz centered at 3 GHz. The signal to the second converter is coupled from an interstage transmission line between the second and third traveling wavetubes. In total, six second-intermediate-frequency amplifiers are provided in the form of five contiguous filters, each 10 MHz wide, and one filter covering the entire 50 MHz band. These six intermediate-frequency-amplifier outputs are separately detected and radiometrically processed by individual IF amplifier, gain modulator, and video circuits. A seventh broad-band (2 GHz) channel response is derived from the output of the third traveling wavetube. For absorption measurements, the comparison load in the Dicke mode of operation is provided by a gas-discharge-noise source fed through a servo-controlled attenuator to the comparison port of the ferrite modulator. The control signal for the servo is derived from the output of the broad-band channel. Frequency calibration is accomplished by injecting the appropriate harmonic of a low-frequency oscillator into the comparison port of a second ferrite modulator, following the Dicke modulator, and adjusting the first local oscillator frequency to obtain an output response

from the desired channel. During the accumulation of observational data, the modulation drive signal is removed from this second ferrite modulator and an appropriate d.c. bias applied so that it performs the function of an isolator. Measured sensitivity for the five 10 MHz wide channels was 2.7° K rms with a postdetection integration time constant of 20 sec.

The observed change in the apparent temperature of the Sun was 67° ± 8° K, or 2.5 per cent of the Sun's antenna temperature, as the frequency of the receiver was tuned to center the line response, first in one of the five 10 MHz contiguous filters and then 50 MHz from the selected filter. Since the receiver responds to the Sun's signal in both the image as well as signal bands of the first superheterodyne converter, and the ozone absorption occurs only in the signal band, the absorption level was twice the observed antenna temperature change, or 5 per cent, corresponding to an atmospheric ozone attenuation of approximately 0.25 db. This does not represent the total ozone attenuation along the entire atmospheric path at the frequency of the line core as a consequence of the method of measurement, i.e., the change in the apparent temperature of the Sun in each of the five contiguous 10 MHz filters was measured relative to the composite 50 MHz filter response as a "zero-reference" level. Based on the measured 0.25-db differential attenuation for that portion of the profile contained within a band width of ±50 MHz centered on the line frequency, our analysis indicates that the total ozone absorption along the atmospheric path at a 64° zenith angle was 0.35 ± 0.03 db during the period of observation.

A computer analysis of anticipated resonant profile characteristics was undertaken prior to the accumulation of observational data. The calculations were based on a model atmosphere of 100 layers of arbitrary thickness. The absorption coefficient of each layer was calculated by introducing model-atmosphere values for temperature, T, pressure, P, water-vapor concentration, and ozone content, N_{O_3} (molecule cm^{-3}). The ozone absorption coefficient α_{O_3} was expressed in the form

$$\alpha_{O_3} = A_1 \frac{e^{-A_2/T}}{T^{5/2}} N_{O_3} \nu^2 \left[\frac{\Delta\nu}{(\nu - A_3)^2 + (\Delta\nu)^2} + \frac{\Delta\nu}{(\nu + A_3)^2 + (\Delta\nu)^2} \right],$$

where

$$\Delta\nu = [(A_4 P T^{-1/2})^2 + (A_5 T^{1/2})^2]^{1/2}.$$

The values for the coefficients A_1 through A_5 introduced in the computer program for the 101.7 GHz transition were

$$A_1 = 1.2 \times 10^{-24} \text{ km}^{-1}, \quad A_2 = 13.1° \text{ K}, \quad A_3 = 101.7368 \times 10^9 \text{ Hz},$$

$$A_4 = 5.28 \times 10^7 \text{ Hz } (° \text{K}^{1/2}) \text{ mm}^{-1}, \quad \text{and} \quad A_5 = 7.31 \times 10^3 \text{ Hz } (° \text{K})^{-1/2}.$$

These coefficient values were obtained from Gora (1959) and from Townes and Schawlow (1955).

The numerical results obtained from the computer analysis of the 101.7 GHz ozone transition are shown in Figure 1. The measured profile obtained on December 20 is shown in Figure 2. The predicted values from Figure 1 are replotted in Figure 2, and the predicted peak-amplitude response of 88° K adjusted to correspond to the measured 134° K in order to provide a direct comparison of the measured with the anticipated line profile. It is of interest to note that the measured ozone absorption was a factor of 1.5 greater than the value predicted by our model-atmosphere analysis.

Measurement of atmospheric ozone in emission at 101.7 GHz is complicated by the additional attentuation of molecular atmospheric oxygen and water vapor. However, the measured intensity of the line in absorption suggested the possibility of detecting the line in emission. During clear, cold weather conditions the line was detected in emission

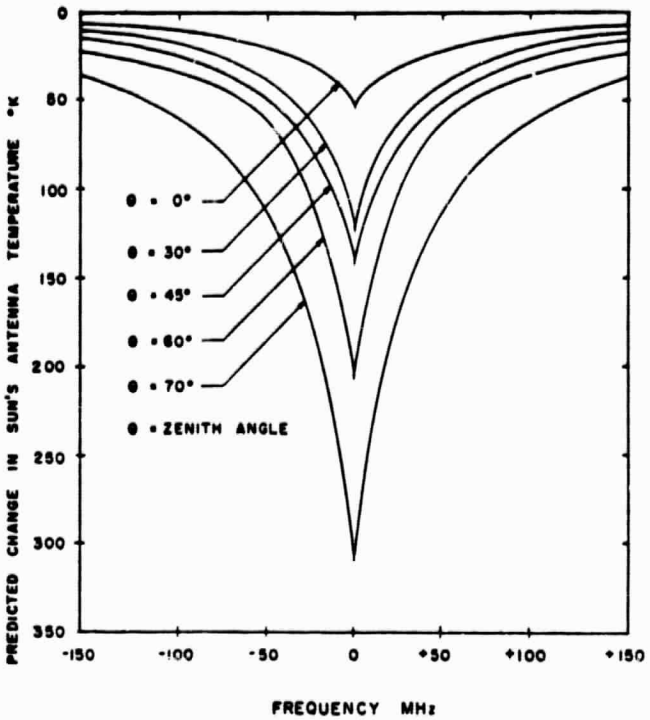

FIG. 1.—Predicted change in the Sun's temperature due to atmospheric ozone absorption as viewed from Earth's surface at a frequency of 101.7 GHz.

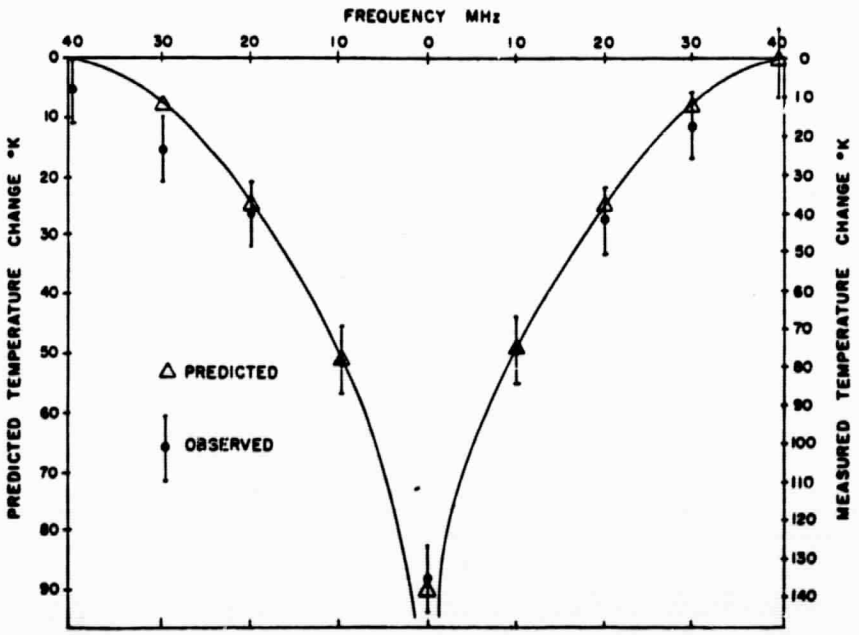

FIG. 2.—Measured and predicted ozone absorption profiles normalized to equal amplitude for a background Sun temperature of 2500° K.

on December 17, with a peak intensity of 6° ± 2° K. Corrected for the receiver-image response, the measured effective temperature was 12° ± 4° K. For these measurements, the frequency of the receiver was fixed throughout the entire period of observation. The integration time constant was adjusted to provide an rms sensitivity of 1.7° K. The antenna beam was scanned in angle from the zenith toward the horizon. An increase in antenna temperature in the channel tuned to the line frequency was noted over the zenith-angle range from 45° to 75°, reaching a peak of 6° ± 2° K at a zenith angle of 75°.

Weather conditions and some equipment difficulties precluded the possibility of nighttime observations during the observing period reported here.

CONCLUSIONS

1. The ozone transition at 101.7 GHz was detected in Earth's atmosphere in both absorption and emission.
2. The observed frequency of the line core was in excellent agreement with the laboratory measured value.
3. Although the measured ozone concentration was higher than anticipated, it was within reasonable limits of prior atmospheric measurements.
4. The measured line profile was in good agreement with the anticipated profile.
5. Due to a lack of nighttime observations, we were unable to confirm the nighttime increase in atmospheric ozone concentration predicted by Dütsch (1961), Paetzold (1961), Hunt (1966), and Carver, Horton, and Burger (1966).

REFERENCES

Barrett, A. H., Neal, R. W., Staelin, D. H., and Weigand, R. M. 1967, *Radiometric Detection of Atmospheric Ozone* (Quart. Prog. Rept., Research Laboratory of Electronics, M.I.T. [July]).
Carver, J. H., Horton, B. H., and Burger, F. G. 1966, *J. Geophys. Res.* (Letter), Vol. 71, No. 17.
Caton, W. M., Welch, W. J., and Silver, S. 1967, *Absorption and Emission in the 8 Mm Region by Ozone in the Upper Atmosphere*, Space Sci. Lab., ser. 8 (issue No. 42), May.
Dütsch, H. U. 1961, *Current Problems in the Photochemical Theory of Atmospheric Ozone*, S.R.I. Conf. on Chem. Reactions in the Lower and Upper Atmosphere, April.
Gora, E. K. 1959, *J. Mol. Spectros.*, 3, 78–99.
Hunt, D. G. 1966, *J. Geophys. Res.*, Vol. 71, No. 5.
Mouw, R. B., and Silver, S. 1960, *Solar Radiation and Atmospheric Absorption for the Ozone Line at 8.3 Millimeters*, Inst. Eng. Res., ser. 60 (issue No. 277) (Berkeley: University of California).
Paetzold, H. K. 1961, *Photochemistry of the Atmospheric Ozone Layer*, S.R.I. Conf. on Chem. Reactions in the Lower and Upper Atmosphere, April.
Townes, C. H., and Schawlow, A. L. 1955, *Microwave Spectroscopy* (New York: McGraw-Hill).

ADDENDA C

DISCUSSION OF ANTENNA EFFECTS

By: C. L. Smith

During a series of observational measurements performed in the Spring of 1968, a diurnal tilt in the base line response of the Earth Based Ozone Measurement Instrument was detected. The effect was localized in the Summer of 1968 by a series of measurements which showed that minor positioning of the feed along the boresight axis about the focal plane of the secondary reflector produced effects of this type.

The reason why positioning of the feed would produce such effects was not immediately apparent. Several possibilities were subjected to detailed analytical study. As a result of these various investigations, it was concluded that the most likely candidates were some form of Fabry-Perot effect and Fresnel effects. This conclusion was supported by discussions with recognized antenna experts at Bell Laboratories, The National Radio Astronomy Observatory, and the Massachusetts Institute of Technology. The effect is produced by multiple reflections within the antenna structure over paths that can extend to hundreds of wavelengths from the plane of the incident wave as it enters the antenna structure to the arrival of the wave at the focal plane of the prime feed. Portions of the incoming wave which travel over these devious paths by reflection and scattering would explain the observed effect if the energy contained in these multiple reflected waves represents less than 1/2% of the total energy in the incident wave. Though more than 99% of the energy may pass through the one normal reflection from the secondary parabola to the prime feed, the extraneous multiply reflected energy arrives at the focal plane of the prime feed in an arbitrary phase relationship, and hence, enhances or constructively interferes with that portion of the wave which travels through the normal path.

One solution to this problem is the introduction of absorbing material on all portions of the antenna structure other than the prime feed and the secondary reflector. An investigation of the most appropriate absorbing material to use was undertaken during the period from November 1, 1968 to February 15, 1969, when the system was inoperative, due to an inadequate supply of klystron tubes. Though absorbing material was readily available from a number of manufacturers, we were unable to obtain data from any manufacturer concerning

the absorbing properties of their material at the 100 GHz frequency of interest. The data available from most manufacturers extends to only 35 GHz. While we were able to verify published data from the manufacturers (Emerson and Cummings and McMillan Radiation Laboratory) at 15 and 35 GHz and to extend measurements to 60 GHz ($\alpha \ll -40$ db), we were unable to check performance at 100 GHz. We were fortunate to find one group at the Aerospace Corporation in El Segundo, California, which had performed measurements on absorbing material at a frequency of 95 GHz. Based on their recommendations and supported by tests performed at our Laboratory on various samples of material, two commercially available absorbing materials were procured in sufficient quantity so that either could be introduced in the antenna system. For several technical reasons, a combination of these two materials was installed in the antenna structure.

The sources of interference and diffraction effects for the 60-inch diameter antenna used in the Earth Based Instrument could be associated with at least five sources. In Figure C-1, these are shown as:

(1) The cylindrical section and the struts form a large scale (dimensions $\gg \lambda_o$) scatterer.

(2) Circular ring diffraction at the end of the hood.

(3) The end of the cylinder and the paraboloid form a Fabry-Perot interferometer.

(4) Fresnel scattering from the cylinder projected as a disk.

(5) A standing wave mismatch at the sub-focal point.

None of these sources are likely to be significant for typical applications since the antenna pattern is seldom defined beyond -35 to -40 db. The effect sought, however, is of the order of -40 db. This is below the level ordinarily regarded as the noise level in antenna tests, (e.g., $\sim$ 35 db). The effect observed could be due, in part, to any or all of the sources noted above.

Fresnel scattering, Fabry-Perot effects, and sub-focal effects will be most noticeable directly below the focal region. Microwave absorber installed below the focus would absorb

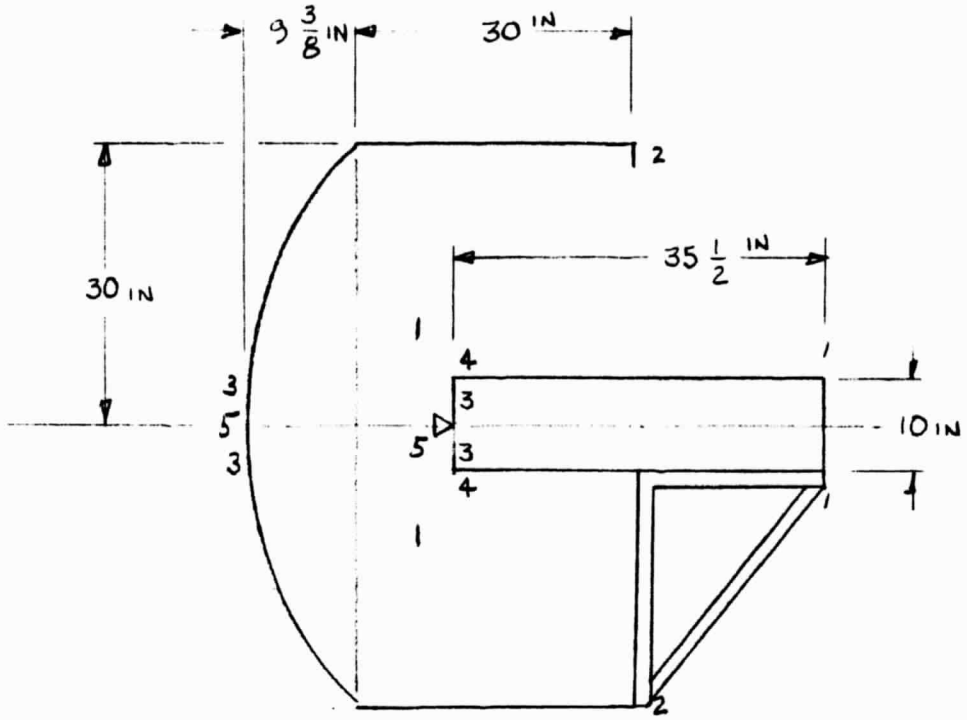

FIGURE 1

SCATTER AND INTEROMETRIC MODES
(DIMENSIONS IN INCHES)

the first and some higher Fresnel zones, reduce the sub-focal standing wave, and lower the Q of the FPI.

Diffraction from shaped surfaces cannot be calculated exactly since, except for certain objects whose surfaces coincide with those of an orthogonal coordinate system, variables of the Laplacian cannot be separated. Even in those cases where separation of variables is possible, the series solutions converge so slowly for objects larger than a wavelength or so that they are virtually useless. Kouyoumjian[1] has introduced a technique from Geometric Optics which is more or less manageable and yields a fairly good approximation. From his discussion, one would conclude that mode (1) is a poor candidate.

Mode 1 -- Diffraction - traveling wave and re-diffraction around the cylinder.

Mode 1 calls for a diffracted wave coupling into a traveling wave in the dielectric cylinder. This wave would be re-radiated at the lower end. While detailed analysis of this problem, by the methods of Kouyoumjian[1] and Walters[2], is possible, the procedures would be tedious.

Upper bounds on the possible relative amount of energy (compared to that incident on the antenna aperture) can be obtained by a somewhat simple argument. The outer surface reflects most of the energy incident upon it. The energy at the approximately outer half wavelength of the radius contributes power to the diffraction pattern:

$$(\mathcal{E})^2 \leq \frac{\pi\left(\frac{25.4}{2}\right)^2 - \pi\left(\frac{25.4}{2} - \frac{300}{101.76\ \ 2}\right)^2}{\pi\left(\frac{60 \times 25.4}{2}\right)^2}$$

$\sim .00064$ or $\quad -32$ db

This is, in turn, scattered through 2π radians. Since two edges, opposite one another, are involved, the contribution to any one point would be π :

$$\frac{1}{\pi}\ db = -4.9$$

$$(\mathcal{E})^2 \sim 37\ db$$

This is the intensity of the source which propagates a wave along the dielectric cylinder. The material dissipates energy at a rate greater than 10^{-3} units/wavelength or about 4 db over the length. The reradiation process could account for another 37 db.

$$|E|^2 \leq \sim 78 \text{ db}$$

This is well below the threshold of the observed phenomenon and does not appear to be significant.

Mode 2, diffraction at the edges, can couple to the feed by direct radiation. The relative amount of energy available for diffraction into the volume containing the feed is that falling on an annulus a half-wavelength or so wide at the radius of the shroud. The feed pattern sees this edge at an angle of 117.7° and at a distance of 292 wavelengths (33.9 in.). The intensity at the diffracting edge is approximately:

$$I_r = \frac{\pi (R\lambda + \lambda)^2 - \pi R\lambda^2}{\pi R_\lambda^2}$$

$$\approx \frac{292.5^2 - 292^2}{292^2} =$$

$$\sim .0034 \sim -24.7 \text{ DB}$$

The radiation is scattered through 360° at each point so that the power launched from the ring is:

$$P_r = (2\pi R) \cdot \frac{P_t G_1 G_2}{(2\pi R)^2}$$

The feed horn is adjusted to provide -10 db edge illumination. $A(\sin X)/X$ pattern would be about -14 db at $\Theta = 117.7°$.

G_1	=	1 or 0 db
G_r	=	-14
$1/R$	=	-24.5
P_t	=	-24.7
2^{-1}	=	-3
$\frac{\pi}{P_r}$	=	$\frac{-4.9}{-71.1}$

or $\sim$ -70 db. This represents an upper bound for a perfectly conducting annulus.

Since the observed phenomenon is of the order of -40 db, direct diffraction from the edge of the shroud does not seem to be a contributing factor.

Fresnel diffraction zones will, however, appear along the inner surface of the shroud because the lip of the outer retaining ring extends inward. The contributions from the edge sources can be quite variable, but if all the energy were to find its way into the feed (assume for illustrative purposes there may be as many as five zones) the intensity would be 38 db higher than the direct diffraction contribution. This, however, would be reduced by 10 log 5 to about -40 db.

Fabry-Perot interferometer effects - (Mode 3). There is a strong similarity between the configuration used in the antenna and the spherical mirror, Fabry-Perot resonators described by Zimmerer[3]. Fabry-Perot Resonators (FPR) are characterized by extremely high Q's and consequently strong frequency effects. The number of modes that can exist along the axis is:

$$m = \frac{2d \cos \theta}{\lambda}$$

The mode density or number of modes per unit wavelength over the band is:

$$\rho_m = \frac{2d\cos\theta}{\lambda_{MAX}} - \frac{2d\cos\theta}{\lambda_{MIN}}$$

$\cos\theta \approx 1$; near normal incidence;

$2d = 2 \times 25.4 \times 24 = 12192$;

$\rho_m = 2.438$ modes/wavelength.

This suggests that the FPR effect at one end of the band is markedly different from the other.

This locates the maxima of the Haidinger fringes as concentric circles of increasing radii until θ is so large that the energy associated with θ_{MAX} escapes the system $0 < \theta < \sim 11\frac{3}{4}°$. The amount of energy that might be coupled into a standing wave pattern is about -35 db (by the argument above) below the principle pattern. Microwave absorber at normal incidence dissipates about 99% of the power (reflection -20 db) which would bring the Q of the FPR down so that the effect would be around -55 db.

The final source of the antenna effect to be considered is Fresnel scattering around the obstacles in the near field of the antenna (Mode 4 in the list). This contribution will be a function of frequency.

The Fresnel region of a circular aperture if given by:

$$E_{(w,z)} = U_{\nu+1}(w,z) + j\, U_{\nu+2}(w,z)$$

where:

$$w = \frac{\beta D^2}{4R} = 2.22$$

$$z = \frac{\beta D \sin\theta}{2} = 1.0656 \sin\theta$$

$$0 < \sin\theta <$$

$$\beta = \frac{2\pi}{\lambda_0}$$

The parameter, ν, in the order of the Lommel functions for circular scatterers is zero.

$$U_{\nu}(w,z) = \sum_{m=0}^{\infty} (-1)^m \left(\frac{w}{2}\right)^{\nu+2m} J_{\nu+2m}(z)$$

$$E(w,z) = U_1(w,z) + j\, U_2(w,z)$$

$$= \sum_{m=0}^{\infty} (-1)^m \left(\frac{w}{2}\right)^{2m+1} J_{2m+1}(z)$$

$$+ j \left[\sum_{m=0}^{\infty} (-1)^m \left(\frac{w}{2}\right)^{2(m+1)} J_{2(m+1)}(z)\right]$$

Ramsay[4] plots $\left[E(w,z)\right]$ for a number of configurations. The case at hand corresponds to a situation where the Fresnel pattern maxima would form a set of concentric rings, with their peak intensity near the outer edge of the projected blockage. These rings would extend toward the sub-focal point in diminishing intensity. The opposite situation occurs for the FPR.

If the same total energy is allowed (-35 db) then we would have two sets of frequency dependent fringes under the feed. If the two effects are assumed to originate at the lower mounting plate, they must divide the energy between them according to some rule. Until better information is available it can be assumed that the two effects, having the same

order of magnitude, divide the energy equally. We then have two sets of fringe rings; a set having a bright spot at the center, and fading to the edge, and a second set having a bright ring near the edge of the cylinder projection and fading rapidly outward toward the edge of the secondary reflector.

The possibility of vertex mismatch (Mode 5) would be eliminated by the introduction of a twelve-inch diameter disk of absorber material as a matter of course. It was, however, investigated separately using a polarization twisting plate.[5] The plate was designed to rotate the polarization of incident energy by 90° and since the feed system is linear, the standing wave (if present) would undergo two round trips before returning in the same polarization sense. Scattering would occur at both ends of the path and the antenna effects from this souce would, hopefully, be attenuated so such effect was observed and other causes were sought with the results discussed above.

RESULTS

The absorber was introduced a few pieces at a time. Improvement was noted as each section was added. The surfaces covered by absorbing material were:

A 12 inch diameter circular area centered on the sub-focal point.

The lower surface of the RF cylindrical unit surrounding the feed itself.

The inner surface of the cylindrical shroud.

The lower surfaces of the RF Unit spar supports.

Measurements performed after the installation of the absorbing material confirmed that this approach was an appropriate remedy as evidenced by the fact that:

1) Mechanical adjustment of the feed position by $\pm$ 1 wavelength along the boresight axis about the focal plane showed no differential frequency response in the signal channel output recordings, to within the rms sensitivity of the system. These measurements were performed when observing the sun. The only effect noted was the normal and anticipated broadband

frequency response in all channels as the feed was de-tuned from the focal position.

2) The accumulation of observational data during the period from February 15 to March 15, 1969 showed no evidence of a base line tilt on any day of observation within the measurement accuracy determined by the rms sensitivity of the system.

The following tentative conclusions were reached:

1) The observed effect was apparently due to internal reflections and standing waves within the antenna structure.

2) There were three possible sources -- Fabry-Perot interferometer and two Fresnel scattering mechanisms.

Antenna effects of the type observed are negligible for most radio telescope measurements. These effects are important only when observing the structure of natural resonant lines typical of atmospheric or interstellar gases. For observations of this type the effect would become noticeable: (a) in the wings of lines measured in emission where the peak response at the line center frequency is at least 30 db above the system sensitivity and (b) throughout the entire line profile when measured in absorption if the background source intensity is at least 30 db above the system sensitivity.

A more thorough analysis of the FPR and near Fresnel zone effects in antenna systems is recommended, since these effects could be significant in large scale ($D > 200\ \lambda$) antennas used in radio astronomy.

REFERENCES

1. Kouyoumjian, R.G., "An Introduction to Geometrical Optics and the Geometrical Theory of Diffraction", The Ohio State University, Antenna and Scattering Theory, Recent Advances, Vol. 1. 1966.

2. Walters, C.H., Traveling Wave Antennas, McGraw-Hill.

3. Zimmerer, R.N., "Sperical Mirror Fabry-Perot Resonators", Trans IEEE MTT-11, No. 5 Sept. 1963, pp. 371-379.

4. Ramsay, J.F., "Lambda Functions", Microwaves June 1967, p. 107.

5. Silver, S., Microwave Antenna Theory and Design, McGraw-Hill, Rad. Lab Series, Vol. 12, pp 443-450.

ADDENDA "D"

ADDENDA D

NEW TECHNOLOGY

"After a diligent review of the work performed under this contract, no new innovation, discover, improvement or invention was made."